ELSEVIER

Mean-field/PDF numerical approach for polydispersed turbulent two-phase flows

E. Peirano [a,*], S. Chibbaro [b], J. Pozorski [c], J.-P. Minier [b]

[a] *ADEME, Renewable Energies Department, 500 route des Lucioles, Sophia Antipolis, 06560 Valbonne, France*
[b] *Electricité de France, Div. R&D, MFTT, 6 Quai Watier, 78400 Chatou, France*
[c] *Institute of Fluid-Flow Machinery, Polish Academy of Sciences, Fiszera 14, 80952 Gdańsk, Poland*

Abstract

   The purpose of this paper is to give an overview in the realm of numerical computations of polydispersed turbulent two-phase flows, using a mean-field/PDF approach. In this approach, the numerical solution is obtained by resorting to a hybrid method, where the mean fluid properties are computed by solving mean-field (RANS) equations with a classical finite volume procedure whereas the local instantaneous properties of the particles are determined by solving stochastic differential equations (SDEs). The fundamentals of the general formalism are recalled and particular attention is focused on a specific theoretical issue: the treatment of the multiscale character of the dynamics of the discrete particles, i.e. the consistency of the system of SDEs in asymptotic cases. Then, the main lines of the particle/mesh algorithm are given and some specific problems, related to the integration of the SDEs, are discussed, for example, issues related to the specificity of the treatment of the averaging and projection operators, the time integration of the SDEs (weak numerical schemes consistent with all asymptotic cases), and the computation of the source terms. Practical simulations, for three different flows, are performed in order to demonstrate the ability of both the models and the numerics to cope with the stringent specificities of polydispersed turbulent two-phase flows.
© 2006 Elsevier Ltd. All rights reserved.

Keywords: Dispersed two-phase flows; Turbulence; PDF methods; Particle/mesh algorithms

Contents

   * Corresponding author. Tel.: +33 4 93 95 79 34; fax: +33 4 93 65 31 96.
   E-mail addresses: eric.peirano@ademe.fr (E. Peirano), chibbaro@chi80bk.der.edf.fr (S. Chibbaro), jp@imp.gda.pl (J. Pozorski), jean-pierre.minier@edf.fr (J.-P. Minier).

1. Introduction

Two-phase flows are relatively easy to observe: to get a first inkling, one can think of throwing small light particles (which then play the role of tracer particles) into a turbulent flow such as a rapid river or a plume coming out of a chimney. The small solid particles reveal the intricate and complex features of turbulent flows: understanding and modelling these features, i.e.

single-phase turbulent flow modelling, is the subject of extensive research [1]. If one introduces larger and larger particles in the flow, more complex phenomena take place: the behaviour of the particles will reflect the interplay between the main physical mechanisms, such as particle inertia and turbulence of the carrying flow. Then, eventually, when particles become large enough, the effect of the fluid may become negligible with respect to particle inertia. Thus, turbulent fluid–particle

Nomenclature

A_i	drift vector
$\mathbf{A}_{p \to f}$	acceleration in Langevin equation for the fluid (m/s^2)
$\mathbf{A}_{p \to s}$	acceleration in Langevin equation for the particles (m/s^2)
$A_{f,i}$	drift vector defined by Eq. (23) (m/s^2)
$A_{s,i}$	drift vector defined by Eq. (24) (m/s^2)
$\mathcal{A}_i$	acceleration defined by Eq. (40) (m/s^2)
$\mathcal{A}_i^n$	approximated value of $\mathcal{A}_i$ at t_n (m/s^2)
$\mathcal{A}_i^{n+1}$	predicted value of $\mathcal{A}_i$ at t_{n+1} (m/s^2)
$\mathfrak{A}_i$	drift vector defined by Eqs. (79) and (120)
$\mathfrak{A}_i^n$	approximated value of $\mathfrak{A}_i$ at t_n
$\tilde{\mathfrak{A}}_i^{n+1}$	predicted value of $\mathfrak{A}_i$ at t_{n+1}
A_1	coefficient defined in Table 4 (s)
A_2	function defined in Table 5
A_{2c}	function defined in Table 5
b_i	coefficient for $\tilde{k}$, $b_i = T_L / T_{L,i}^*$
B	diffusion coefficient in Eq. (31) (m/s$^{3/2}$)
$B.(N)$	bias for variable·
B_{ij}	diffusion matrix (m/s$^{3/2}$)
$\check{B}_i$	diagonal elements of B_{ij}, i.e. $\check{B}_i = B_{ii}$ (m/s$^{3/2}$)
$\check{B}_i^n$	approximated value of $\check{B}_i$ at t_n (m/s$^{3/2}$)
$\tilde{\check{B}}_i^{n+1}$	predicted value of $\check{B}_i$ at t_{n+1} (m/s$^{3/2}$)
B_i^*	approximated value defined by Eq. (88) (m/s$^{3/2}$)
$\mathfrak{B}_{ij}$	diffusion matrix defined by Eqs. (79) and (120)
$\mathfrak{B}_{ij}^n$	approximated value of $\mathfrak{B}_{ij}$ at t_n
$\tilde{\mathfrak{B}}_{ij}^{n+1}$	predicted value of $\mathfrak{B}_{ij}$ at t_{n+1}
$B_{f,ij}$	diffusion matrix defined by Eq. (23) (m/s$^{3/2}$)
$B_{s,ij}$	diffusion matrix defined by Eq. (24) (m/s$^{3/2}$)
B_1	coefficient defined in Table 4 (s)
B_2	function defined in Table 5
B_{2c}	function defined in Table 5
C	proportionality constant, cf. Eq. (51)
$C(T)$	proportionality constant, cf. Eq. (67)
C_D	drag coefficient
C_i	acceleration defined by Eq. (40) (m/s^2)
C_i^n	approximated value of C_i at t_n (m/s^2)
C_i^{n+1}	predicted value of C_i at t_{n+1} (m/s^2)
C_β	coefficient for $T_{L,i}^*$, cf. Eq. (25)
C_0	Kolmogorov constant, cf. Eq. (22)
C_1	coefficient defined in Table 4 (s)
C_{2c}	function defined in Table 5
d_p	particle diameter (m)
dt	time increment or observation timescale (s)

D	diffusion coefficient or cyclone diameter (m^2/s or m)
D_{ij}	positive-definite matrix, $\mathbf{D} = \mathbf{B}B^T$
D_1	coefficient defined in Table 4
E_1	coefficient defined in Table 4
f	function
f_Φ	pdf of Φ
$\mathcal{F}_f^E$	fluid Eulerian mass density function
g	function
$\mathbf{g}$	gravitational acceleration (m/s^2)
G_{ij}	return-to-equilibrium matrix, cf. Eq. (23) (s^{-1})
G_{ij}^a	anisotropy matrix, cf. Eq. (23) (s^{-1})
$\mathcal{G}_{p,i}$	standard Gaussian random variable, Eq. (72)
$\mathcal{G}_{p,i}'$	standard Gaussian random variable, Eq. (96)
$\mathcal{G}_{x,i}$	standard Gaussian random variable, Eq. (73)
$\mathcal{G}_{1,i}$	standard Gaussian random variable, cf. Table 4
$\mathcal{G}_{2,i}$	standard Gaussian random variable, cf. Table 4
$\mathcal{G}_{3,i}$	standard Gaussian random variable, cf. Table 4
$\mathbf{H}(t)$	stochastic process, cf. Eq. (68)
$\mathcal{H}(\mathbf{V}_f)$	function of $\mathbf{V}_f$
$I_x(t)$	stochastic integral in model problem, cf. Eq. (36) (m)
$I_U(t)$	stochastic integral in model problem, cf. Eq. (36) (m/s)
k	turbulent kinetic energy (m^2/s^2)
$\tilde{k}$	modified turbulent kinetic energy (m^2/s^2)
k_p	deposition velocity (m/s)
$m(x)$	deterministic function, cf. Section 5.2.1
N	total number of discrete particles or samples
N_k	number of discrete particles in cell k
N_{pc}	number of discrete particles per cell or per class
N_{pc}^i	number of discrete particles in cell i
p	probability density function (pdf) for $\mathbf{Z}(t)$
p_f^E	Eulerian fluid distribution function
p^r	probability density function (pdf) for $\mathbf{Z}^r(t)$
$P(t,\mathbf{x})$	local instantaneous pressure field (Pa)
$\langle P^n \rangle$	approximated value of $P(t,\mathbf{x})$ at $(t_n, \mathbf{x}_p^n)$ (Pa)
$\langle P^{n+1} \rangle$	predicted value of $P(t,\mathbf{x})$ at $(t_{n+1}, \mathbf{x}_p^{n+1})$ (Pa)
P_{ij}	coefficients defined in Table 4, $(i,j) \in (1,2,3)^2$ (m or m/s)

Re_p — Reynolds number (discrete particles)

R_{ij} — Reynolds stress tensor (m^2/s^2)

$s(x)$ — deterministic function, cf. Section 5.2.1

S_U — source term in Eq. (125) (m/s^2)

S_k — trace of source term tensor in Eq. (126) (m^2/s^3)

$S_{R_{ij}}$ — source term in Eq. (126) (m^2/s^3)

t — time (s)

t^+ — dimensionless time, $t^+ = t(u^*)^2/\nu_f$

T — characteristic timescale (s)

T_E — fluid Eulerian integral timescale (s)

T_i — fluid seen integral timescale (in Section 5) (s)

T_i^n — approximated value of T_i at t_n (s)

$\tilde{T}_i^{n+1}$ — predicted value of T_i at t_{n+1} (s)

T_L — fluid Lagrangian integral timescale (s)

$T_{L,i}^*$ — fluid seen integral timescale (s)

$\mathbf{u}(t, \mathbf{x})$ — fluctuating fluid velocity field (m/s)

u^* — friction velocity (m/s)

$U(t)$ — velocity in model problem, cf. Eq. (31) (m/s)

$\mathbf{U}(t, \mathbf{x})$ — local instantaneous fluid velocity field (m/s)

$\langle U_i \rangle$ — mean fluid velocity field at $(t, \mathbf{x})$ or $(t, \mathbf{x}_p(t))$ (m/s)

$\langle U_i^n \rangle$ — approximated value of $\langle U_i \rangle$ at $(t_n, \mathbf{x}_p^n)$ (m/s)

$\langle U_i^{n+1} \rangle$ — approximated value of $\langle U_i \rangle$ at $(t_{n+1}, \mathbf{x}_p^{n+1})$ (m/s)

$\mathbf{U}_f(t)$ — velocity of fluid particles (m/s)

$U_{f,i}^n$ — approximated value of $\mathbf{U}_f(t)$ at t_n (m/s)

$\tilde{U}_{f,i}^{n+1}$ — predicted value of $\mathbf{U}_f(t)$ at t_{n+1} (m/s)

$U_{f,i}^{n+1}$ — approximated value of $\mathbf{U}_f(t)$ at t_{n+1} (m/s)

$\mathbf{U}_p(t)$ — velocity of the discrete particles (m/s)

$U_{p,i}^n$ — approximated value of $\mathbf{U}_p(t)$ at t_n (m/s)

$\tilde{U}_{p,i}^{n+1}$ — predicted value of $\mathbf{U}_p(t)$ at t_{n+1} (m/s)

$U_{p,i}^{n+1}$ — approximated value of $\mathbf{U}_p(t)$ at t_{n+1} (m/s)

$\mathbf{U}_r(t)$ — particle relative velocity (m/s)

$\mathbf{U}_s(t)$ — fluid velocity seen (m/s)

$U_{s,i}^n$ — approximated value of $\mathbf{U}_s(t)$ at t_n (m/s)

$\tilde{U}_{s,i}^{n+1}$ — predicted value of $\mathbf{U}_s(t)$ at t_{n+1} (m/s)

$U_{s,i}^{n+1}$ — approximated value of $\mathbf{U}_s(t)$ at t_{n+1} (m/s)

$\mathbf{V}_f$ — sample space value for $\mathbf{U}_f(t)$ (m/s)

$\mathcal{V}_f^{[k]}$ — volume of fluid in cell $[k]$ (m^3)

$w(\mathbf{x})$ — weighting function (continuous form)

$\tilde{w}(\mathbf{x})$ — weighting function (discrete form)

$W_i(t)$ — Wiener process ($s^{1/2}$)

$x(t)$ — position in model problem, cf. Eq. (31) (m)

$\mathbf{x}_f(t)$ — position of the fluid particles (m)

$\mathbf{x}_p(t)$ — position of the discrete particles (m)

$x_{p,i}^n$ — approximated value of $\mathbf{x}_p(t)$ at t_n (m)

$x_{p,i}^{n+1}$ — approximated value of $\mathbf{x}_p(t)$ at t_{n+1} (m)

$\mathbf{X}(t)$ — stochastic process or deterministic variable, X

y^+ — dimensionless distance from wall

Y — sample space value of $\mathbf{Y}(t)$

$Y(t)$ — stochastic process or deterministic variable, Y

$\mathbf{Y}(t)$ — set of external variables

$\mathbf{z}$ — sample space value of $\mathbf{Z}(t)$

$\mathbf{z}_f^i$ — sample space value of $\mathbf{Z}_f^i(t)$

$\mathbf{z}_p^i$ — sample space value of $\mathbf{Z}_p^i(t)$

$\mathbf{Z}(t)$ — state vector

$Z_{f,j}^i$ — variable j for fluid particle i

$Z_{p,j}^i$ — variable j for discrete particle i

$\mathbf{Z}^r(t)$ — reduced state vector

Greek letters

$\alpha_f(t, \mathbf{x})$ — volume fraction of fluid

$\alpha_p(t, \mathbf{x})$ — volume fraction of particles

β_i, β — constants defined in Eq. (25)

$\gamma_i(t)$ — stochastic process defined by Eq. (133) (m/s)

γ_i^n — approximated value of $\gamma_i(t)$ at t_n (m/s)

$\tilde{\gamma}_i^{n+1}$ — predicted value of $\gamma_i(t)$ at t_{n+1} (m/s)

$\Gamma_i(t)$ — stochastic process defined by Eq. (134) (m/s)

Γ_i^n — approximated value of $\Gamma_i(t)$ at t_n (m/s)

$\tilde{\Gamma}_{n+1}^i$ — predicted value of $\Gamma_i(t)$ at t_{n+1} (m/s)

$\delta(\cdot)$ — Dirac delta function

δ_{ij} — Kronecker's symbol

Δt — time step (s)

Δx — characteristic cell size (m)

$\epsilon(t, \mathbf{x})$ — dissipation rate of k (m^2/s^3)

$\varepsilon(t)$ — energy dissipation for fluid particles (m^2/s^3)

$\eta(t)$ — Gaussian white noise

θ_i — ratio, $\theta_i = T_i/(T_i - \tau_p)$

θ_i^n — approximated value of θ_i at t_n

μ_f — dynamic viscosity of fluid (Pa s)

ν_f — kinematic viscosity of fluid (m^2/s)

ξ — standard Gaussian random variable, cf. Eq. (51)

ξ_x — standard Gaussian random variable, cf. Eq. (37)

ξ_U — standard Gaussian random variable, cf. Eq. (37)

$\Pi_p(t)$ — random acceleration defined by Eq. (A2) (m/s^2)

ρ_f — density of fluid (kg/m^3)

ρ_p — density of discrete particles (kg/m^3)

σ — diffusion matrix in Eq. (45)

$\sigma[\cdot]$ — standard deviation of $\cdot$

σ_Φ^2 — variance of Φ

τ — characteristic timescale (s)

τ_p — particle relaxation time (s)

τ_p^+ — dimensionless particle relaxation time

$\tilde{\tau}_p^n$ — approximated value of τ_p at t_n (s)

$\tilde{\tau}_p^{n+1}$	predicted value of τ_p at t_{n+1} (s)
τ_η	Kolmogorov timescale (s)
Φ	random variable or deterministic function
χ	ratio, $\chi = \alpha_f \rho_f / \alpha_p \rho_p$
Ψ	sample space value of Φ
$\Omega_i(t)$	stochastic process defined by Eq. (135) (m)
Ω_i^n	approximated value of $\Omega_i(t)$ at t_n (m)

Subscripts

f	continuous phase (fluid)
p	discrete phase (particles)
s	fluid properties sampled along particle trajectories (fluid seen)

Superscripts

[i]	variable calculated at cell centre i
[k]	variable calculated in cell k
n	approximated values at $t = t_n$
$n+1$	approximated values at $t = t_n + \Delta t$
$(n), (N)$	variables calculated at particle locations
r	reduced information
T	transpose of a matrix
[x]	variables calculated on the mesh/at cell centres
$+$	dimensionless quantities
$\sim$	predicted quantities (numerical schemes)

Special notation

$\{\cdot\}$	set of variables
$\langle\cdot\rangle$	mathematical expectation
$\langle\cdot\rangle_N$	mean value, i.e. $(1/N)\sum_{i=1}^{N} \bullet$
$\langle\cdot\rangle_\Delta$	spatial average
$\langle\cdot\rangle_{N,\Delta}$	approximation of $\langle\cdot\rangle$, spatial average on N samples
$\langle\cdot\rangle_\infty$	$=\langle\bullet\rangle_N$ with $N \to \infty$, i.e. $\langle\cdot\rangle$
$\langle\bullet\vert\bullet\rangle$	conditional expectation
$\vert\cdot\vert$	norm of a vector
∂	partial derivative
$\mathbf{U}$	bold style for vector notation
$D\bullet/Dt$	$\partial\bullet/\partial t + \langle U_i\rangle\partial\bullet/\partial x_i$
$d\bullet(t)$	time increment, e.g. $d\mathbf{U}_f(t) = \mathbf{U}_f(t + dt) - \mathbf{U}_f(t)$

Abbreviations

CIC	cloud in cell
CPU	central processing unit
cst	a given constant
CTE	crossing trajectory effect
DNS	direct numerical simulation
DSMC	direct simulation Monte Carlo
LES	large eddy simulation
NGP	nearest grid point
ODE	ordinary differential equation
PDE	partial differential equation
pdf/PDF	probability density function
PIC	particle in cell
RANS	Reynolds-averaged Navier–Stokes
RHS	right-hand side
r.m.s.	root-mean square
RSM	Reynolds stress models
SDE	stochastic differential equation
SPH	smoothed particle hydrodynamics
VRT	variance reduction technique

flow modelling appears as a link between subjects such as turbulence and granular flows [2]. In general, two-phase flows are even more complex since, in the case of air and water, for example, different configurations of the interface between the two phases may be present. Yet, in the present study, attention will be focused on the motion of particles embedded in a turbulent fluid, i.e. *polydispersed turbulent two-phase flows*, where the geometrical configuration does not change.

Polydispersed turbulent two-phase flows are found in numerous environmental and industrial processes, very often in contexts that involve additional issues, for example chemical and combustion ones. Therefore, modelling these flows raises very difficult theoretical questions and, at the same time, one has to provide answers to what we can refer to as engineering concerns. As a consequence, a theoretical and numerical model represents an attempt to find a

satisfactory compromise between these sometimes conflicting expectations. Before trying to outline what is meant by satisfactory, let us describe the characteristics of the polydispersed turbulent two-phase flows we consider here.

In the present study, only non-reacting incompressible fluid–particle flows, with no collisions between particles, are investigated (particle dispersion and turbulence modulation induced by the presence of the particles are the physical mechanisms under consideration). This is not a strict limitation of the approach that will be adopted since, as mentioned below, the probability density function (PDF) formalism that shall be followed is precisely well-suited for the extension to more complex physics, such as combustion. However, for the sake of simplicity, we limit ourselves to the core physics embodied by particle dynamics. In addition, only the case of solid heavy

particles is treated, i.e. density of the particles is much greater than that of the fluid, $\rho_p \gg \rho_f$. This hypothesis simplifies the equation of motion of discrete particles in a turbulent flow which, retaining only drag and gravity forces, can be written as:

$$\begin{cases} \dfrac{d\mathbf{x}_p(t)}{dt} = \mathbf{U}_p(t), \\[2mm] \dfrac{d\mathbf{U}_p(t)}{dt} = \dfrac{1}{\tau_p}(\mathbf{U}_s(t) - \mathbf{U}_p(t)) + \mathbf{g}. \end{cases} \quad (1)$$

In these equations, $\mathbf{U}_s(t) = \mathbf{U}(t,\mathbf{x}_p(t))$ is the fluid velocity 'seen', i.e. the fluid velocity sampled along the particle trajectory $\mathbf{x}_p(t)$, where $\mathbf{U}(t,\mathbf{x})$ is the local instantaneous (Eulerian) fluid velocity field. The particle relaxation time, τ_p, is defined as

$$\tau_p = \frac{\rho_p}{\rho_f} \frac{4d_p}{3C_D|\mathbf{U}_r|}, \quad (2)$$

where the local instantaneous relative velocity is $\mathbf{U}_r(t) = \mathbf{U}_p(t) - \mathbf{U}_s(t)$. The drag coefficient, C_D, is a non-linear function of the particle-based Reynolds number, $Re_p = d_p|\mathbf{U}_r|/\nu_f$, which means that C_D is a non-linear function of the particle diameter, d_p [3]. This last point represents a major theoretical difficulty for a statistical treatment since we do not consider mono-dispersed two-phase flows (where d_p is constant), but *polydispersed* two-phase flows, where d_p covers a range of possible values (from very light particles acting as fluid tracers to high-inertia particles in the ballistic regime, where the effect of the fluid on the particle dynamics can be neglected). In the particle dynamical equations, it is important to note that we are dealing with the instantaneous fluid velocities, $\mathbf{U}(t,\mathbf{x}_p(t))$. Yet, for high-Reynolds turbulent flows, which are the most common ones, such an information is not available due to the very large number of degrees of freedom of turbulent flows [4]. A modelling step is necessary and most models adopt a statistical approach where only some limited information is sought for the fluid fields whereas particles are tracked individually. In practical models, this information consists of, for the fluid, the first two velocity moments, as in $R_{ij}–\epsilon$ models [5], or even filtered velocity fields as in LES calculations, e.g. [6,7]. In the present work, $R_{ij}–\epsilon$ models (RANS equations) will be used in practical computations, but the PDF approach (for the particles) to come is fully compatible with other approaches for the fluid, for example LES.

As indicated above, in order to track the particles, a *satisfactory* model must be built for the evaluation of particle properties, cf. Eqs. (1). By *satisfactory*, we mean a model, which has the following properties:

(i) the model treats the important phenomena, such as convection and the polydispersed nature of the particles, without approximation;
(ii) the approach is naturally set into a general formalism, which allows additional variables, for more complex physics such as combustion issues, to be directly introduced;
(iii) the complete theoretical model must be tractable in complex geometries and applicable for engineering problems.

The first two issues have been addressed in a previous review work [8], where a PDF approach has been developed. In practice, the PDF approach has the form of a particle stochastic method where the velocity of the fluid seen, $\mathbf{U}_s(t)$, is modelled as a stochastic diffusion process, i.e. the dynamics of the particles are calculated from stochastic differential equations (SDEs), the so-called Langevin equations [8]. In polydispersed two-phase flows, a particle point of view seems rather natural, given the physics considered. Yet, the particles, which are to be simulated, represent samples of the pdf and should not be confused with real particles. Within the PDF formalism, this particle point of view is helpful to build the theoretical model and, at the same time, represents directly a discrete formulation of the model. However, in order to devise a consistent framework, it is important to separate the two steps by formulating the model in continuous time *before* addressing the questions of numerical methods for practical computations.

The purpose of the present review is to address point (iii) above, and to discuss the general numerical methodology used for particle stochastic or PDF models for polydispersed turbulent two-phase flows. More specifically, it is aimed at providing answers to several interrogations:

(a) what do the stochastic particles represent?
(b) how do we compute the stochastic differential equations?
(c) what are the various difficulties and sources of numerical errors in the complete numerical method?

More than trying to present definitive answers to the questions of what numerical scheme should be used, the objective is to propose a general numerical approach and to show how PDF models, Langevin stochastic

equations, particle/mesh and dynamical Monte Carlo methods are closely connected and actually represent different translations of the same idea. Within that context, a major goal is to emphasise that although numerical schemes are separated from the construction of the theoretical model, they cannot be addressed only from a mathematical point of view. Indeed, it is important that they reflect the physical properties of the continuous stochastic model, namely the multiscale character of the Langevin equations presented in Section 3.

The paper is organised as follows. The mathematical background on PDF equations and stochastic diffusion processes is recalled in Section 2. General and state-of-the-art Langevin models for polydispersed turbulent two-phase flow modelling are briefly presented in Section 3. A central point is the analysis of the multiscale properties of the Langevin equations, and the expression of various physical limits when characteristic timescales become negligible with respect to the observation timescale, cf. Section 4. This analysis serves as a guideline for the development of the numerical model in Section 5 that contains both particle/mesh and time-integration issues. Then, a discussion is given on specific issues related to two-way coupling, Section 6. Several numerical applications representative of practical concerns are presented in Section 7.

2. General formalism

The general formalism, on which the derivation of the system of equations (RANS equations for the fluid and SDEs for the discrete particles) relies, is based on the Lagrangian point of view: the system (the fluid–particle mixture) is treated as an ensemble of fluid and discrete particles. The discretisation of a continuous medium (the fluid) with particles is not a natural step, but it is a practical way, in the frame of the probabilistic formalism briefly outlined here, to treat important physical phenomena without approximation [8]. In the present formalism, a fluid particle is an independent sample of the flow, with a given pdf. Physically, a fluid particle can be seen as a small element of fluid whose characteristic length scale is much larger than the molecular mean free path and much smaller than the Kolmogorov length scale. The fluid particles have a mass m_f, a volume V_f and a velocity that equals the fluid velocity field at the location of the particle, $\mathbf{U}_f(t) = \mathbf{U}(t, \mathbf{x}_f(t))$.

2.1. Statistical approach

Let us consider an ensemble composed by N_f fluid particles and N_p discrete particles interacting through forces that can be expressed as functions, or functionals, of the variables attached to each particle, e.g. l variables for the fluid particles and q variables for the discrete particles (these variables can be, for example, position, velocity, etc.). All available information is then contained in the following state vector

$$\mathbf{Z}(t) = \{Z_{f,1}^1(t), \ldots, Z_{f,l}^1(t); \ldots; Z_{f,1}^{N_f}(t), \ldots, Z_{f,l}^{N_f}(t); \\ Z_{p,1}^1(t), \ldots, Z_{p,q}^1(t); \ldots; Z_{p,1}^{N_p}(t), \ldots, Z_{p,q}^{N_p}(t)\}, \tag{3}$$

where $Z_{f,j}^i(t)$ represents the variable j attached to the fluid particle labelled i and $Z_{p,j}^i(t)$ represents the variable j attached to the discrete particle labelled i. The dimension of the state vector is then $lN_f + qN_p$. Let us suppose that the dynamical behaviour of the closed system can be described in terms of ordinary differential equations (the Navier–Stokes equations, in Lagrangian form, for fluid particles and for discrete particles, the equation of motion of a single particle in a turbulent fluid–particle mixture), i.e.

$$\frac{d\mathbf{Z}(t)}{dt} = \mathbf{A}(t, \mathbf{Z}(t)). \tag{4}$$

Here, it is assumed that in the Navier–Stokes equations, the local instantaneous pressure gradient, the viscous forces and the source term (due to the force exerted by the discrete particles on the fluid) can be expressed as functionals of the state vector $\mathbf{Z}(t)$. In sample space, this system of ordinary differential equations (ODEs) corresponds to the Liouville equation [9]

$$\frac{\partial p(t; \mathbf{z})}{\partial t} + \frac{\partial}{\partial \mathbf{z}}(\mathbf{A}(t, \mathbf{z})p(t; \mathbf{z})) = 0, \tag{5}$$

where $p(t; \mathbf{z})$, the associated pdf, represents the probability to observe at time t the system in state $\mathbf{z}$. In the present paper, we distinguish between physical space, $\mathbf{Z}$, and sample space, $\mathbf{z}$. A distinction is also made, for the pdf, between parameters and variables by separating them with a semi-colon, i.e. $(t; \mathbf{z})$.

In practice, the number of degrees of freedom of such a system is huge (turbulent flow with a large number of particles) and one has to resort to a contracted description in order to come up with a model that can be simulated with modern computer technology. For single-phase turbulent reactive flows, a one-point pdf, $p(t; \mathbf{z}_f^i)$, is often retained [10,11]. For the description of the dynamics of discrete particles in

turbulent dispersed two-phase flows, a one-point pdf, $p(t; \mathbf{z}_p^i)$, is also encountered [5,8,12]. In this work, as we shall see in Section 3.2, both approaches are gathered in the form of a two-point pdf, $p(t; \mathbf{z}_f^i, \mathbf{z}_p^j)$ and the associated reduced state vector (henceforth denoted by superscript r) is

$$\mathbf{Z}^r(t) = \{Z_{f,1}(t), ..., Z_{f,l}(t), Z_{p,1}(t), ..., Z_{p,q}(t)\}. \quad (6)$$

The time evolution equations, in physical space, for this sub-system have the form

$$\frac{d\mathbf{Z}^r(t)}{dt} = \mathbf{A}(t, \mathbf{Z}^r(t), \mathbf{Y}(t)), \quad (7)$$

where there is a dependence on the external variable $\mathbf{Y}(t)$ (related to the particles not contained in $\mathbf{Z}^r(t)$ as only pairs of particles, a fluid one and a discrete one, are under consideration). In sample space, the marginal pdf $p^r(t; \mathbf{z}^r)$ verifies

$$\frac{\partial p^r(t; \mathbf{z}^r)}{\partial t} + \frac{\partial}{\partial \mathbf{z}^r}[\langle \mathbf{A}|\mathbf{z}^r \rangle p^r(t; \mathbf{z}^r)] = 0, \quad (8)$$

where the conditional expectation is given by

$$\langle \mathbf{A}|\mathbf{z}^r \rangle = \int \mathbf{A}(t, \mathbf{z}^r, \mathbf{y})p(t; \mathbf{y}|\mathbf{z}^r)d\mathbf{y}$$

$$= \frac{1}{p^r(t; \mathbf{z}^r)} \int \mathbf{A}(t, \mathbf{z}^r, \mathbf{y})p(t; \mathbf{z}^r, \mathbf{y})d\mathbf{y}. \quad (9)$$

Eq. (8) is now unclosed showing that a reduced description of a system implies a loss of information and thus the necessity to introduce a model.

A practical way to close the system is to resort to stochastic differential equations (SDEs), as it shall be briefly explained in Section 3.1. Further detailed explanations for this move can be found in Refs. [8,13]. The stochastic differential equations treated in this work have the following form ($\mathbf{Z}^r(t)$ is called a diffusion process)

$$dZ_i^r(t) = A_i(t, \mathbf{Z}^r(t))dt + B_{ij}(t, \mathbf{Z}^r(t))dW_j(t), \quad (10)$$

where $\mathbf{W}(t) = (W_1(t), ..., W_d(t))$ is a set of independent Wiener processes [14] and $d = l + q$ is the dimension of the reduced state vector. These equations are often referred to as *Langevin equations* in the physical literature [9]. In Eq. (10), $\mathbf{A} = (A_i)$ is called the drift vector and $\mathbf{B} = (B_{ij})$ is the diffusion matrix. SDEs require a strict mathematical definition of the stochastic integral as it shall be explained in Section 2.2. If one adopts the Itô definition of the stochastic integral (see Section 2.2) in Eq. (10), it can be shown, see [9] for example, that the corresponding equation in sample space for $p^r(t; \mathbf{z}^r)$ is the Fokker–Planck equation

$$\frac{\partial p^r(t; \mathbf{z}^r)}{\partial t} = -\frac{\partial}{\partial z_i^r}[A_i(t, \mathbf{z}^r)p^r(t; \mathbf{z}^r)] + \frac{1}{2}\frac{\partial^2}{\partial z_i^r \partial z_j^r}$$

$$\times [D_{ij}(t, \mathbf{z}^r)p^r(t; \mathbf{z}^r)], \quad (11)$$

where $D_{ij} = B_{il}B_{jl} = (BB^T)_{ij}$ is a positive-definite matrix. In a weak sense (when one is only interested in statistics of the process), one can speak of an equivalence between SDEs and Fokker–Planck equations. As we shall see below, this correspondence is the cornerstone of the proposed numerical approach: the pdf can be obtained by simulating the motion of stochastic particles, i.e. Eq. (10). In other words, real particles are replaced by stochastic particles, which, if the model is suitable, reproduce the same statistics as the real ones. Indeed, in many problems of practical concern, the dimension of the reduced state vector is large and properties of the coefficients $\mathbf{A}$ and $\mathbf{B}$ make the direct solution of the above partial differential equation (PDE), i.e. the Fokker–Planck equation, numerically difficult. Instead, it is more appropriate to calculate $p^r(t; \mathbf{z}^r)$ (or any moment extracted from it) from Eq. (10). Practically, this is done by resorting to a dynamical Monte Carlo method, i.e. by simulating a large number N of independent realisations of $\mathbf{Z}^r(t)$. Then, at each time step, the *discrete* pdf, $p_N^r(t; \mathbf{z}^r)$, can be computed from the set of N independent samples $\{\mathbf{Z}^{r,n}(t)\}$ as

$$p_N^r(t; \mathbf{z}) = \frac{1}{N}\sum_{n=1}^{N} \delta(z_1^r - Z_1^{r,n}(t))\delta(z_2^r - Z_2^{r,n}(t))$$

$$\cdots \delta(z_d^r - Z_d^{r,n}(t)), \quad (12)$$

where d is the dimension of the reduced state vector and n stands for the sample index. The question to be answered is: in what sense does the ensemble $\{\mathbf{Z}^{r,n}(t)\}$, from which the discrete pdf $p_N^r(t; \mathbf{z}^r)$ is extracted, represent the underlying pdf $p^r(t; \mathbf{z}^r)$? The answer to this question can be given in a weak sense, i.e. when *convergence in distribution* is ensured, i.e. $p_N^r(t; \mathbf{z}^r) \rightarrow p^r(t; \mathbf{z}^r)$ when $N \rightarrow \infty$.

A sequence of random variables $\{X^n\}$ converges in distribution to X if and only if, for any bounded continuous function g on $\mathbb{R}$, one has $\langle g(X^n) \rangle \rightarrow \langle g(X) \rangle$ when $n \rightarrow \infty$. In calculations, the mathematical expectation $\langle \cdot \rangle$ is estimated by the ensemble average $\langle \cdot \rangle_N$ over N independent samples. The *law of large numbers* tells us that $\langle g(X) \rangle_N$ is an unbiased estimation of $\langle g(X) \rangle$, i.e. $\langle g(X) \rangle_N \rightarrow \langle g(X) \rangle$ when $N \rightarrow \infty$. Then, according to the *central limit theorem*, the error $\epsilon_N = \langle g(X) \rangle_N - \langle g(X) \rangle$, which is a random variable, converges in distribution to a Gaussian random variable of zero mean and standard

deviation $\sigma[g(X)]/\sqrt{N}$ provided that the variance of $g(X)$, $\sigma^2[g(X)]$, is finite.

In the following, the PDF approach shall always be understood as the numerical solution of the set of SDEs equivalent, in a weak sense as explained above, to the corresponding Fokker–Planck equation.

2.2. Stochastic integrals and calculus

Stochastic differential equations require a strict mathematical treatment. The mathematical specificities of SDEs have far-reaching consequences for the derivation of accurate numerical schemes, cf. Section 5.3. Some basic explanations are now given to highlight the important points that are needed for practical purposes. As a matter of fact, Eq. (10) is just a shorthand notation for

$$Z_i^{\mathrm{r}}(t) = Z_i^{\mathrm{r}}(t_0) + \int_{t_0}^{t} A_i(s, \mathbf{Z}^{\mathrm{r}}(s))\mathrm{d}s + \int_{t_0}^{t} B_{ij}(s, \mathbf{Z}^{\mathrm{r}}(s))\mathrm{d}W_j(s),$$
(13)

where the first integral on the right-hand side (RHS) is a classical Riemann–Stieltjes one. In the second integral, integration is performed with a measure, $\mathrm{d}W(t)$, that has non-conventional properties. The Wiener process can be defined [14] as *the only stochastic process with independent Gaussian increments and continuous trajectories* (an increment, over a time step $\mathrm{d}t$, is defined as $\mathrm{d}W_j(t) = W_j(t + \mathrm{d}t) - W_j(t)$). The Wiener process has the following properties [14,15]:

   (i) the trajectories of $W_j(t)$ are continuous, yet nowhere differentiable (even on small time intervals, $W_j(t)$ fluctuates enormously),

  (ii) each increment is a Gaussian random variable: $\langle \mathrm{d}W_j(t)^{2p+1}\rangle = 0$ for the odd moments, $\langle \mathrm{d}W_j(t)^2\rangle = \mathrm{d}t$ and $\langle \mathrm{d}W_j(t)^{2p}\rangle = o(\mathrm{d}t)$, $\forall p > 1$, for the even moments. Increments over small time steps are stationary and independent, $\langle \mathrm{d}W_j(t)\rangle = 0$, $\forall t$, and $\langle \mathrm{d}W_j(t)\,\mathrm{d}W_j(t')\rangle = 0$ with $t \neq t'$,

 (iii) the trajectories are of unbounded variation in every finite interval.

The last property is the reason why the treatment of stochastic integrals differs from that of classical (Riemann–Stieltjes) ones (the Wiener process is not of finite variation [15]). Without going too deep into mathematical details, property (iii) simply implies that speaking of a stochastic integral without specifying in

what sense it is considered lacks rigour (in this work, all stochastic integrals will be considered in the Itô sense). In classical integration, the limit of the following sum ($\tau_k \in [t_k, t_{k+1}]$)

$$\int_{t_0}^{t} B_{ij}(s, \mathbf{Z}^{\mathrm{r}}(s))\mathrm{d}W_j(s)$$

$$= \lim_{N \to +\infty} \sum_{k=0}^{N} B_{ij}(\tau_k, \mathbf{Z}^{\mathrm{r}}(\tau_k))(W_j(t_{k+1}) - W_j(t_k)), \quad (14)$$

should be independent of the choice of τ_k. This is not true in the above integral because of property (iii).[1] As a consequence, a choice has to be made for the sake of consistency. Two main choices (there exist others) are encountered in the literature, the Itô and the Stratonovich definitions. In the Itô definition, $\tau_k = t_k$ and the following limit is under consideration

$$\lim_{N \to +\infty} \sum_{k=1}^{N} B_{ij}(t_k, \mathbf{Z}^{\mathrm{r}}(t_k))(W_j(t_{k+1}) - W_j(t_k)). \quad (15)$$

This choice has a major drawback, i.e. the rules of ordinary differential calculus are no longer valid. However, this drawback is balanced by *the zero mean and isometry properties*, which are of great help when deriving weak numerical schemes, see Section 5.3.1

$$\left\langle \int_{t_0}^{t_1} X(s)\,\mathrm{d}W(s) \right\rangle = 0,$$

$$\left\langle \int_{t_0}^{t_2} X(s)\,\mathrm{d}W(s) \int_{t_1}^{t_3} Y(s)\,\mathrm{d}W(s) \right\rangle = \int_{t_1}^{t_2} \langle X(s)Y(s)\rangle\,\mathrm{d}s. \quad (16)$$

where $\langle \cdot \rangle$ is the mathematical expectation ($t_0 \leq t_1 \leq t_2 \leq t_3$, $X(t)$ and $Y(t)$ are two stochastic processes). These properties no longer hold in the case of the Stratonovich interpretation but the rules of ordinary differential calculus remain valid. In the Stratonovich interpretation of the stochastic integral, the basic idea is to choose τ_k as the middle point of the intervals, i.e. $2\tau_k = t_k + t_{k+1}$. There are, as a matter of fact, several possible choices, the most commonly

---

[1] Here, the different modes of convergence of the random variable—the stochastic integral—are not dealt with. For further information, see [14,16] for example.

encountered in the mathematical literature being

$$\int_{t_0}^{t} B_{ij}(s, \mathbf{Z}^{\mathrm{r}}(s)) \circ \mathrm{d}W_j(s) = \lim_{N \to +\infty} \sum_{k=0}^{N} \frac{1}{2} [B_{ij}(t_k, \mathbf{Z}^{\mathrm{r}}(t_k)) \\ + B_{ij}(t_{k+1}, \mathbf{Z}^{\mathrm{r}}(t_{k+1}))] \\ \times (W_j(t_{k+1}) - W_j(t_k)), \qquad (17)$$

where o indicates that the stochastic integral is treated in the Stratonovich sense.

The distinction between the Itô and the Stratonovich interpretations is critical, especially when ensuring consistency in the derivation of weak numerical schemes. There is actually an equivalence between the two interpretations. It can be shown [14,16] that Eq. (10) written in the Stratonovich sense

$$\mathrm{d}Z_i^{\mathrm{r}}(t) = A_i(t, \mathbf{Z}^{\mathrm{r}}(t))\mathrm{d}t + B_{ij}(t, \mathbf{Z}^{\mathrm{r}}(t)) \circ \mathrm{d}W_j(t), \qquad (18)$$

is equivalent to the following SDE, written in the Itô sense

$$\mathrm{d}Z_i^{\mathrm{r}}(t) = A_i(t, \mathbf{Z}^{\mathrm{r}}(t))\mathrm{d}t + B_{kj}(t, \mathbf{Z}^{\mathrm{r}}(t)) \\ \times \frac{\partial B_{ij}(t, \mathbf{Z}^{\mathrm{r}}(t))}{\partial z_k} \mathrm{d}t + B_{ij}(t, \mathbf{Z}^{\mathrm{r}}(t))\mathrm{d}W_j(t). \qquad (19)$$

This result can explain why, in some works, computations performed with identical models can lead to contradictory results (the difference between the results is a drift term which is, most of the time, not negligible). Let us stress, once again, that even though the purpose of the present paper is not to present mathematical subtleties, a good understanding of stochastic calculus is needed when deriving weak numerical schemes for SDEs encountered in fluid mechanics.

As in the present work the Itô interpretation is retained, let us briefly present the basics of stochastic calculus. It has been mentioned that in the frame of the Itô interpretation, the rules of ordinary differential calculus are no longer valid. As a matter of fact, this non-trivial consequence can be understood by going back to the properties of the Wiener process. For the second-order moment of the increments of $W(t)$, one has $\langle \mathrm{d}W(t)^2 \rangle = \mathrm{d}t$. This non-trivial result (in classical calculus one would expect a second-order term) is inherent to the nature of the Wiener process (it is a non-differentiable process). As a consequence, the rules of classical calculus must be modified when considering terms of at least order 2. This is the well-known Itô formula. For any stochastic process $\mathbf{X}(t)$ which verifies the following

SDE

$$\mathrm{d}X_i(t) = A_i(t, \mathbf{X}(t))\mathrm{d}t + B_{ij}(t, \mathbf{X}(t))\mathrm{d}W_j(t), \qquad (20)$$

the SDE verified by any smooth function $f(t, \mathbf{X}(t))$ is

$$\mathrm{d}f(t, \mathbf{X}(t)) = \frac{\partial f}{\partial t}(t, \mathbf{X}(t))\mathrm{d}t + \mathrm{d}X_i(t)\frac{\partial f}{\partial x_i}(t, \mathbf{X}(t)) \\ + \frac{1}{2}(\mathbf{B}\mathbf{B}^{\mathrm{T}})_{ij}(t, \mathbf{X}(t))\frac{\partial^2 f}{\partial x_i \partial x_j}(t, \mathbf{X}(t))\mathrm{d}t, \qquad (21)$$

where the last term on the RHS is a new term with respect to classical differential calculus.

The main tools of the general formalism and the basics of stochastic calculus have now been introduced. This short presentation is a brief summary and a reader willing to derive weak numerical schemes for SDEs may refer to Refs. [14,16] for the mathematical background, Ref. [9] for the physical background and more importantly Ref. [17] for the derivation of numerical schemes. A key point, which is not developed here (the main point being that stochastic integrals require a careful treatment), is the derivation of stochastic Taylor series, a tool which is needed when attempting to develop weak numerical schemes for SDEs. There exists a comprehensive book on these techniques, see Ref. [17].

3. PDF models

The purpose of this section is to put forward the system of equations, which is solved in the present mean-field/PDF approach, and to reveal the existing link between the physics of the problem and the tools that were presented in Section 2. Once this is done, attention shall be focused on a central specific theoretical issue: the treatment of the multiscale character of the dynamics of discrete particles, cf. Section 4.

3.1. Derivation of a PDF model

If the trajectories of a pair of particles (a fluid particle and a discrete particle) can be modelled by writing a system of equations given by Eq. (10), two issues must be solved:

(i) what is the dimension of the reduced state vector (what variables should be retained)?
(ii) and what is the form of coefficients (the drift vector and the diffusion matrix)?

A physical answer can be given to issue (i) when there is a separation of (time) scales. Let dt be the

reference timescale at which the physical phenomena are observed. The separation of scales is defined in terms of slow and fast variables. A slow variable is a variable whose integral timescale, T, is much larger than dt and vice-versa for a fast variable whose integral timescale is τ, i.e. $\tau \ll dt \ll T$. The answer comes from the application of ideas known in synergetics, the so-called slaving principle [18]. In this equilibrium hypothesis, the fast variables are assumed to relax 'very rapidly' to their equilibrium values which can be expressed as a function of the values taken by the slow modes. A practical application of this principle is the fast-variable elimination technique, where the fast variables are replaced by models which represent their equilibrium values and usually involve white-noise terms [9]. The fast-variable elimination technique can be used in the derivation of one-point PDF models for single-phase turbulent flows.

In this work, answers to issues (i) and (ii) are given separately for the fluid and the particles in the form of one-point PDF models. In the one-point PDF approach for the fluid (see Section 3.1.1), single-phase turbulence is under consideration whereas in one-point PDF models for the discrete particles, the fluid–particle mixture is under investigation with known properties for the fluid (see Section 3.1.2). The two-point description briefly introduced in Section 2 will be addressed in Section 3.2.

3.1.1. One-point PDF models for single-phase turbulent flows

When the Reynolds number is sufficiently large, for a reference timescale dt in the inertial range ($\tau_\eta \ll dt \ll T_L$, where T_L is the integral Lagrangian timescale and τ_η is the Kolmogorov timescale), the Kolmogorov theory [4] tells us that for Lagrangian statistics, the covariance matrix of velocity increments has the form

$$\langle dU_{f,i}(t) dU_{f,j}(t + dt) \rangle = C_0 \langle \epsilon \rangle dt \, \delta_{ij}, \tag{22}$$

where $\epsilon(t,\mathbf{x})$ is the local instantaneous energy dissipation rate and C_0 is a constant. Eq. (22) implies that one has for the autocorrelation coefficients $R_U = 1 - [(C_0 \, dt)/(2T_L)] \simeq 1$ (velocity) and $R_A = \tau_\eta/T_L \ll 1$ (acceleration) [8]. This shows that for dt in the inertial range, the velocity of a fluid particle, $\mathbf{U}_f(t)$, is a slow variable whereas the acceleration, $\mathbf{A}_f(t)$, is a fast variable. This suggests, according to the slaving principle, that $\mathbf{A}_f(t)$ should be eliminated and replaced by a function of the slow modes, position and velocity, i.e. $\mathbf{Z}^r(t) = \{\mathbf{x}_f(t), \mathbf{U}_f(t)\}$. The Kolmogorov theory gives answers to issues (i) and (ii): the

dimension of the reduced state vector is 2 and the diffusion matrix should be given by $B_{ij} = \sqrt{C_0 \langle \epsilon \rangle} \delta_{ij}$. The use of a SDE is not enforced by Eq. (22) but the linear dependence in time of the covariance matrix is a strong indication. For further justifications concerning the use of SDEs for modelling purposes, see Ref. [8].

Using different arguments, several researchers [13,19] have shown that a Langevin equation model for single-phase turbulence is

$$dU_{f,i}(t) = -\frac{1}{\rho_f} \frac{\partial \langle P \rangle}{\partial x_i} dt + G_{ij}(U_{f,j} - \langle U_j \rangle) dt$$
$$+ \sqrt{C_0 \langle \epsilon \rangle} dW_i(t), \tag{23}$$

where $P(t,\mathbf{x})$ is the local instantaneous pressure field. All mean fields, i.e. $\langle P \rangle$, $\langle U \rangle$ and $\langle \epsilon \rangle$ are evaluated at time t for $\mathbf{x} = \mathbf{x}_f(t)$. The return-to-equilibrium matrix, G_{ij}, depends on mean fields and is usually written $G_{ij} = -\delta_{ij}/T_L + G_{ij}^a$ where T_L is a timescale given by $1/T_L = (1/2 + 3C_0/4)\langle \epsilon \rangle/k$ (k is the turbulent kinetic energy). The anisotropy matrix, G_{ij}^a, also depends on mean fields only and can take different forms [13].

Eq. (23) has two noteworthy properties:

– the coefficients of this SDE depend not only on time and $\mathbf{Z}^r(t)$ (as in Eq. (10)) but also on the expected values of functionals of the state vector. This dependence of the coefficients has important consequences, not only for the mathematical formalism, but also for the numerical algorithm, see Section 5.1. These equations are often called Mac-Kean SDEs in the mathematical literature.
– the model is not self-contained since external fields are needed to compute the drift vector and the diffusion matrix, i.e. the state vector should rather be written $\mathbf{Z}^r(t) = \{\mathbf{x}_f(t), \mathbf{U}_f(t), \varepsilon(t)\}$. In complete models, a specific SDE is written for $\varepsilon(t) = \epsilon(t, \mathbf{x}_f(t))$ and the mean pressure field is given by a Poisson equation, see Ref. [13] for example.

3.1.2. One-point PDF models for the discrete particles

Let us suppose that the discrete particles are moving in a turbulent flow whose mean fields are known (only one-way coupling is considered for the moment, i.e. the presence of particles does not modulate the turbulence). These mean fields are most commonly the two first velocity moments, $\langle \mathbf{U}(t,\mathbf{x}) \rangle$ and $\langle \mathbf{U}(t,\mathbf{x}) \otimes \mathbf{U}(t,\mathbf{x}) \rangle$, and $\langle P(t,\mathbf{x}) \rangle$ and $\langle \epsilon(t,\mathbf{x}) \rangle$.

In the case of discrete particles, the choice of a suitable state vector is more difficult than in the fluid

case since there are no general results indicating a clear separation of scales. However, an extension of Kolmogorov theory [8,20] shows that a linear dependence for the covariance matrix of the increments of the fluid velocity seen, i.e. $\langle \mathrm{d}U_{\mathrm{s},i}(t)\mathrm{d}U_{\mathrm{s},j}(t+\mathrm{d}t)\rangle$, can be obtained under some specific hypotheses, for $\mathrm{d}t$ in the inertial range. Without being a formal proof, this result suggests to include the fluid velocity seen in the state vector, $\mathbf{Z}^{\mathrm{r}}(t)=\{\mathbf{x}_{\mathrm{p}}(t),\mathbf{U}_{\mathrm{p}}(t),\mathbf{U}_{\mathrm{s}}(t)\}$, and to model the increments of $\mathbf{U}_{\mathrm{s}}(t)$ with a Langevin equation. This choice differs from the one inherent to kinetic models, where $\mathbf{Z}^{\mathrm{r}}(t)=\{\mathbf{x}_{\mathrm{p}}(t),\mathbf{U}_{\mathrm{p}}(t)\}$ [12,21]. The existing correspondence between these two approaches has been discussed elsewhere [8]: it can be shown that including the fluid velocity seen in the state vector presents several advantages from the modelling point of view. Furthermore, kinetic models can be retrieved from the Langevin models for $\mathbf{U}_{\mathrm{s}}(t)$ [8]. Issue (i) has now been addressed; the dimension of the state vector is 3. Let us move to issue (ii), i.e. to write an SDE for the increments of $\mathbf{U}_{\mathrm{s}}(t)$.

From a physical point of view, the problem of modelling particle dispersion (i.e. deriving a model for $\mathbf{U}_{\mathrm{s}}(t)$, see Eq. (1)) is more complicated than the diffusion one (fluid particles, cf. Section 3.1.1) since two additional physical mechanisms have to be accounted for: particle inertia characterised by the timescale τ_{p} and external force fields (gravity in our case), Eq. (1). Two main approaches can be found in the literature:

– *Approaches based on paths (trajectories).* A two-step construction is considered: a Lagrangian step and an Eulerian step. The Lagrangian step corresponds to the trajectory, over a time interval $\mathrm{d}t$, of a fluid particle located at time t in the vicinity of the discrete particle (this step is directly given by Eq. (23)). The Eulerian step corresponds to a spatial correction, which gives, from the location of the fluid particle at $t+\mathrm{d}t$, the fluid velocity seen by the discrete particle at time $t+\mathrm{d}t$. This modelling point of view has two major drawbacks: it leads to an artificial decrease of the integral timescale of $\mathbf{U}_{\mathrm{s}}(t)$ (denoted $T^{*}_{\mathrm{L},i}$ in the present paper) and there is no clear separation between the effects of τ_{p} and $\mathbf{g}$ [8].
– *Approaches based on the physical effects* [22]. A two-step construction is also considered by decoupling the two physical mechanisms: the first step corresponds to the effects of τ_{p} in the absence of external forces (in that case $T^{*}_{\mathrm{L},i}$ varies between two limit values, T_{E}—the integral Eulerian timescale—when $\tau_{\mathrm{p}}\rightarrow+\infty$ and T_{L} when $\tau_{\mathrm{p}}\rightarrow 0$). The second step corresponds to the effects of gravity alone which

induces a mean drift and result in a decorrelation of $\mathbf{U}_{\mathrm{s}}(t)$ with respect to $\mathbf{U}_{\mathrm{f}}(t)$. This effect is called the crossing trajectory effect (CTE) and is related to the mean relative velocity $\langle\mathbf{U}_{\mathrm{r}}\rangle=\langle\mathbf{U}_{\mathrm{p}}-\mathbf{U}_{\mathrm{s}}\rangle$.

In the present work, the derivation of a model for $\mathbf{U}_{\mathrm{s}}(t)$ is carried out by resorting to an approach based on the physical effects where the influence of the first step is neglected. This assumption allows us to extend Kolmogorov theory since the increments of the fluid velocity seen are only governed by mean quantities [8].

Assuming, for the sake of simplicity, that the mean drift (the mean relative velocity $\langle\mathbf{U}_{\mathrm{r}}\rangle$) is aligned with one of the coordinate axes (the general case is discussed in Ref. [8]), it can be shown [8,20] that a possible model for the increments of the fluid velocity seen is (the summation convention by repeated indices does not apply to the third and fourth term on the RHS)

$$\mathrm{d}U_{\mathrm{s},i}(t) = -\frac{1}{\rho_{\mathrm{f}}}\frac{\partial\langle P\rangle}{\partial x_i}\mathrm{d}t + (\langle U_{\mathrm{p},j}\rangle - \langle U_j\rangle)\frac{\partial\langle U_i\rangle}{\partial x_j}\mathrm{d}t$$
$$-\frac{1}{T^{*}_{\mathrm{L},i}}(U_{\mathrm{s},i}-\langle U_i\rangle)\mathrm{d}t$$
$$+\sqrt{\langle\epsilon\rangle\left(C_0 b_i\tilde{k}/k + \frac{2}{3}(b_i\tilde{k}/k-1)\right)}\mathrm{d}W_i(t).$$
(24)

The CTE has been modelled by changing the timescale, compared to the fluid case, in the drift term (third term on the RHS) and by adding a mean drift term (second term on the RHS). The timescale is modified according to Csanady's analysis [23]

$$T^{*}_{\mathrm{L},i} = T_{\mathrm{L}}\left(1 + \beta_i^2\frac{|\langle\mathbf{U}_{\mathrm{r}}\rangle|^2}{2k/3}\right)^{-1/2},$$
(25)

where $\beta_1=\beta$, if axis 1 is aligned with the mean drift, with $\beta=T_{\mathrm{L}}/T_{\mathrm{E}}$, and in the transversal directions (axes labelled 2 and 3) $\beta_i=2\beta$. In the diffusion matrix, a new kinetic energy has been introduced

$$\tilde{k} = \frac{3}{2}\frac{\displaystyle\sum_{i=1}^{3} b_i\langle u_i^2\rangle}{\displaystyle\sum_{i=1}^{3} b_i},$$
(26)

where $\mathbf{u}(t,\mathbf{x})=\mathbf{U}(t,\mathbf{x})-\langle\mathbf{U}\rangle$ and $b_i=T_{\mathrm{L}}/T^{*}_{\mathrm{L},i}$.

Eq. (24) has two noteworthy properties:

– it is consistent, by construction, with Eq. (23) when

$\tau_{\mathrm{p}} \to 0$, i.e. when the discrete particles behave like fluid particles,

– it is a Mac-Kean SDE even though the mean fields of the fluid are known (they are given by solving RANS equations). Indeed, it is necessary to compute the mean velocity of the particles $\langle \mathbf{U}_{\mathrm{p}} \rangle$ to calculate not only the mean drift term (second term on the RHS) but also the integral timescale of $\mathbf{U}_{\mathrm{s}}(t)$, T_{L}^* ($\langle \mathbf{U}_{\mathrm{s}} \rangle$ is also needed for the computation of this timescale).

Moreover, it must be emphasised that Eq. (24) is a possible choice among others and that the exact form of a Langevin equation for $\mathbf{U}_{\mathrm{s}}(t)$ still remains an open issue, see for example Refs. [24,25] for models suited for homogeneous turbulence. There exists an alternative to Eq. (24) in the literature [26] where the coefficients are slightly different (the drift vector and the diffusion matrix), the main difference being the form of the mean drift term which is written in terms of instantaneous velocities rather that mean velocities, i.e. $(U_{\mathrm{p},j} - U_{\mathrm{s},j})(\partial \langle U_i \rangle / \partial x_j)$. This difference has been discussed elsewhere [8]. This form of the mean drift term does not change the methodology which is presented in the rest of the paper, but it modifies the structure of the system of SDEs, i.e. $\mathbf{U}_{\mathrm{s}}(t)$ depends explicitly on the particle velocity, $\mathbf{U}_{\mathrm{p}}(t)$. This matter will be discussed in Section 6.

When two-way coupling occurs, i.e. when the mass of particles per unit volume of fluid is sufficient to influence the characteristics of turbulence, Eq. (24) can be supplemented by an acceleration term $\mathbf{A}_{\mathrm{p} \to \mathrm{s}}$ which accounts for the influence of the discrete particles on the statistics of the fluid velocity sampled along the trajectory of a discrete particle, i.e.

$$\mathrm{d}U_{\mathrm{s},i}(t) = A_{\mathrm{s},i}\,\mathrm{d}t + A_{\mathrm{p} \to \mathrm{s},i}\,\mathrm{d}t + B_{\mathrm{s},ij}\,\mathrm{d}W_j(t), \qquad (27)$$

where the drift vector $\mathbf{A}_{\mathrm{s}}$ and the diffusion matrix $\mathbf{B}_{\mathrm{s}}$ are directly given by Eq. (24).

For $\mathbf{A}_{\mathrm{p} \to \mathrm{s}}$, the underlying force corresponds to the exchange of momentum between the fluid and the particles (drag force). The acceleration acting on the fluid element surrounding a discrete particle can be obtained as the sum of all elementary accelerations (due to the neighbouring particles) [8]

$$\mathbf{A}_{\mathrm{p} \to \mathrm{s}} = -\frac{\alpha_{\mathrm{p}} \rho_{\mathrm{p}}}{\alpha_{\mathrm{f}} \rho_{\mathrm{f}}} \frac{\mathbf{U}_{\mathrm{s}} - \mathbf{U}_{\mathrm{p}}}{\tau_{\mathrm{p}}}, \qquad (28)$$

i.e. at the discrete particle location $\mathbf{x}_{\mathrm{p}}$, the elementary acceleration $(\mathbf{U}_{\mathrm{p}} - \mathbf{U}_{\mathrm{s}})/\tau_{\mathrm{p}}$ is multiplied by the probable mass of particles divided by the probable mass of fluid (since the total force is distributed only on the

fluid phase). In Eq. (28), it is implicitly assumed that all particles under consideration have the same acceleration. Moreover, $\alpha_{\mathrm{f}}(t,\mathbf{x})$ and $\alpha_{\mathrm{p}}(t,\mathbf{x})$ represent the probability of presence of fluid and the particles, respectively ($\alpha_{\mathrm{f}} + \alpha_{\mathrm{p}} = 1$).

The complete set of SDEs, which describes the one-point dynamical behaviour of the discrete particles is

$$\begin{cases} \mathrm{d}x_{\mathrm{p},i}(t) = U_{\mathrm{p},i}\,\mathrm{d}t, \\[2mm] \mathrm{d}U_{\mathrm{p},i}(t) = \dfrac{U_{\mathrm{s},i} - U_{\mathrm{p},i}}{\tau_{\mathrm{p}}}\,\mathrm{d}t + g_i\,\mathrm{d}t, \\[2mm] \mathrm{d}U_{\mathrm{s},i}(t) = A_{\mathrm{s},i}\,\mathrm{d}t + A_{\mathrm{p} \to \mathrm{s},i}\,\mathrm{d}t + B_{\mathrm{s},ij}\,\mathrm{d}W_j(t), \end{cases} \qquad (29)$$

where $\mathbf{A}_{\mathrm{s}}$ and $\mathbf{B}_{\mathrm{s}}$ are calculated by resorting to Eqs. (24)–(26). This set of SDEs is under investigation in the present paper and the numerical methods needed to solve it will be discussed in Section 5.

3.2. Mean-field/PDF approach

As specified in Section 1, a mean-field/PDF approach is adopted here for the computation of polydispersed turbulent two-phase flows, i.e. the fluid is described by solving RANS equations whereas the dynamics of the discrete particles are simulated with SDEs. The general formalism presented in Section 2 and the models presented in Sections 3.1.1 and 3.1.2 are sufficient to derive the mean-field/PDF model, which is used in the present work. As a matter of fact, the set of SDEs, from which the pdf of the discrete phase can be extracted, has already been presented, cf. Eqs. (29). Only the derivation of the set of mean-field (RANS) equations for the continuous phase has to be put forward. This derivation can be done using different techniques [27–29]. An interesting technique, which is in line with the tools introduced in Section 2, is to resort to a two-point description. This new approach hardly provides further physical information but it allows both the fluid and the particles to be described under the same formalism. This description is briefly outlined here, supplementary information is given in Appendix A.

3.2.1. PDF models for polydispersed turbulent two-phase flows

The path which is adopted is to gather the preceding results that have just been presented for the time increments of the fluid velocity seen along discrete particle trajectories, Eq. (29), and for the time increments of the fluid velocity along fluid particle trajectories, Eq. (23). The system of SDEs is, however,

supplemented by one term (an acceleration) $\mathbf{A}_{p\to f}$, which reflects the influence of discrete particles on the fluid. The time rate of change of $\mathbf{Z}^r(t) = \{\mathbf{x}_f(t), \mathbf{U}_f(t), \mathbf{x}_p(t), \mathbf{U}_p(t), \mathbf{U}_s(t)\}$ is given by

$$\begin{cases} dx_{f,i}(t) = U_{f,i}\, dt, \\ dU_{f,i}(t) = A_{f,i}\, dt + A_{p\to f,i}\, dt + B_{f,ij}\, dW_j(t), \\ dx_{p,i}(t) = U_{p,i}\, dt, \\ dU_{p,i}(t) = ((U_{s,i} - U_{p,i})/\tau_p)dt + g_i\, dt, \\ dU_{s,i}(t) = A_{s,i}\, dt + A_{p\to s,i}\, dt + B_{s,ij}\, dW_j'(t), \end{cases} \quad (30)$$

where the drift vector $\mathbf{A}_f$ and the diffusion matrix $\mathbf{B}_f$ are given by Eq. (23). The form of $\mathbf{A}_{p\to f}$ is discussed in Appendix A. By assuming that the trajectories of a pair of particles can be obtained in such a way, i.e. Eqs. (30), one should be aware that several assumptions have been made. Further explanations on these assumptions are given in Refs. [8,29].

3.2.2. Mean-field/PDF model

It can be shown that the mean-field (RANS) equations for the fluid can be extracted from Eqs. (30), see Appendix A. A complete set of equations is given in Table 1. Depending on the closures chosen for the return-to-equilibrium matrix, G_{ij}, different RSM equations can be obtained. In practical computations, these mean-field equations are supplemented with a PDE for $\langle \epsilon \rangle$ obtained by the same path (as mentioned in Section 3.1.1, an SDE can be written for $\varepsilon(t)$).

The mean-field/PDF model has now been presented, i.e. the mean field equations for the fluid and the set of SDEs for the discrete particles. In practical computations, the mean fluid properties are computed with classical finite volume techniques whereas the dynamics of the stochastic particles are calculated by resorting to stochastic calculus, i.e. by integrating in time a set of SDEs (weak numerical schemes). The finite volume algorithms are well known and no discussion on these methods is given here. However, some specific issues related to the computation of the source terms in Eqs. (125) and (126) will be addressed in Section 6.1. These source terms are computed from the stochastic particles (the numerical solution of the SDEs) and, as we shall see in Section 5.1, information has to be exchanged between the stochastic particles and the mesh on which the mean-fluid properties are calculated. Before carrying on with the derivation of weak numerical schemes for the set of SDEs, a very important issue has to be put forward: the multiscale character of the model for the discrete phase.

Table 1
Complete mean-field (RANS)/PDF model

Mean-field (RANS) equations for the fluid
Continuity equation:
$$\frac{D}{Dt}(\alpha_f \rho_f) = -\alpha_f \rho_f \frac{\partial \langle U_i \rangle}{\partial x_i} \quad (124)$$

Momentum equation:
$$\frac{D}{Dt}\langle U_i \rangle = -\frac{1}{\rho_f}\frac{\partial \langle P \rangle}{\partial x_i} - \frac{1}{\alpha_f \rho_f}\frac{\partial}{\partial x_j}(\alpha_f \rho_f \langle u_i u_j \rangle) + \chi \langle (U_{p,i} - U_{s,i})/\tau_p \rangle \quad (125)$$

Reynolds stress equation:
$$\frac{D}{Dt}\langle u_i u_j \rangle = -\frac{1}{\alpha_f \rho_f}\frac{\partial}{\partial x_k}(\alpha_f \rho_f \langle u_i u_j u_k \rangle) - \langle u_i u_k \rangle \frac{\partial \langle U_j \rangle}{\partial x_k} - \langle u_j u_k \rangle$$
$$\times \frac{\partial \langle U_i \rangle}{\partial x_k} + G_{jk}\langle u_i u_k \rangle + G_{ik}\langle u_j u_k \rangle + C_0 \langle \epsilon \rangle \delta_{ij}$$
$$+ \chi \left\langle \frac{1}{\tau_p}[(U_{p,i} - U_{s,i})U_{s,j} + (U_{p,j} - U_{s,j})U_{s,i}] \right\rangle \quad (126)$$

with $\quad \dfrac{D}{Dt} = \dfrac{\partial}{\partial t} + \langle U_k \rangle \dfrac{\partial}{\partial x_k} \quad$ and $\quad \chi = \dfrac{\alpha_p \rho_p}{\alpha_f \rho_f}$

SDEs for the discrete particles:
$$\begin{cases} dx_{p,i}(t) = U_{p,i}\, dt, \\ dU_{p,i}(t) = \dfrac{U_{s,i} - U_{p,i}}{\tau_p}\, dt + g_i\, dt, \\ dU_{s,i}(t) = A_{s,i}\, dt + A_{p\to s,i}\, dt + B_{s,ij}\, dW_j(t), \end{cases}$$

$$A_{s,i} = -\frac{1}{\rho_f}\frac{\partial \langle P \rangle}{\partial x_i} + (\langle U_{p,j} \rangle - \langle U_j \rangle)\frac{\partial \langle U_i \rangle}{\partial x_j} - \frac{1}{T_{L,i}^*}(U_{s,i} - \langle U_i \rangle)$$

$$B_{s,i}^2 = \langle \epsilon \rangle \left(C_0 b_i \tilde{k}/k + \frac{2}{3}(b_i \tilde{k}/k - 1) \right)$$

$$A_{p\to s,i} = -\chi(U_{s,i} - U_{p,i})/\tau_p$$

$$T_{L,i}^* = T_L/\sqrt{1 + \beta_i^2 \frac{|\langle \mathbf{U}_r \rangle|^2}{2k/3}}, \qquad b_i = T_L/T_{L,i}^*, \qquad \tilde{k} = \frac{3}{2}\frac{\sum\limits_{i=1}^{3} b_i \langle u_i^2 \rangle}{\sum\limits_{i=1}^{3} b_i}$$

The discussions to come on the multiscale character of the set of SDEs, Section 4, and on the derivation of weak numerical schemes for these equations, Section 5.3, are presented in the case of one-way coupling. This is not due to the limitation of the method but it simply reflects the current status of the present work. Indeed, the methodology, which is presented in Sections 4 and 5, remains valid in the case of two-way

coupling. The presentation of the general algorithm, Section 5.1, and the discussion on issues related to projection and averaging in particle-mesh method, Section 5.2, are put forward in the case of two-way coupling. Specific issues related to two-way coupling will be discussed in Section 6, namely the computations of the source terms in the set of PDEs (RANS equations) and the extension of the material presented in Sections 4 and 5.3 to two-way coupling.

4. Multiscale properties of the SDEs

There are three different timescales describing the dynamics of the discrete particles, cf. Eq. (29): dt, the timescale at which the process is observed, $T_{L,i}^*$ the integral timescale of the fluid velocity seen, $\mathbf{U}_s(t)$, and τ_p the particle relaxation time. Once again, it must be recalled that these SDEs have a physical meaning only in the case where $dt \ll T_{L,i}^*$ and $dt \ll \tau_p$. What happens if one of these conditions or both are not verified? It is in fact possible to show that the system of SDEs converges towards several limit cases, which are consistent with the physics. The mathematical details are not given here, see Ref. [30] for further explanations. Nevertheless, the fast-variable elimination technique is now presented in a simple case in order to help the reader understand the form of two of the limit cases of system (29).

4.1. Fast-variable elimination technique

Let us consider a model problem to illustrate this technique. A good historical example is the treatment of Brownian motion. There exist two points of view to address this problem: Einstein's point of view where only position is retained in the state vector, $\mathbf{Z}(t) = \{\mathbf{x}(t)\}$, and Langevin's approach, where the state vector is composed of position and velocity, $\mathbf{Z}(t) = \{\mathbf{x}(t), \mathbf{U}(t)\}$. Let us consider one-dimensional Brownian motion for the sake of simplicity. Langevin's model reads

$$\begin{cases} dx(t) = U(t)dt, \\ dU(t) = -(U(t)/T)dt + B\,dW(t), \end{cases} \quad (31)$$

this system being valid when $dt \ll T$ (T is the integral timescale of $U(t)$, B is the diffusion coefficient). What happens if this condition is not verified, i.e. when $T \to 0$? The velocity, $U(t)$, becomes a fast variable and, according to the slaving principle, it should be eliminated and its influence should be expressed as a function of the slow modes (here position, $x(t)$). This new description should then be consistent with

Einstein's model, $dx(t) = \sqrt{2D}\,dW(t)$, where D is the diffusion coefficient.

By applying the rules of stochastic calculus (see Section 2.2), one can show that

$$U(t) \simeq BT\eta(t)$$

$$\text{with } \eta(t) = \frac{1}{T}\exp(-t/T)\int_{-\infty}^{t}\exp(s/T)dW(s), \quad (32)$$

where the influence of initial conditions has been neglected (one integrates from $-\infty$). Here, $\eta(t)$ is a Gaussian random variable [15] (it is a stochastic integral of a deterministic function) with $\langle\eta(t)\rangle = 0$ (zero mean property) and (isometry property)

$$\langle\eta(t)\eta(t')\rangle = \frac{1}{2T}\exp(-|t-t'|/T)\xrightarrow[T\to 0]{}\delta(t-t'). \quad (33)$$

Therefore, $\eta(t)$ is a Gaussian white noise and consequently $dW(t) = \eta(t)dt$. The limit system for Langevin's model, Eqs. (31), when $T \to 0$ and BT remains finite, is then given by

$$dx(t) = \sqrt{2D}\,dW(t), \quad (34)$$

where $D = (BT)^2/2$. The velocity, whose integral timescale becomes zero and whose variance becomes infinite (Gaussian white noise), has been eliminated, i.e. the process is observed at a timescale dt large in comparison to the velocity fluctuations (characteristic timescale, T). Its influence is, however, left in the diffusion coefficient of the reduced model (Einstein's model) provided that the product BT remains finite. As we shall see shortly in Section 4.2, this model problem is going to be helpful to understand two of the four limit cases to come.

The above analysis of the model problem has been presented in the *continuous sense*, i.e. when both variables are continuous functions of time. In practical applications, i.e. in numerical computations or in experiments, both variables would have been observed at discrete times. In numerical calculations, one computes the solutions at discrete times where the time step corresponds to the observation timescale dt. In experiments, the variables of interest are measured at a given sampling frequency f and one has $dt = 1/f$. The development of the numerics is slightly anticipated and the limit case $T \to 0$ is now investigated in the *discrete sense*, i.e. when $T \ll \Delta t$. A good understanding of the subtle difference between the continuous case and the discrete case will be helpful in the development of weak numerical schemes to come, see Section 5.3.1.

In the *discrete sense*, the limit case does not correspond to $T \to 0$ but rather to $T \ll \Delta t$. Applying

the rules of stochastic calculus, the solution to system (31) at $t = t_0 + \Delta t$ is given by

$$\begin{cases} x(t) = x(t_0) + U(t_0)T[1 - \exp(-\Delta t/T)] + I_x(t), \\ U(t) = U(t_0)\exp(-\Delta t/T) + I_U(t), \end{cases}$$

(35)

where the stochastic integrals are defined as

$$\begin{cases} I_x(t) = BT \int\limits_{t_0}^{t} dW(s) - BT \exp(-t/T) \int\limits_{t_0}^{t} \exp(s/T) dW(s), \\ I_U(t) = B \exp(-t/T) \int\limits_{t_0}^{t} \exp(s/T) dW(s). \end{cases}$$

(36)

Here, (I_x, I_U) is a vector composed of two dependent, centred (zero mean property, see Section 2.2) Gaussian random variables (Gaussian since I_x and I_U are stochastic integrals of deterministic functions [15]). It can be shown that a centred Gaussian vector can be expressed as the product of two matrices by resorting to the Choleski algorithm: these matrices are the covariance matrix and a vector composed of independent standard Gaussian random variables ($\mathcal{N}(0, 1)$, i.e. zero mean and variance equal to unity). This decomposition is well suited to numerical applications since a set of independent standard Gaussian random variables can easily be generated on computers by using suitable random number generators. By applying the Choleski algorithm to (I_x, I_U), one can write

$$\begin{cases} I_x(t) = (\langle I_x I_U \rangle / \sqrt{\langle I_U^2 \rangle})\xi_U + \sqrt{\langle I_x^2 \rangle - \langle I_x I_U \rangle^2 / \langle I_U^2 \rangle}\xi_x, \\ I_U(t) = \sqrt{\langle I_U^2 \rangle}\xi_U, \end{cases}$$

(37)

where ξ_x and ξ_U are two independent standard Gaussian random variables. The components of the covariance matrix are given by

$$\begin{cases} \langle I_x^2 \rangle = (BT)^2\{\Delta t - T[1 - \exp(-\Delta t/T)][3 - \exp(-\Delta t/T)]/2\}, \\ \langle I_U^2 \rangle = B^2 T[1 - \exp(-2\Delta t/T)]/2, \\ \langle I_x I_U \rangle = \{BT[1 - \exp(-\Delta t/T)]\}^2/2. \end{cases}$$

(38)

Therefore, in the *discrete sense*, the limit system to Langevin's model becomes

$$\begin{cases} x(t) = x(t_0) + U(t_0)T + BT\left(\sqrt{\dfrac{T}{2}}\xi_U + \sqrt{\Delta t}\xi_x\right), \\ U(t) = \sqrt{\dfrac{B^2 T}{2}}\xi_U. \end{cases}$$

(39)

In the discrete sense, the velocity $U(t)$ does not 'disappear' (in the continuous case, it becomes Gaussian white noise). This result is physically sound since the velocity is only observed at time steps, which are large compared to its memory (integral timescale). Finally, the above results are consistent with the observation of Einstein, i.e. for long diffusion times, one has $\langle x(t)^2 \rangle \sim (BT)^2 t$.

4.2. Limit cases

From now on, the summation rule by repeating indices is dropped to avoid confusion, as in Eq. (24) for example. The system of SDEs describing the dynamics of the discrete particles reads (*from now on, $B_{s,ij}$ is denoted B_{ij} for the sake of simplicity*)

$$\begin{cases} dx_{p,i}(t) = U_{p,i}\, dt, \\ dU_{p,i}(t) = \dfrac{1}{\tau_p}(U_{s,i} - U_{p,i})dt + \mathcal{A}_i\, dt, \\ dU_{s,i}(t) = -\dfrac{1}{T_{L,i}^*} U_{s,i}\, dt + C_i\, dt + \sum_j B_{ij}\, dW_j(t), \end{cases}$$

(40)

where C_i is a term that includes all mean contributions: the mean pressure gradient, $-(\partial\langle P\rangle/\partial x_i)/\rho_f$, the mean drift term, $(\langle U_{p,j}\rangle - \langle U_j\rangle)(\partial\langle U_i\rangle/\partial x_j)$, and the mean part of the return-to-equilibrium term, $\langle U_i\rangle/T_{L,i}^*$. As explained above, two-way coupling is left out of the present analysis. $\mathcal{A}_i$ is an acceleration (gravity in the present work, but it can be extended for practical reasons to the case of other external force fields). Once again, system (40) has a physical meaning only in the case where $dt \ll T_{L,i}^*$ and $dt \ll \tau_p$. When these conditions are not satisfied, it is possible to show that in the *continuous sense* (time and all coefficients are continuous functions which can go to zero), the system converges towards several limit systems [30].

Case 1. When $\tau_p \to 0$, the particles behave as fluid particles and one has

$$
\text{system (40)} \xrightarrow{[\tau_p \to 0]}
\begin{cases}
dx_{p,i}(t) = U_{p,i}\, dt, \\[2mm]
U_{p,i}(t) = U_{s,i}(t), \\[2mm]
dU_{s,i}(t) = -\dfrac{1}{\rho_f}\dfrac{\partial \langle P \rangle}{\partial x_i}\, dt \\[2mm]
\qquad\qquad -\dfrac{1}{T_L}(U_{s,i} - \langle U_i \rangle)dt \\[2mm]
\qquad\qquad +\sqrt{C_0 \langle \varepsilon \rangle}\, dW_i(t),
\end{cases}
\tag{41}
$$

i.e. the model is consistent with a known turbulent fluid PDF model [11] as explained in Section 3.1.2. This shows that the model is a coherent generalisation of the fluid one, which can be recovered as a limit case.

Case 2. When $T_{L,i}^* \to 0$ and $B_{ij}T_{L,i}^* \to \text{cst}$, the fluid velocity seen becomes a fast variable. It is then eliminated and one can write

$$
\text{system (40)} \xrightarrow[T_{L,i}^* \to 0]{(B_{ij}T_{L,i}^* \to \text{cst})}
\begin{cases}
dx_{p,i}(t) = U_{p,i}dt, \\[2mm]
dU_{p,i}(t) = \dfrac{1}{\tau_p}(\langle U_i \rangle \\[2mm]
\qquad\qquad - U_{p,i})dt + \mathscr{A}_i dt \\[2mm]
\qquad\qquad + \displaystyle\sum_j \dfrac{B_{ij}T_{L,i}^*}{\tau_p}dW_j(t).
\end{cases}
\tag{42}
$$

This result can be understood from the model problem of Section 4.1. $U_s(t)$ has been eliminated but its influence is left in the diffusion coefficient $B_{ij}T_{L,i}^*/\tau_p$. In this case, the equations are equivalent to a Fokker–Planck model for particles of significant inertia.

Case 3. When τ_p, $T_{L,i}^* \to 0$ and at the same time $B_{ij}T_{L,i}^* \to \text{cst}$, the fluid velocity seen becomes a fast variable and the discrete particles behave as fluid particles. It can be shown that

$$
\text{system (40)} \xrightarrow[\tau_p, T_{L,i}^* \to 0]{(B_{ij}T_{L,i}^* \to \text{cst})}
\begin{cases}
dx_{p,i}(t) = \langle U_i \rangle dt + \mathscr{A}_i\, dt \\[2mm]
\qquad\qquad + \sum_j (B_{ij}T_{L,i}^*)dW_j(t).
\end{cases}
\tag{43}
$$

We retrieve a pure diffusive behaviour, i.e. the equations of *Brownian motion*, cf. Section 4.1.

Case 4. At last, when $T_{L,i}^* \to 0$ with no condition on $B_{ij}T_{L,i}^*$, the velocity of the fluid seen is no longer random and the system becomes deterministic. The flow is laminar and it can be proven that

$$
\text{system (40)} \xrightarrow[T_{L,i}^* \to 0]{}
\begin{cases}
dx_{p,i}(t) = U_{p,i}dt, \\[2mm]
dU_{p,i}(t) = \dfrac{1}{\tau_p}(\langle U_i \rangle - U_{p,i})dt + \mathscr{A}_i dt, \\[2mm]
U_{s,i}(t) = \langle U_i \rangle.
\end{cases}
\tag{44}
$$

Limit cases 1–3 reflect the multiscale character of the problem. When the timescales go to zero (with a condition on their products with the coefficients of the diffusion matrix), a hierarchy of stochastic differential systems is obtained. Moreover, the elimination of the fast variables (the velocities $U_p(t)$ and $U_s(t)$) does not mean that these variables do not (physically) exist anymore: they simply become Gaussian white noise. As we shall see in Section 5.3.1, both $U_p(t)$ and $U_s(t)$ become independent Gaussian random variables, in the discrete sense, in limit case (3) (in limit case (2), only $U_s(t)$ becomes a Gaussian random variable). These results are in line with the previous model problem, cf. Eq. (39) in Section 4.1.

The existence of limit systems is a key point in the development of weak numerical schemes to integrate in time the set of SDEs describing the dynamics of discrete particles, i.e. Eqs. (40). As we shall see in Section 5, in numerical computations, dt the observation timescale of the process, is the time step. A suitable weak numerical scheme should therefore be consistent with all limit cases since, as we shall see, it is not possible to control the time step to enforce the conditions necessary for the validity of Eqs. (40). Before we carry on to the time integration of Eqs. (40), let us give a general overview of the numerical procedure which is needed to solve the whole set of equations (the mean-field (RANS) equations for the fluid and the SDEs for the discrete particles).

5. Numerical approach

The mean-field/PDF model used in the present paper for practical computations has now been given, see Table 1. It consists of a set of PDEs describing the dynamics of mean-fluid quantities and a set of SDEs from which the joint pdf of the variables of interest for the discrete particles can be extracted. In this approach, the numerical solution is obtained by resorting to a hybrid method, where the mean-fluid properties are

computed by solving the mean-field (RANS) equations with a classical finite volume procedure whereas the local instantaneous properties of the discrete particles are determined by solving the set of SDEs, Eqs. (29). Therefore, the mean fluid properties are computed on a mesh whereas the statistics of the discrete phase are calculated from particles moving in the computational domain.

A closer look at the equation system presented in Table 1 shows that the set of equations has the following properties:

(i) in the set of PDEs from which the mean-fluid properties are computed, mean fields involving discrete particles' properties are needed in order to compute the source terms, see Eqs. (125) and (126).

(ii) in the set of SDEs, the knowledge of statistical moments (for the fluid and the discrete particles), such as mean values and variances, at the locations of the stochastic particles, is required in order to compute the time evolution of discrete particle properties and, thus, of the statistics derived from them. Indeed, from a mathematical standpoint, the set of SDEs can formally be written as (from now on, the notation is slightly changed: $\mathbf{Z}(t)$ denotes the state vector for the discrete particles, i.e. the superscript r is dropped for the sake of clarity)

$$d\mathbf{Z}(t) = \mathbf{A}(t, \mathbf{Z}(t), p(t; \mathbf{z}), \mathbf{Y}(t))dt$$
$$+ \sigma(t, \mathbf{Z}(t), p(t; \mathbf{z}), \mathbf{Y}(t))d\mathbf{W}(t), \qquad (45)$$

where $p(t;\mathbf{z})$ stands for the pdf of $\mathbf{Z}(t)$ and $\mathbf{Y}(t)$ represents external mean fields, i.e. the fluid mean fields defined at particle locations. For each time t, $p(t;\mathbf{z})$ has to be calculated in order to compute the coefficients of the SDE: in the present approach, the pdf (or any necessary moment extracted from it) is computed out of all stochastic particles that are tracked (all values taken by $\mathbf{Z}(t)$), cf. Section 2.1. Thus, as mentioned in Sections 3.1.1 and 3.1.2, a kind of integro-differential equation, no longer local in the space of $\mathbf{Z}(t)$, is obtained; it is called a Mac-Kean SDE and is inherently difficult to solve [31,32]. In other words, we are dealing with a system where particles interact weakly (or indirectly) through the mean fields that they create (it is the leading idea of one-point PDF models).

As far as property (ii) is concerned, in practice, probabilistic expectations of particle properties at a given point are approximated by spatial averages over nearby particles, i.e. the statistics extracted from the stochastic particles (which are needed to compute the coefficients of system (29)) are not calculated for each particle (this would cost too much CPU time) but are evaluated at each cell centre of the mesh (generated for the solution of the set of PDEs) following a given spatial average (*averaging operator*). These moments can then be evaluated for each particle by interpolation or projection (*projection operator*). The same projection operator is used to compute the statistics of the fluid at the locations of the stochastic particles. The source terms in the PDEs, cf. property (i), are directly computed by resorting to the averaged particle quantities.

This is the principle of particle-mesh methods: exchange data between particles and mesh points. In the present work, the main advantage of such methods is of course the reduction of CPU time but the use of projection and averaging operators has some drawbacks, i.e. it creates additional numerical errors and, in the general algorithm, each particle has to be located in the mesh.

5.1. Particle-mesh methods

Historically, particle-mesh methods have been widely used in other areas of physics like the dynamics of plasmas, astrophysical simulations, electrostatics, etc. [33]. In these applications, the system of equations, which is solved, is deterministic and the mesh is uniform, most of the time for unbounded domains or bounded domains with periodic boundary conditions. These models are often referred to as the particle-in-cell (PIC) approach [33–35].

In fluid dynamics, apart from calculations of dispersed two-phase flows, particle-mesh methods are mainly encountered in computations of single-phase turbulence with stand-alone particle models [36–38], in hybrid particle/field models [39], in calculations of turbulent reactive flows with PDF methods [10], and in numerical simulations of non-Newtonian polymeric fluids [31]. In these applications, the situation is different from the classical PIC approach. Indeed, the systems of equations are stochastic and the domains are bounded with various boundary conditions. Let us present the main lines of the particle-mesh algorithm used in the present work. It is implemented in the ESTET software [40].

5.1.1. General algorithm

Let $\{\mathbf{Y}^{[\mathbf{x}]}\}$ stand for the set of fluid mean fields at the different mesh points and let $\{\mathbf{Y}^{(N)}\}$ be the fluid mean fields interpolated at particle locations. Let $\{\mathbf{Z}^{(N)}\}$ denote the set of variables attached to the stochastic particles and $\{\mathbf{Z}^{[\mathbf{x}]}\}$ the set of statistics, defined at cell centres, extracted from $\{\mathbf{Z}^{(N)}\}$. Time is discretised with a constant time step $\Delta t = t_{n+1} - t_n$ and space with a uniform mesh of cell size Δx.

The first step (operator F) of the algorithm is to solve the PDEs describing the fluid

$$\{\mathbf{Y}^{[\mathbf{x}]}\}(t_n) \text{ and } \{\mathbf{Z}^{[\mathbf{x}]}\}(t_n) \xrightarrow{F} \{\mathbf{Y}^{[\mathbf{x}]}\}(t_{n+1}). \tag{46}$$

The F operator corresponds to a classical finite volume RANS solver and it gives the evolution in time of the statistical moments of the fluid (the particle properties are needed to compute source terms when two-way coupling is accounted for).

The second step (projection, operator P) consists of calculating mean-particle properties and mean-fluid properties at particle locations

$$\{\mathbf{Z}^{[\mathbf{x}]}\}(t_n) \text{ and } \{\mathbf{Y}^{[\mathbf{x}]}\}(t_n) \xrightarrow{P} \{\mathbf{Z}^{(N)}\}(t_n) \text{ and } \{\mathbf{Y}^{(N)}\}(t_n). \tag{47}$$

Then, the stochastic differential system can be integrated in time (operator T)

$$\{\mathbf{Z}^{(N)}\}(t_n) \text{ and } \{\mathbf{Y}^{(N)}\}(t_n) \xrightarrow{T} \{\mathbf{Z}^{(N)}\}(t_{n+1}). \tag{48}$$

Finally, from the new computed set of variables, at particle locations, new statistical moments are evaluated at cell centres

$$\{\mathbf{Z}^{(N)}\}(t_{n+1}) \xrightarrow{A} \{\mathbf{Z}^{[\mathbf{x}]}\}(t_{n+1}), \tag{49}$$

and so on. The general algorithm is therefore defined by iterating the four operators, $F \rightarrow P \rightarrow T \rightarrow A$. The purpose of the present section, Section 5, is to discuss different implementation aspects of the general algorithm and more especially issues related to:

  (i) the specificity of the treatment of averaging and projection operators, Section 5.2,
 (ii) the time integration of the SDEs (operator T), i.e. the determination of a suitable weak numerical scheme for system (29) which is consistent with the multiscale character of the physics (asymptotic cases), Section 5.3.

Before discussing these issues, some last clarifications are given on the nature of the numerical errors generated by the particle-mesh algorithm sketched above.

5.1.2. Numerical errors in particle-mesh methods

The numerical particle-mesh solution of evolution equations like Eq. (45) involves several kinds of errors. These errors have been described in the context of PDF methods for turbulent reactive flows [37,41]. The overall error of the PDF computation ($P \rightarrow T \rightarrow A$) can be separated into a deterministic and a random part, the former involving the bias, spatial and temporal discretisation errors. Numerical errors occur due to:

  (i) spatial discretisation, represented by a typical mesh size Δx,
 (ii) finite temporal resolution, determined by the time step Δt,
(iii) the use of a finite number of particles, both in the whole domain (N) and per cell (N_{pc}); these are further decomposed into the statistical error (of zero average) and the bias.

The spatial discretisation error (i) is akin to the classical error in numerical methods for solving PDEs and depends on the mesh size. In the present approach (Mac-Kean SDEs), it is inherent to the use of projection and averaging operators (A and P). This numerical error does not occur when the coefficients of the SDEs depend only on local values of the state vector. This is the case, for instance, in numerical computations of stand-alone PDF methods for homogeneous turbulence [37]. To date, only Xu and Pope [41] have addressed this issue for non-linear SDEs and have found some characteristics of the error for an infinite number of particles per cell. Note that the spatial discretisation error also occurs in grid-free methods, such as SPH [42], and is, in this case, directly related to the smoothing parameter (kernel size).

The temporal discretisation error (ii) is basically the same as in any numerical method for solving the time evolution of the solutions to deterministic ODEs or PDEs. Numerical schemes for the SDEs (operator T) must be developed and analysed with care due to the specificity of stochastic calculus, cf. Section 5.3.

The statistical error, which is inherent to any Monte Carlo method, is due to the use of a finite number of particles per cell (samples) to compute the statistics and is proportional to the inverse of the square root of N, according to the central limit theorem. In specific applications (e.g. [36]), the coefficient of proportionality can be reduced considerably when appropriate variance reduction techniques (VRT) are applied [37,43].

The bias is the difference between the mean value of a quantity for a finite number (N) of particles and the mean value for infinitely many particles (all other parameters being unchanged), i.e. for any random variable Z

$$B_Z(N) = \langle\langle Z \rangle_N\rangle - \langle Z \rangle \quad \text{with} \; \langle Z \rangle_N = \frac{1}{N}\sum_{i=1}^{N} Z^i, \qquad (50)$$

where Z^i stands for different sample values of Z. The bias is thus a deterministic error, important for non-linear stochastic models [37,41]. The issue is worth explaining with a simple example. Consider a random variable X with a certain law (pdf), say standard Gaussian, i.e. $\langle X \rangle = 0$ and $\langle X^2 \rangle = 1$. We note $X \in \mathcal{N}(0,1)$. For the mean value $\langle X \rangle_N$ computed out of N samples, the central limit theorem gives (for N sufficiently large)

$$\langle X \rangle_N = \langle X \rangle_\infty + C\xi/\sqrt{N}, \qquad (51)$$

where $\xi \in \mathcal{N}(0,1)$ and C is a proportionality constant for the statistical error; obviously $\langle X \rangle_\infty = \langle X \rangle = 0$. Consider next a function $Y = \langle X \rangle^2$. Now $Y_\infty = 0$, but for a finite number N of samples $Y_N = C^2\xi^2/N$ and after averaging $\langle Y_N \rangle = C^2/N$. The bias $B_Y(N) = \langle Y_N \rangle - Y_\infty$ is thus proportional to N^{-1}. In more general terms [37], for $Y = g(\langle X \rangle)$ we have $Y_\infty = g(\langle X \rangle_\infty)$, and the development into a Taylor series, accounting for Eq. (51), yields

$$Y_N = g(\langle X \rangle_N) = g\left(\langle X \rangle_\infty + \frac{C}{\sqrt{N}}\xi\right)$$

$$= Y_\infty + \frac{Cg'}{\sqrt{N}}\xi + \frac{C^2 g''}{2N}\xi^2 + \mathcal{O}\left(\frac{g'''}{N^{3/2}}\right). \qquad (52)$$

After averaging the above, the bias is computed as

$$B_Y(N) = C^2 \frac{g''}{2N} + \mathcal{O}\left(\frac{g'''}{N^{3/2}}\right). \qquad (53)$$

It depends on the local second derivative of g and is proportional to N^{-1}. In a general case of random fields, the bias interplays with the spatial error because of the kernel estimation, which is applied to compute averages [13,44].

5.2. Averaging and projection operators

We recall that, in the numerical solution process of Eq. (45), moments of $\mathbf{Z}(t)$, like $\langle \mathbf{Z} \rangle$ and $\langle Z_i Z_j \rangle$ need to be extracted from the particle data. A correct computation of these quantities is crucial for the overall numerical solution, since the moments are put back into the SDE and serve to advance the particle properties to the next

time step of the simulation, see Section 5.1.1. These ingredients of the algorithm, i.e. the computation of mean fields (or averaging) and their interpolation at (or projection to) particle locations are well known in the PIC approach [33–35]. For those particle models (deterministic equations on a regular mesh), optimum averaging and projection schemes have been worked out. In the present case, a new problem is addressed: stochastic models with boundary conditions typical of fluid mechanics. Consequently, some new important numerical features appear.

(i) The first specificity is related to the computation of statistics: in most applications, we not only need the mean values, but also (at least) second-order moments present in the evolution equations. These moments are usually position-dependent (non-homogeneous in space).

(ii) A second specificity here (often present in applications in fluid mechanics) is that the computational domain is bounded and the associated mesh is non-uniform; as argued further, adequate boundary conditions may affect the computation of statistics.

Here, attention is focused specifically on the errors due to the exchange of information between particles and the mesh, i.e. how mean fields (usually the first and second-order moments) are computed and projected at particle locations, the main issue being to investigate whether classical techniques already used in particle simulations are also suitable for our present particle-mesh problem.

5.2.1. Averaging operators, weighting functions

In order to introduce the numerical issues related to the exchange of information between the particles and the mesh, let us first discuss the difference between the ensemble mean (expected value) and the spatial average. For the case of a deterministic function $\Phi(\mathbf{x})$, the spatial average $\langle \cdot \rangle_\Delta$ (with a characteristic smoothing length Δ) in the cell centred at $\mathbf{x}^{[i]}$, $i = 1,\dots,I$, can be thought of as the integral

$$\langle \Phi^{[i]} \rangle_\Delta = \int \Phi(\mathbf{x})\tilde{w}(\mathbf{x} - \mathbf{x}^{[i]})\mathrm{d}\mathbf{x}, \qquad (54)$$

where $\Phi^{[i]} = \Phi(\mathbf{x}^{[i]})$ and $\tilde{w}$ is a given weighting function (smoothing kernel) satisfying $\int \tilde{w}(\mathbf{x})\mathrm{d}\mathbf{x} = 1$. For a random field $\Phi(t,\mathbf{x})$ with a pdf $f_\Phi(t,\mathbf{x};\Psi)$, the mean at $\mathbf{x}^{[i]}$ corresponds to the probabilistic expectation, i.e.

$$\langle \Phi^{[i]} \rangle = \int_{-\infty}^{+\infty} \Psi f_\Phi(t, \mathbf{x}^{[i]}; \Psi) \mathrm{d}\Psi, \qquad (55)$$

where Ψ is a sample-space variable of Φ. In classical Monte Carlo methods, the pdf $f_\Phi(t, \mathbf{x}^{[i]}; \Psi)$ at each point $\mathbf{x}^{[i]}$ is approximated by using a number N of independent samples of the random variable, say $\Phi^{(n)}$, $n = 1, \dots, N$. In other words, a set of variables $\Phi^{(n)}$ is attached to every particle, located at $\mathbf{x}^{(n)}$ in the computational domain (NB, the superscript convention helps to distinguish between particles $^{(n)}$ and cell-related quantities $^{[i]}$).

The mathematical expectation, $\langle \Phi^{[i]} \rangle$ in Eq. (55), is computed *exactly* at $\mathbf{x}^{[i]}$, whereas $\langle \Phi^{[i]} \rangle_\Delta$ in Eq. (54) represents the spatial average *centred* on $\mathbf{x}^{[i]}$; both are equal in the spatially homogeneous case only. However, space-dependent moments cannot be calculated exactly from a Monte Carlo estimation, given a finite number of particles used in the simulation. In practice, under a local homogeneity assumption, expectations $\langle \Phi^{[i]} \rangle$ are approximated by (local) spatial averages $\langle \Phi^{[i]} \rangle_{N,\Delta}$, based on a discrete particle set:

$$\langle \Phi^{[i]} \rangle \simeq \langle \Phi^{[i]} \rangle_{N,\Delta} = \sum_{n=1}^{N} \Phi^{(n)} w(\mathbf{x}^{(n)} - \mathbf{x}^{[i]}). \qquad (56)$$

This expression, also known as kernel estimate [13], is derived from Eq. (54) as a quadrature formula; the weights w are the discrete equivalents of $\tilde{w}$, $\sum_{n=1}^{N} w(\mathbf{x}^{(n)} - \mathbf{x}^{[i]}) = 1$.

A generalisation of the above discussion to centred moments of any order is straightforward. Here, the explicit formulation is given for the variance because of its importance in further considerations, cf. Sections 5.2.2–5.2.4. By analogy to Eq. (55), the local value (at $\mathbf{x}^{[i]}$) of the variance σ_Φ^2 of the random field $\Phi(t, \mathbf{x})$ is

$$(\sigma_\Phi^2)^{[i]} = \int_{-\infty}^{+\infty} (\Psi - \langle \Phi^{[i]} \rangle)^2 f_\Phi(t; \mathbf{x}^{[i]}, \Psi) \mathrm{d}\Psi. \qquad (57)$$

As an extension of formula (56) for the mean value, the expression for the variance σ_Φ^2 with the use of spatial averaging becomes

$$(\sigma_\Phi^2)^{[i]} \simeq (\sigma_\Phi^2)_{N,\Delta}^{[i]} = \sum_{n=1}^{N} (\Phi^{(n)} - \langle \Phi \rangle)^2 w(\mathbf{x}^{(n)} - \mathbf{x}^{[i]}),$$

$$(58)$$

where $\langle \Phi \rangle$ stands either for a cell average $\langle \Phi^{[i]} \rangle$ or is interpolated at $\mathbf{x}^{(n)}$. From the algorithmic standpoint,

Eq. (58) has some disadvantages. Firstly, the double pass over particles (the mean has to be computed in advance) results in some computational overhead. Secondly and more important, for first-order weighting functions (cf. Sections 5.2.2 and 5.2.3), it implies a risky extrapolation of mean fields at the locations outside the computational domain. We propose to get around the difficulty by computing the central moments directly from the standard (non-centred) moments; for example, the variance of a random variable Q satisfies $\langle (Q - \langle Q \rangle)^2 \rangle = \langle Q^2 \rangle - \langle Q \rangle^2$. Yet, some precaution is needed since such an expression for the variance cannot be guaranteed to remain always non-negative because of round-off errors.

As far as the choice of the weighting function is concerned, two methods are widely used and are under investigation in the following: the NGP (Nearest-Grid-Point) and CIC (Cloud-in-Cell) methods. They correspond to weighting functions of zero (constant) and first (linear) order, respectively. These methods have been thoroughly discussed [33], as mentioned above, for deterministic systems solved on uniform meshes and in the particular case of unbounded domains or bounded domains with periodic boundary conditions. In the present work, we address the problem for the numerical solutions of specific stochastic systems (Mac-Kean SDEs) on non-uniform meshes for bounded domains and non-periodic boundary conditions.

In the NGP method, particle properties are associated with the centre of the cell containing the particle (for a uniform mesh, it is the grid point nearest to the particle, hence the name), and the weighting function is top-hat (or piecewise constant, Fig. 1a), i.e. $w(\mathbf{x}^{(n)} - \mathbf{x}^{[i]}) = 1/N_{\mathrm{pc}}^i$ for particle n in cell i and 0 otherwise (N_{pc}^i is the number of particles in cell i). The NGP average is thus found from the sum over all N_{pc}^i particles in a given cell i

$$\langle \Phi^{[i]} \rangle = \frac{1}{N_{\mathrm{pc}}^i} \sum_{n=1}^{N_{\mathrm{pc}}^i} \Phi^{(n)}. \qquad (59)$$

In the CIC method, for a uniform mesh in D spatial dimensions, the weighting function is piecewise-linear (Fig. 1b)

$$w(\mathbf{x}) = \prod_{j=1}^{D} \frac{1}{\Delta_j} \max\{1 - |x_j|/\Delta_j, 0\}, \qquad (60)$$

where Δ_j is the width of the cell in direction j. The particle is thus regarded not as a single point but rather as a linear distribution of properties: a cloud centred at $\mathbf{x}^{(n)}$, with a width of $2\Delta_j$. The CIC method is less local
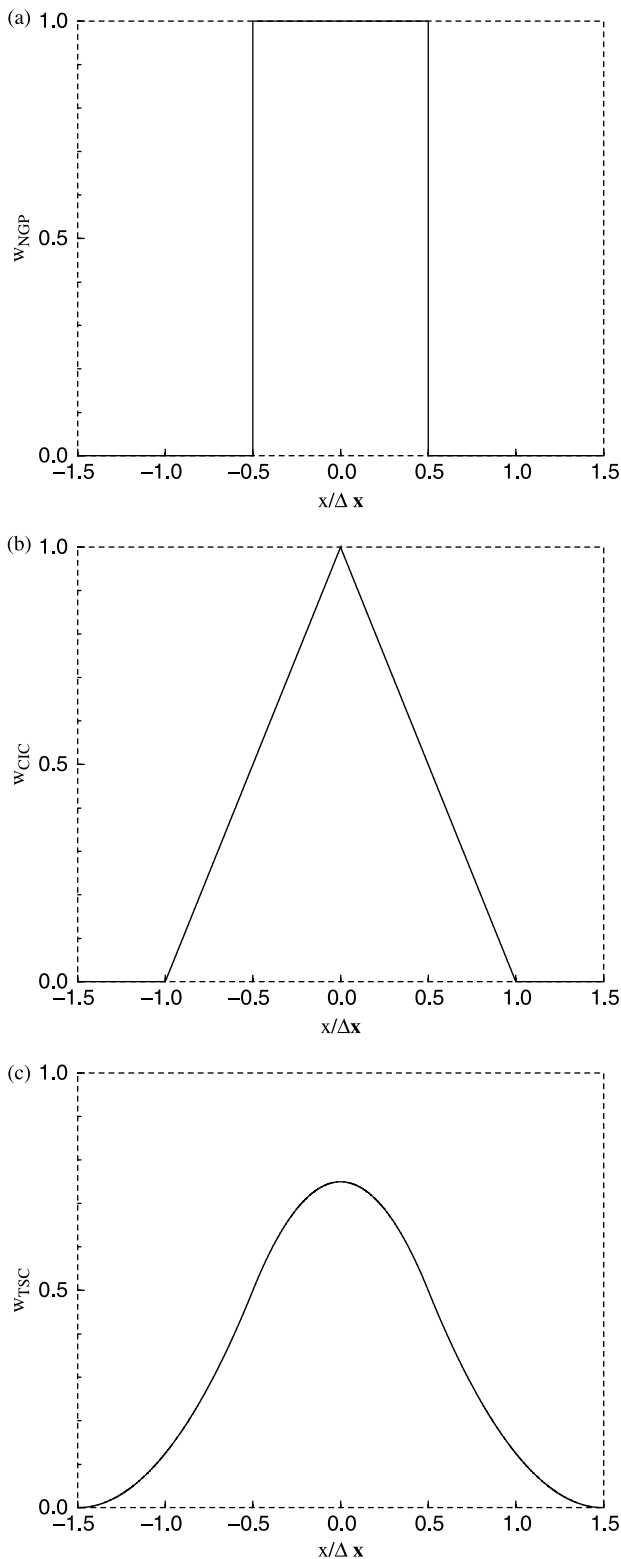
Fig. 1. Weighting functions of different orders used for averaging: (a) top hat (constant) or Nearest-Grid-Point (NGP); (b) linear or Cloud-In-Cell (CIC); (c) piecewise quadratic.

than NGP: the average at a given cell centre is computed not only from the particles located in this very cell, but also from those in the neighbouring cells.

Higher order, but less local, weighting functions can be used, for instance a piecewise-quadratic polynomial (Fig. 1c) or a cubic spline as in Smoothed Particle Hydrodynamics (SPH) [45]; quartic and quintic splines as well as Gaussian kernels are also quite popular [42,46]. An alternative to kernel estimators, cf. Eq. (56) is offered by somewhat more costly (especially in 2D/3D) formulae with least-squares or local least-squares approximations, as well as cross-validated splines [10,44].

The projection of averaged (cell) values onto the particle locations is an interpolation procedure, in a sense akin to averaging, Eq. (56), with $^{(n)}$ and $^{[i]}$ replaced by each other (it is the reverse operation). The consistency of averaging and projection steps has been a serious concern in PIC applications. Indeed, it has been demonstrated (see [33], Section 5.2.4) that, in the case of a system of charged particles moving in an electric field generated by themselves, unphysical forces may appear if the averaging scheme is not of order equal to (acceptably also higher than) the projection scheme. Those authors have also stated that the CIC method performs better than NGP.

5.2.2. CIC statistics on a non-uniform mesh

Although the usual presentation of CIC formulae is made for a uniform mesh, in typical applications of the present mean-field/PDF approach for polydispersed turbulent two-phase flows, a non-uniform mesh may be of advantage (wall-bounded flows). A number of difficulties arise in this generalisation, depending whether the mean density computed from the particle masses or the mean of a variable attached to the particles is sought. For the sake of simplicity, we will illustrate the issue in a 1D setting; extension to 2D and 3D is straightforward through the Cartesian products.

First, consider the computation of fluid density. A particle located at $x^{(n)}$ where $x^{[i]} \leq x^{(n)} < x^{[i+1]}$, cf. Fig. 2(a), will contribute to the mean density at $x^{[i]}$ and $x^{[i+1]}$. Here, we treat the particle as a 'cloud' (or a linear distribution of mass) centred at $x^{(n)}$ and stretched on the interval $\delta x_i = \min(\Delta x_i, \Delta x_{i+1})$. With this assumption, the particle mass is contained between $x_0^{[i-1]}$ and $x_0^{[i+1]}$ and does not contribute to other cell averages (three possible locations of a 'stretched' particle are shown in Fig. 2a). The fraction of the cloud that belongs to the cell $[i+1]$, $R_x = (x^{(n)} + \delta x_i/2 - x_0^{[i]})/\delta x_i$, adds to the average at $x^{[i+1]}$, whereas $(1 - R_x)$ adds to the cell average at $x^{[i]}$. For a boundary cell, the whole mass of
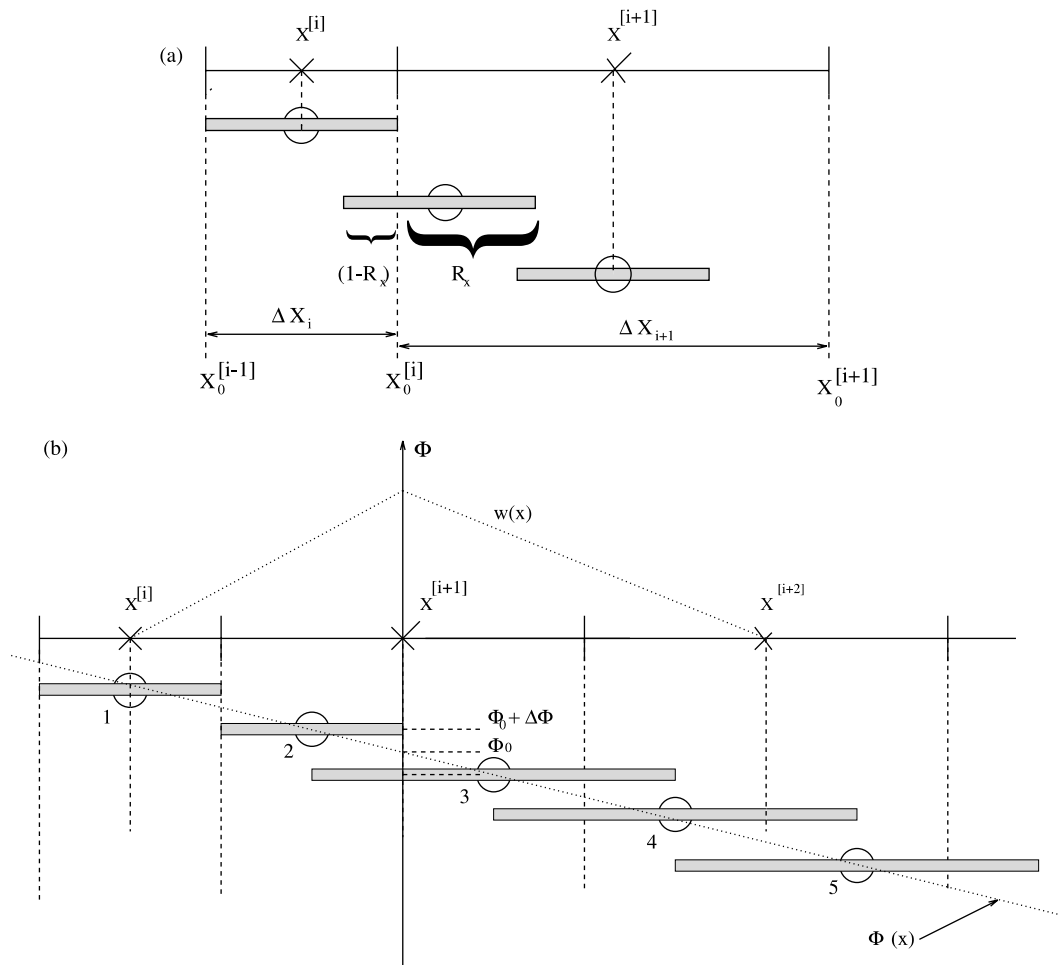
Fig. 2. CIC scheme used to compute cell averages for (a) particle density and (b) a linear function attached to particles (the linear function is defined by its slope $\Delta\Phi$ and Φ_0 which is the value of Φ at $x = x^{[i+1]}$). The cells are characterised by the cell boundary coordinates $x_0^{[i-1]}, x_0^{[i]}, x_0^{[i+1]}, \ldots$ and by the coordinates of the cell centres $x^{[i-1]}, x^{[i]}, x^{[i+1]}, \ldots$; Δx_i and Δx_{i+1} represent the cell sizes.

particles located close to the boundary (between the boundary and the centre of the cell closest to it) is attributed to the centre of the cell next to the boundary. Fig. 3 presents 2D computation results of the r.m.s. density (r.m.s. deviation from the mean particle density) on a 10×10 mesh, both uniform and non-uniform, using the standard NGP averaging and the CIC method described above. For the uniform mesh, particle locations in the domain are generated randomly from the uniform random distribution. The non-uniform mesh has been generated using random numbers from a uniform distribution on the interval $(0.5\Delta x, 1.5\Delta x)$; in this case, particle locations have been generated deterministically with a constant number density. To reduce the statistical error of the r.m.s. density deviation, it has been computed as an average of four different runs with different seeding

values for pseudorandom number generator. As expected, the statistical error is higher for the NGP average and varies as $N_{pc}^{-1/2}$. We note that although the r.m.s. density on the non-uniform mesh is higher, there is no systematic error for the CIC computation which confirms the correctness of the method above.

Next, consider the computation of cell-averaged values for any variable Φ assigned to the particles (a typical example is the calculation of the mean velocity at a given point from the set of particle instantaneous velocities). In this case, both the particle masses and the values of Φ attached to the particles come into play (it has been mentioned in Appendix A that in the frame of the present formalism, one has to resort to mass-weighted expected values). The first idea could be to use the method described above for the calculation of the mean density. However, in a basic
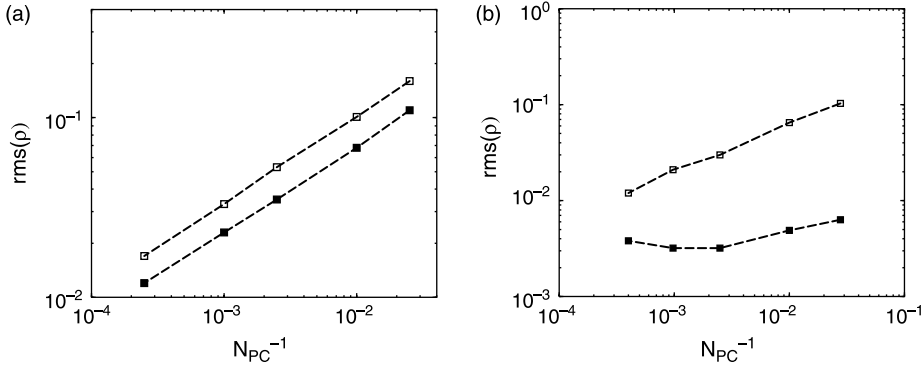
Fig. 3. Computations of the r.m.s. of particle density on a mesh using NGP and CIC averaging: (a) uniform mesh, (b) non-uniform mesh. NGP method ($\square$), CIC method ($\blacksquare$).

test of a linear deterministic function and particles distributed uniformly on the interval, this method is readily shown not to retrieve given values of particle variables at cell centres for a non-uniform grid. Fig. 2(b) illustrates this point, where cell [i] is half the size of its neighbours. To compute the average value of Φ at $x^{[i+1]}$, the particles labelled 2, 3 and 4 contribute with the respective weights of 1, 3/4, and 1/4

$$2\langle\Phi^{[i+1]}\rangle = 1(\Phi_0 + \Delta\Phi) + \frac{3}{4}(\Phi_0 - \Delta\Phi) + \frac{1}{4}(\Phi_0 - 3\Delta\Phi). \tag{61}$$

For this simple example, it is readily checked that $\langle\Phi^{[i+1]}\rangle$ depends on $\Delta\Phi$ (it should not) and that $\Phi^{[i+1]} \neq \Phi_0$. The reason for this behaviour can be traced into the formula of particle weights which is not symmetric with respect to $x^{[i+1]}$. Indeed, the same behaviour can be noticed when non-symmetric CIC weight functions are used though they seem to be a natural generalisation of Eq. (60). This point is also

illustrated in Fig. 2(b) that includes one such basis function $w(x)$ decreasing linearly from a maximum at the considered cell centre, here $x^{[i+1]}$, to zero at the neighbouring cell centres, here $x^{[i]}$ and $x^{[i+2]}$. Using these weighting functions, we readily find again

$$\frac{5}{3}\langle\Phi^{[i+1]}\rangle = \frac{2}{3}(\Phi_0 + \Delta\Phi) + \frac{3}{4}(\Phi_0 - \Delta\Phi) + \frac{1}{4}(\Phi_0 - 3\Delta\Phi), \tag{62}$$

i.e. $\langle\Phi^{[i+1]}\rangle \neq \Phi_0$, a result that would explicitly depend upon the gradient of the function and size of the mesh. Instead, we propose the following method that works correctly for particle variables on a non-uniform mesh. We generalise Eq. (60) by taking Δ as $\min\{\Delta x_{i-1}, \Delta x_i\}$ to preserve the symmetry of $w(x)$. This expression gives the correct result for the example of Fig. 2(b). An alternative to the above is the use of a two-stage algorithm [44], satisfactory but arguably more time-consuming. Again, a 2D computation has been performed for the r.m.s. of a variable assigned to
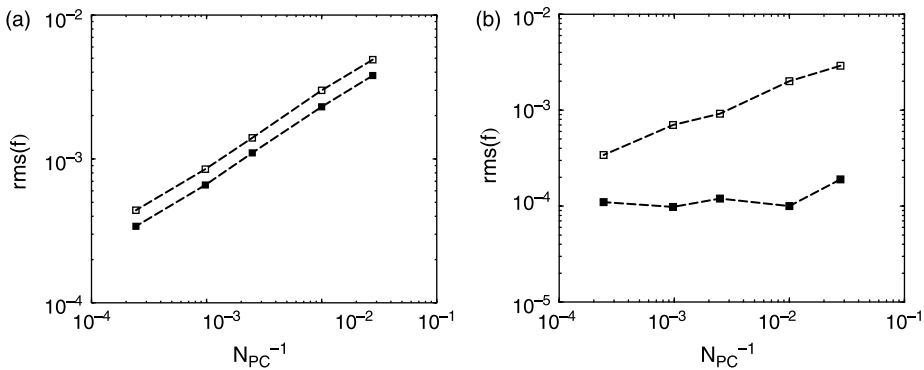

Fig. 4. The r.m.s. value of the mean of a linear deterministic function computed on a mesh using NGP and CIC averaging: (a) uniform mesh, (b) non-uniform mesh. NGP method ($\square$), CIC method ($\blacksquare$).
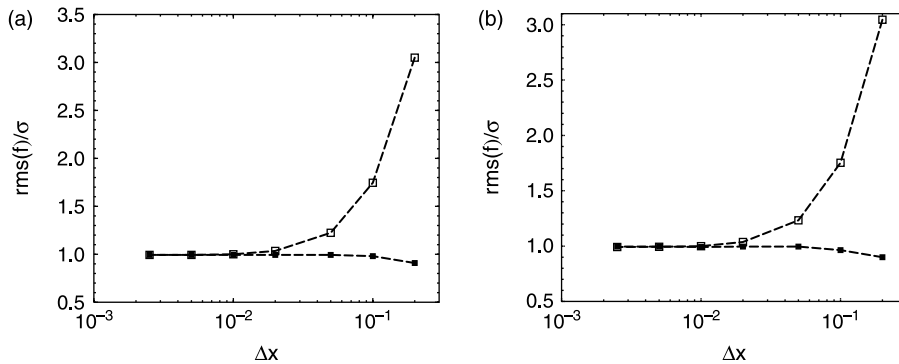
Fig. 5. Normalised r.m.s. of a linear random function computed on a mesh using NGP and CIC averaging: (a) uniform mesh, (b) non-uniform mesh. NGP method ($\square$), CIC method ($\blacksquare$).

particles from a deterministic linear profile in space with the same procedure as above for particle density computations. Both the standard NGP averaging and the CIC method described above have been used. Results shown in Fig. 4 confirm the advantages of CIC averaging in this case. To continue, let us now remove the deterministic assumption for Φ and consider averaging of a random variable assigned to particles

$$\Phi^{(n)} = \Phi(x^{(n)}) = m(x^{(n)}) + s(x^{(n)})\xi, \qquad (63)$$

where $\xi \in \mathcal{N}(0,1)$, $m(x) = a_0 + a_1 x$ is a linear function and $s(x) = \Delta$ (where Δ denotes the average mesh size) to study the effect of spurious variance resulting from the NGP averaging. A numerical test has been performed again with the same methodology as described above. Fig. 5 shows the normalised r.m.s. of this linear random function (i.e. the square root of its variance computed at the cell centres divided by the prescribed r.m.s.) computed out of particle locations. A systematic error is readily noticed for NGP statistics, unless $a_1 \Delta \ll \mathcal{O}(1)$.

5.2.3. CIC statistics with boundary conditions

In wall-bounded flow applications, the CIC method has to be modified so that suitable boundary conditions (BC) are properly accounted for. Dreeben and Pope [44] describe their application of CIC statistics in the PDF method but the treatment of flow boundaries is not reported there. In Fig. 6, a schematic plot shows clearly why the CIC averaging requires some care in the presence of flow boundaries (here walls). The NGP statistics are local (in a cell) and they can thus be computed in border cells without any change. However, for the CIC method this is not the case. As it transpires from Fig. 6, the CIC average of the particle density in a border cell, computed with the weight $w_1(x)$, incorrectly gives a smaller value than the density in the

neighbouring internal cell, computed with $w_2(x)$. The obvious reason is that less particles contribute to the mass in the border cell. The problem differs depending upon whether we consider the particle density field or the mean of any variable Φ (such as velocity) assigned to particles. To compute the mean density, for the particles located between the cell centre and the boundary, it is sufficient to assign all their mass to the centre of this boundary cell. For other particle variables, this treatment is not applicable: even for a linear function $\Phi(x)$, the higher spatial accuracy (compared to NGP) of CIC is lost.

A working remedy to this situation is the addition of 'ghost' or 'mirror' particles outside the actual computational domain in order to compensate for the incorrect CIC computation at the cell centres close to the boundaries. The idea of these 'ghost' particles is
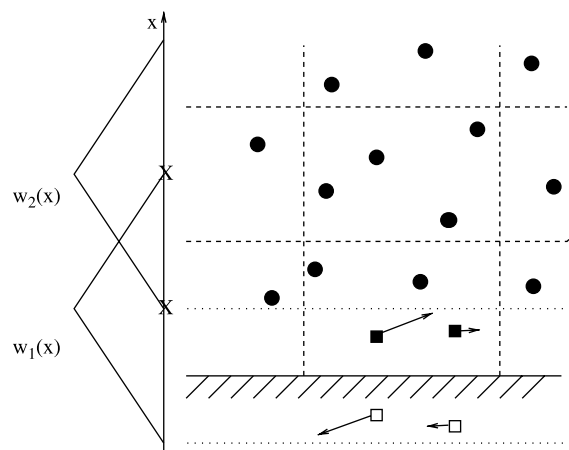

Fig. 6. Cells and particles—schematic plot. Mirror particles ($\square$), corresponding to ($\blacksquare$) are added outside the computational domain. The values of variables attached to them (like velocity) correspond to those of their 'host' particles in border cells. Dashed lines delimit cells and dotted lines indicate where mirror particles are needed.

known in the context of SPH simulation [46]. The very presence of ghost particles with masses equal to their 'hosts' allows for a correct CIC density computation in boundary cells. Next, to compute CIC statistics of any variable Φ attached to the particles, values Φ' of the variables are to be determined also for the mirror ones, as they enter Eq. (56) with a corresponding weight. The procedure is relatively straightforward for the CIC averaging of given functions (either deterministic or random) where the value of the function at a mirror particle location is known. However, the main interest for using ghost particles is in actual particle simulations where precisely these functions are unknown. The values of the variables attached to the mirror particles are to be determined directly from those of the host particles through the application of relevant BCs. For example, if Φ stands for a particle velocity component, then the no-slip, impermeable wall implies $\Phi' = -\Phi$ (Fig. 6) so that at the boundary $\langle\Phi\rangle = 0$. Generalisation is possible for more complex, yet still block-structured, 2D and 3D geometries. Other types of possible boundary conditions in the PDF method for turbulent flow computations, e.g. where particle boundary conditions are determined from a physical reasoning for the near-wall region [36], are also readily implemented this way.

5.2.4. Test case: space-dependent SDE

Let us now analyse the behaviour of a simple nevertheless realistic example of the generic SDE, Eq. (45), where emphasis is put on the averaging and projection operators. Both the NGP and CIC techniques are going to be used with the suitable modifications presented in Sections 5.2.2 and 5.2.3. We consider a one-dimensional Ornstein–Uhlenbeck process on $0 \leq x \leq 1$ interval

$$
\mathrm{d}\Phi(t) = -\frac{\Phi(t) - m(x)}{T}\mathrm{d}t + \sqrt{\frac{2s^2(x)}{T}}\mathrm{d}W(t), \tag{64}
$$

with a fixed timescale T; the space-dependence of the mean value $m(x)$ and the variance $s^2(x)$ is essential to study the spatial discretisation error, cf. Section 5.1.2. In Eq. (64), there is no physical coupling in x; it would occur if convection was added (e.g., $\mathrm{d}x = f(\Phi)\mathrm{d}t$) or if non-local operators were present (e.g., $\alpha\nabla^2\langle\Phi\rangle\mathrm{d}t$ term on the RHS). Here, only a 'numerical' coupling exists; it is due to the approximate computation of ensemble averages through spatial averages, Eq. (56).

For a given time step, $\Delta t = t_{l+1} - t_l$, trajectories of the stochastic process (64) can be integrated analytically [9,17], thus avoiding any temporal discretisation

error; this yields (the location x is a parameter)

$$
\begin{aligned}
\Phi_{l+1} =\ & \Phi_l \exp\left(-\frac{\Delta t}{T}\right) + m(x)\left[1 - \exp\left(-\frac{\Delta t}{T}\right)\right] \\
& + \sqrt{s^2(x)\left[1 - \exp\left(-\frac{2\Delta t}{T}\right)\right]}\,\xi,
\end{aligned} \tag{65}
$$

where ξ is a standard Gaussian random variable, $\xi \in \mathcal{N}(0, 1)$.

The actual test case consists in using the computed values of $\langle\Phi\rangle$ and σ_Φ^2 in Eq. (65) in place of $m(x)$ and $s^2(x)$, respectively. The computed profiles (at different times) for a quadratic mean $m(x)$ and a constant variance $s^2(x)$ are presented in Fig. 7. Qualitatively, a typical behaviour of CIC averaging is to modify the shape of the mean $\langle\Phi\rangle(t,x)$ (ultimately towards a linear profile) and to produce an increase of the variance in the centre of the computational interval. On the contrary, the NGP mean value remains basically unchanged, while the variances in separate cells become increasingly uncorrelated in time. Indeed, in the CIC method, neighbouring cells are linked through the averaging procedure, thus the profile of the variance stays relatively smooth. The NGP computation of Eq. (64) is local and as a result, separate cells become independent of one another, cf. the upper right plot in Fig. 7. These numerical outcomes raise the question of the existence of a bias (cf. Section 5.1.2). A detailed numerical study of this issue has been performed by analysing the temporal behaviour of the r.m.s. of Φ averaged over all cells, denoted by $\sigma_\Phi(t)$ and given by

$$
\sigma_\Phi(t) = \frac{1}{I}\sum_{i=1}^{I}\sigma^{[i]}(t), \tag{66}
$$

where $\sigma^{[i]}(t)$ are the r.m.s. values obtained in cell i. Indeed, for the NGP method, calculations done in each cell are uncorrelated and $\sigma^{[i]}(t)$, $i = 1,\ldots,I$, can be regarded as independent samples. The simplest case to be discussed now is that of constant mean $m(x)$ and variance $s^2(x)$ in Eq. (64). Fig. 8(a) shows how $\sigma_\Phi(t)$, normalised by its initial value, evolves in time. The procedure, in the NGP case, is sensitive to the number of particles per cell. In subsequent time steps, the recomputed variance decreases. The decrease is faster for a smaller number of particles per cell. This phenomenon is identified to be related to the bias and is due to the finite value of N_{pc}. Fig. 8(b) clearly indicates that there is a bias; however, computations of the variance of $\sigma_\Phi(t)$ (results presented as error bars in the same figure) show that the statistical
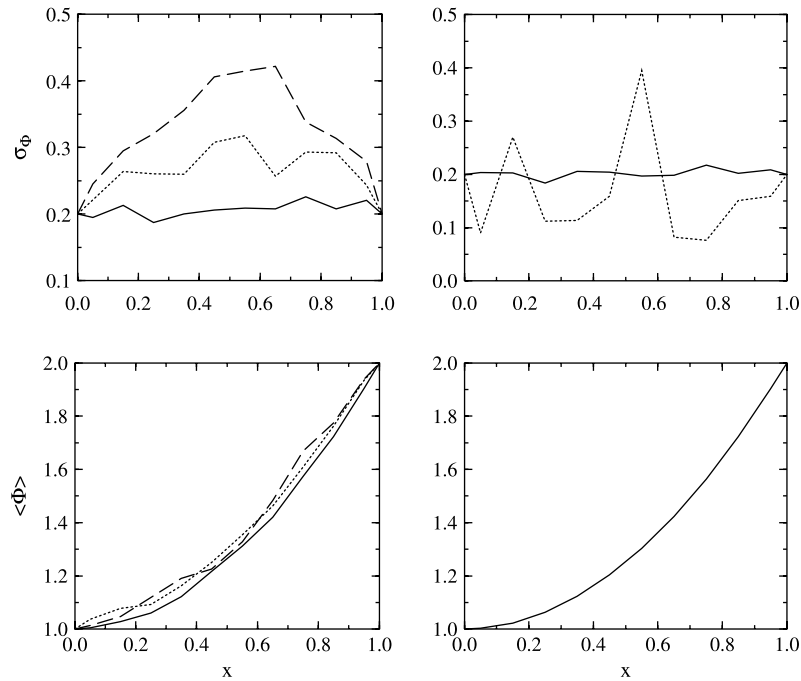
Fig. 7. Temporal evolution of the mean (lower plots), $\langle\Phi\rangle$, and variance (upper plots), (σ_ϕ^2), profiles for quadratic initial mean profile and constant initial non-zero variance. Left plots: CIC; right plots: NGP. Three successive time instants (solid, dotted and dashed lines).

fluctuations of this quantity are significant. With this precaution in mind, the bias (resulting from several different runs for several number of cells, etc.) has been plotted as a function of the number of particles per cell N_{pc}. Results in Fig. 9(a) indicate that the slope for different runs is indeed close to the theoretical prediction of the bias, $B_\Phi \sim N_{pc}^{-1}$ (plotted as a dotted line). The computed probability distributions of σ_Φ are shown in Fig. 9(b).

5.2.5. NGP or CIC in practical computations?

In Fig. 7, the centred second-order moment, i.e. the variance, has been computed using the non-centred moments in order to avoid problems with the correct statement of boundary conditions, which are necessary for CIC averages. It is readily seen that the computed profiles of $\langle\Phi\rangle(x)$ and $\sigma^2(x)$ tend to become linear (both are fixed to the respective $m(x)$ and $s(x)$ values at the boundaries $x=0$ and 1). In Fig. 9, it is seen that
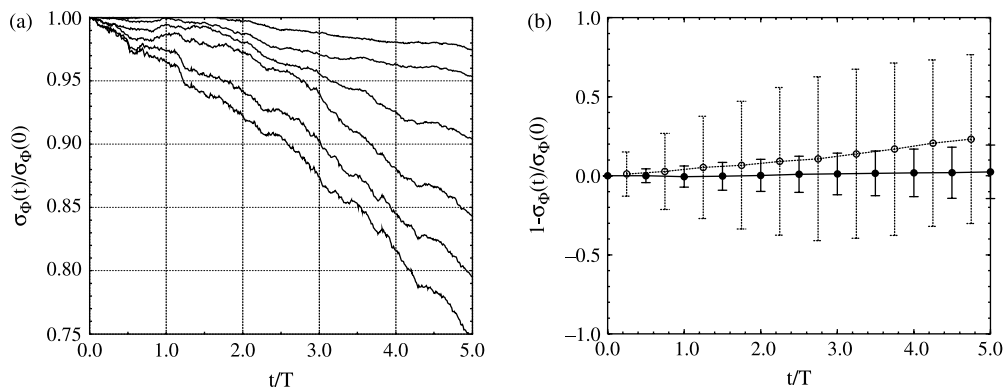

Fig. 8. Temporal evolution of the r.m.s. of Φ in scaled time; NGP computation over 1000 cells. (a) Results for $N_{pc}=20$, 25, 40, 80, 160, and 320, respectively (from the lowest to the highest curve); (b) the r.m.s. of Φ with its standard deviation for $N_{pc}=25$ (dotted line with $\bigcirc$) and $N_{pc}=320$ (solid line with $\bullet$).
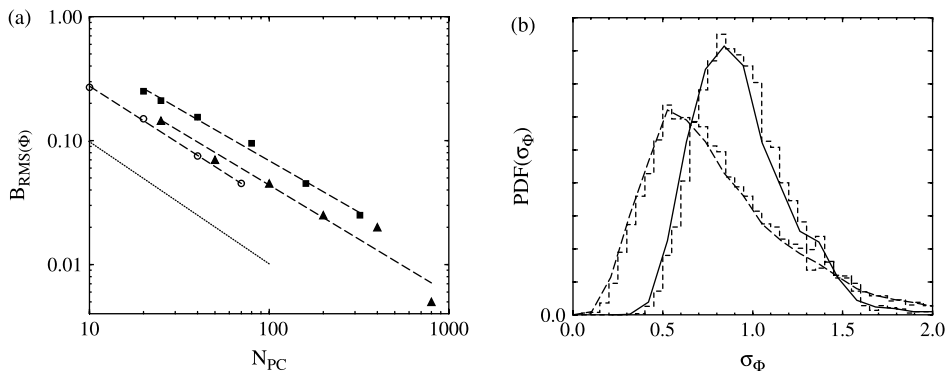
Fig. 9. (a) Analysis of the bias of the r.m.s. of Φ as a function of the number of particles per cell N_{pc} for three different NGP computations; dotted line: -1 slope. (b) PDF of the r.m.s. of Φ at $t/T=3$ in the NGP computation over 5000 cells. Solid line: $N_{pc}=20$, dashed line: $N_{pc}=70$. Results are smoothed histograms (dashed lines).

the NGP computation generates a non-zero spurious variance.

The comparison between the NGP and CIC methods for stochastic processes reveals that none of the results are entirely satisfactory. Compared to classical deterministic particle systems, where the CIC has a known advantage over NGP, new features have been revealed. NGP is a local and robust method, which does not require specific developments. It respects given mean profiles but leads to spurious variances. The spurious variances are shown to be related to a bias, which decreases linearly with the number of particles. On the contrary, when using CIC, developments are needed to account for non-uniform meshes and for boundary conditions. It is a less local (higher order) method than NGP but it is more complicated to implement in the general case. The results obtained in a prototypical SDE, cf. Section 5.2.4, show that the CIC method does not present advantages in accuracy. Furthermore, in the particular case considered (no convection), the CIC technique performs globally worse than the NGP one. Indeed, CIC does not preserve the mean and shows a systematic error in the variance.

As a consequence, all practical computations performed in the rest of the present paper (cf. Section 7) will be based upon the NGP technique.

5.3. Accurate schemes for SDE integration

It has now been explained how information is exchanged between the discrete particles and the mesh (operators P and A, cf. Section 5.1.1). We recall that this is done here in the case of one-way coupling and the extension of the numerical schemes, presented in

this section, to the case of two-way coupling will be discussed in Section 6.

As shown in Sections 3.1.2 and 3.2, and as explained at the beginning of this section, cf. Eq. (45), the SDEs reproducing the dynamics of the discrete particles are Mac-Kean SDEs since the coefficients depend not only on the state vector but also on expected values of functions of $\mathbf{Z}(t)$. In particle-mesh methods, as explained above, quantities such as $\langle f(\mathbf{Z}) \rangle$ (where f is a linear or quadratic function of $\mathbf{Z}(t)$ in our problem) are extracted from the particle data and evaluated at grid points. In Section 5.2, the difficulties inherent to the projection and averaging procedures have been detailed.

Attention is now focused on the time integration of the set of SDEs (operator T). The development of a suitable weak numerical scheme for the time integration of SDEs is a much more difficult task than the corresponding one for ODEs. Indeed, SDEs do not obey the rules of classical differential calculus, see Section 2.2, and one has to rely on the theory of stochastic processes [15]. In that sense, particular attention has to be paid to the problem of consistency between discretised equations and the original continuous set of SDEs. It is recalled that, in the present paper, Itô's calculus is adopted and therefore all SDEs are written in the *Itô' sense*, see Section 2.2. This choice has no physical motivation: Itô's calculus is very convenient in the development of weak numerical schemes for SDEs because of the zero mean and isometry properties, cf. Eqs. (16).

An essential preliminary is to clearly frame the development of the weak numerical scheme in the general methodology that has been followed here. We propose, indeed, to describe the problem of turbulent polydispersed two-phase flows within an engineering

context but with a rigorous treatment of the multiscale character, which is a distinctive feature of these flows, cf. Section 4. The model, Eqs. (40), contains several characteristic timescales and this system of SDEs becomes stiff, from a mathematical point of view, whenever one of these timescales goes to zero. In those cases, various limit systems are obtained, see Section 4, which represent the asymptotic limits of the physical model. A proper treatment of the physics of the multiscale aspect imposes to put forward weak numerical schemes, which are consistent with all asymptotic limits when different timescales go to zero.

It is worth emphasising that this corresponds to a practical concern. Indeed, in the numerical simulation of a complex flow, the timescales may be negligible (much smaller than the time step) in some areas of the computational domain. For example, in a wall-bounded flow, the integral timescale of the fluid velocity seen, $T_{L,i}^*$, goes to zero when the distance to the wall decreases. Furthermore, when dealing with polydispersed particles, or with phenomena involving evaporation or combustion (when particle diameters decrease in time), one has to handle often a whole range of particle diameters (say from 1 to 100–200 μm) and thus a whole range of values for τ_p (for example, 10^{-6} s $\lesssim \tau_p \lesssim 10^{-2}$ s). It would be inefficient to carry out computations with a time step limited by the smallest possible value of τ_p and/or $T_{L,i}^*$. This is the very reason why in the simulations of particle dispersion in wall-bounded flows, based on discrete models, it is necessary to use different time steps for different classes of diameters (and thus of τ_p) and to lower the time step in the wall region.

As a consequence of the above discussion, the constraints, which are required for a suitable weak numerical scheme, can now be summarised, considering both physical and numerical issues. Since a particle-mesh method is adopted here, the PDEs for the fluid are first solved and then the dynamics of the stochastic particles are computed (see Section 5.1.1), thus, the scheme has to be *explicit* for the fluid mean fields. By choice, the scheme will also be explicit for the particle properties. Furthermore, the time step, which has to be the same for the integration of the PDEs and the SDEs, is imposed by stability conditions required by the finite volume algorithm solving the mean-field equations for the fluid. This implies that since there is no possibility to control the time step when integrating the SDEs, the numerical scheme has to be *unconditionally stable*. At last, since particle localisation on a mesh (needed for projection and averaging, see Section 5.1) is CPU-

demanding, the numerical scheme should minimise these operations.

The constraints required for a suitable weak numerical scheme are:

(i) the numerical scheme must be explicit, stable and the number of calls to particle localisation (sub)routine has to be minimum,
(ii) the numerical scheme must be consistent with all limit systems.

5.3.1. Weak numerical schemes for SDEs

In Section 2, the correspondence (in a weak sense) between a set of SDEs and a Fokker–Planck equation (for the associated law) has been established. In this work, weak numerical schemes shall be developed for Eqs. (40), i.e. we are not interested in the exact trajectories of the process but instead in statistics (the pdf) extracted from the stochastic particles (the real particles are replaced by stochastic ones, which should reproduce the same statistics). The numerical method proposed in this work is therefore nothing else than the simulation of an underlying pdf, or in other words, the equivalent Fokker–Planck equation is solved by simulating the trajectories of stochastic particles, i.e. by a dynamical Monte Carlo method. As briefly explained in Section 2.1, this non-trivial numerical procedure, i.e. to resort to SDEs to solve a PDE, is well suited for PDEs with a large number of degrees of freedom.

Since the Itô interpretation of stochastic integrals has been chosen, it is *implicitly* assumed, in the discretisation of the stochastic integral, that B_{ij} should not anticipate the future, i.e. for each time step $\Delta t = t_{k+1} - t_k$, B_{ij} should be computed at $t = t_k$. As a result, classical numerical schemes for ODEs, for example Runge-Kutta schemes, cannot be applied directly. More precisely, careless applications of such schemes for SDEs can introduce spurious drifts, which may not be easy to detect. An illuminating example of this kind of error is illustrated in Ref. [47]. The key point here is that the numerical discretisation of the stochastic integral must be in line with its mathematical definition.

Let $\mathbf{Z}^{\Delta t}(t)$ be a numerical approximation of $\mathbf{Z}(t)$ obtained with a uniform time discretisation, Δt. A numerical scheme of order m will converge, in a weak sense, if at time $t = T$ (T is called the stopping time), for all sufficiently smooth functions f, there exists a constant C (function of T) such that

$$\sup_{t \leq T} |\langle f[\mathbf{Z}(t)] - f[\mathbf{Z}^{\Delta t}(t)] \rangle| \leq C(T)(\Delta t)^m. \tag{67}$$

Other convergence modes are possible, for example *strong convergence* in the mean-square sense, if one is interested in the exact trajectories of the process. It is fairly rare that this is the case for engineering problems. Indeed, in most engineering applications, one is mainly interested in the expected values (statistics) of functionals of the variables of interest. For further discussion on the convergence modes, see the book of Kloeden and Platen [17].

5.3.2. Analytical solution to the system of SDEs

In the present work, the weak numerical schemes, with the required features, are developed based on the analytical solution to Eqs. (40) *with constant coefficients* (independent of time), the main idea being to derive a numerical scheme by freezing the coefficients on the integration intervals. This methodology ensures *stability* and *consistency with all limit systems*:

- stability because the form of the equations gives analytical solutions with exponentials of the type $\exp(-\Delta t/T)$ where T is one of the characteristic timescales (τ_p, $T_{\mathrm{L},i}^*$),
- consistency with all limit systems by construction, since the schemes are based on an analytical solution.

Different techniques shall be used to derive first- and second-order (in time) schemes from the analytical solutions with constant coefficients. A first-order scheme can be obtained by computing, at each time step, the variables on the basis of the analytical solutions (all coefficients are frozen at the beginning of the integration interval), i.e. a numerical scheme of the *Euler* kind is obtained. A second-order scheme can be derived by resorting to a predictor–corrector technique, where the prediction step is the first-order scheme.

Before presenting the weak numerical schemes, it is a prerequisite to give the analytical solutions to system (40), with constant coefficients (in time). These solutions are obtained by resorting to Itô's calculus in combination with the method of the variation of the constant. For instance, for the fluid velocity seen, one seeks a solution of the form $U_{\mathrm{s},i}(t) = H_i(t)\exp(-t/T_i)$, where $H_i(t)$ is a stochastic process defined by (from now on the notation is slightly changed: $T_{\mathrm{L},i}^*$ is noted T_i for the sake of clarity in the complex formulae to come)

$$dH_i(t) = \exp(t/T_i)[C_i \, dt + \breve{B}_i \, dW_i(t)], \tag{68}$$

i.e. by integration on a time interval $[t_0, t]$ ($\Delta t = t - t_0$),

$$\begin{aligned} U_{\mathrm{s},i}(t) = {}& U_{\mathrm{s},i}(t_0)\exp(-\Delta t/T_i) + C_i T_i[1 - \exp(-\Delta t/T_i)] \\ & + \breve{B}_i \exp(-t/T_i) \int_{t_0}^{t} \exp(s/T_i) dW_i(s), \end{aligned} \tag{69}$$

where $\breve{B}_i = B_{ii}$ since B_{ij} is a diagonal matrix, cf. Eq. (24). By proceeding in the same way for the other equations (position and velocity), the analytical solution is obtained for the entire system, cf. Table 2. The three stochastic integrals, Eqs. (130)–(132) in Table 2, are centred Gaussian processes (they are stochastic integrals of deterministic functions [15]). These integrals are defined implicitly, but they can be simplified by integration by parts, cf. Table 2. As explained in Section 4.1, for the numerical representation of the stochastic integrals, the knowledge of the covariance matrix (second-order moments) is needed, see Table 3. Using the isometry property, see Section 2.2, the second-order moments, i.e. Eqs. (136)–(141) in Table 3, can be calculated. The analytical solutions are now known. Before presenting the first-order scheme, let us verify that the analytical solution given by Tables 2 and 3 is consistent with the limit cases obtained in Section 4.2, i.e. Eqs. (41)–(44).

5.3.2.1. Limits systems of analytical solution.
In limit case 1, where the discrete particles behave as fluid particles, the limit system is given by Eq. (41). When $\tau_\mathrm{p} \to 0$, Eq. (128) becomes

$$\begin{aligned} U_{\mathrm{p},i}(t) = {}& U_{\mathrm{s},i}(t_0)\exp(-\Delta t/T_i) + C_i T_i \exp(-\Delta t/T_i) \\ & + \Gamma_i(t), \end{aligned} \tag{70}$$

and for the stochastic integral $\Gamma_i(t)$, one has

$$\begin{cases} \langle \Gamma_i^2(t) \rangle [\overrightarrow{\tau_\mathrm{p} \to 0}] \dfrac{\breve{B}_i^2 T_i}{2}[1 - \exp(-2\Delta t/T_i)] = \langle \gamma_i^2(t) \rangle, \\[2ex] \langle \Gamma_i(t)\gamma_i(t) \rangle [\overrightarrow{\tau_\mathrm{p} \to 0}] \langle \gamma_i^2(t) \rangle. \end{cases} \tag{71}$$

The last two equations indicate that $\Gamma_i(t) \to \gamma_i(t)$ when $\tau_\mathrm{p} \to 0$. By comparing Eq. (70) to Eq. (129) with $\Gamma_i(t) = \gamma_i(t)$, the results of Eq. (41) are retrieved, i.e. $\mathbf{U}_\mathrm{p}(t) = \mathbf{U}_\mathrm{s}(t)$.

In limit case 2, the fluid velocity seen, $\mathbf{U}_\mathrm{s}(t)$, is a fast variable which is eliminated. The results obtained in Tables 2 and 3 with $T_i \to 0$ and $\breve{B}_i T_i = \mathrm{cst}$, give

Table 2
Analytical solutions to system (40) for time-independent coefficients

---

$x_{\text{p},i}(t) = x_{\text{p},i}(t_0) + U_{\text{p},i}(t_0)\tau_{\text{p}}[1-\exp(-\Delta t/\tau_{\text{p}})] + U_{\text{s},i}(t_0)\theta_i\{T_i[1-\exp(-\Delta t/T_i)] + \tau_{\text{p}}[\exp(-\Delta t/\tau_{\text{p}})-1]\} + [C_iT_i]\{\Delta t - \tau_{\text{p}}[1-\exp(-\Delta t/\tau_{\text{p}})]$

$\qquad -\theta_i(T_i[1-\exp(-\Delta t/T_i)] + \tau_{\text{p}}[\exp(-\Delta t/\tau_{\text{p}})-1])\} + \Omega_i(t),$ (127)

with $\theta_i = T_i/(T_i - \tau_{\text{p}})$

$U_{\text{p},i}(t) = U_{\text{p},i}(t_0)\exp(-\Delta t/\tau_{\text{p}}) + U_{\text{s},i}(t_0)\theta_i[\exp(-\Delta t/T_i) - \exp(-\Delta t/\tau_{\text{p}})] + [C_iT_i]\{[1-\exp(-\Delta t/\tau_{\text{p}})] - \theta_i[\exp(-\Delta t/T_i) - \exp(-\Delta t/\tau_{\text{p}})]\} + \Gamma_i(t)$

(128)

$U_{\text{s},i}(t) = U_{\text{s},i}(t_0)\exp(-\Delta t/T_i) + C_iT_i[1-\exp(-\Delta t/T_i)] + \gamma_i(t)$ (129)

The stochastic integrals $\gamma_i(t)$, $\Gamma_i(t)$, $\Omega_i(t)$ are given by:

$$\gamma_i(t) = \check{B}_i \exp(-t/T_i) \int_{t_0}^{t} \exp(s/T_i)\mathrm{d}W_i(s),$$ (130)

$$\Gamma_i(t) = \frac{1}{\tau_{\text{p}}}\exp(-t/\tau_{\text{p}}) \int_{t_0}^{t} \exp(s/\tau_{\text{p}})\gamma_i(s)\mathrm{d}s,$$ (131)

$$\Omega_i(t) = \int_{t_0}^{t} \Gamma_i(s)\mathrm{d}s.$$ (132)

By resorting to stochastic integration by parts, $\gamma_i(t)$, $\Gamma_i(t)$, $\Omega_i(t)$ can be written:

$\gamma_i(t) = \check{B}_i \exp(-t/T_i)I_{1,i},$ (133)

$\Gamma_i(t) = \theta_i\check{B}_i[\exp(-t/T_i)I_{1,i} - \exp(-t/\tau_{\text{p}})I_{2,i}],$ (134)

$\Omega_i(t) = \theta_i\check{B}_i\{(T_i - \tau_{\text{p}})I_{3,i} - [T_i \exp(-t/T_i)I_{1,i} - \tau_{\text{p}}\exp(-t/\tau_{\text{p}})I_{2,i}]\},$ (135)

with $I_{1,i} = \int_{t_0}^{t} \exp(s/T_i)\mathrm{d}W_i(s), \quad I_{2,i} = \int_{t_0}^{t} \exp(s/\tau_{\text{p}})\mathrm{d}W_i(s) \quad$ and $\quad I_{3,i} = \int_{t_0}^{t} \mathrm{d}W_i(s).$

$$\begin{aligned} U_{\text{p},i}(t) = {} & U_{\text{p},i}(t_0)\exp(-\Delta t/\tau_{\text{p}}) \\ & + [\langle U_i \rangle + \mathcal{A}_i\tau_{\text{p}}][1-\exp(-\Delta t/\tau_p)] \\ & + \sqrt{\frac{\check{B}_i^2 T_i^2}{2\tau_{\text{p}}}[1-\exp(-2\Delta t/\tau_{\text{p}})]}\mathcal{G}_{\text{p},i}, \end{aligned}$$ (72)

where $\mathcal{G}_{\text{p},i}$ is a $\mathcal{N}(0,1)$ vector (composed of independent standard Gaussian random variables) and we recall that $\langle U_i \rangle = \langle U_i(t,\mathbf{x}_{\text{p}}(t)) \rangle$. It can be rapidly verified, by applying Itô's calculus, that Eq. (72) is the solution to system (42) when the coefficients are constant.

In limit case 3, both the fluid velocity seen and the velocity of the discrete particles become rapid variables. When $\tau_{\text{p}} \to 0$ and $T_i \to 0$ with $\check{B}_i T_i = \text{cst}$, Eq. (127) becomes

$$x_{\text{p},i}(t) = x_{\text{p},i}(t_0) + [\langle U_i \rangle + \mathcal{A}_i\tau_{\text{p}}]\Delta t + \sqrt{\check{B}_i^2 T_i^2 \Delta t}\,\mathcal{G}_{x,i},$$ (73)

which is the solution to Eq. (43) when the coefficients are constant ($\mathcal{G}_{x,i}$ is a $\mathcal{N}(0,1)$ vector).

In limit case 4, when $T_i \to 0$ (with no condition on $\check{B}_i T_i$) the system becomes deterministic, the results are in agreement with Eq. (44). When $T_i \to 0$, Eqs. (127)–(129) become

Table 3
Derivation of the covariance matrix for constant coefficients

$$\langle \gamma_i^2(t) \rangle = \breve{B}_i^2 \frac{T_i}{2}[1 - \exp(-2\,\Delta t/T_i)], \quad \text{where } \breve{B}_i^2 = B_{ii}^2 \tag{136}$$

$$\langle \Gamma_i^2(t) \rangle = \breve{B}_i^2 \theta_i^2 \left\{ \frac{T_i}{2}[1 - exp(-2\,\Delta t/T_i)] - \frac{2\tau_p T_i}{T_i + \tau_p}[1 - exp(-\Delta t/T_i)exp(-\Delta t/\tau_p)] + \frac{\tau_p}{2}[1 - exp(-2\Delta t/\tau_p)] \right\} \tag{137}$$

$$\frac{1}{\breve{B}_i^2 \theta_i^2}\langle \Omega_i^2(t) \rangle = (T_i - \tau_p)^2 \Delta t + \frac{T_i^3}{2}[1 - \exp(-2\Delta t/T_i)] + \frac{\tau_p^3}{2}[1 - \exp(-2\Delta t/\tau_p)] - 2T_i^2(T_i - \tau_p)[1 - \exp(-\Delta t/T_i)]$$
$$+ 2\tau_p^2(T_i - \tau_p)[1 - \exp(-\Delta t/\tau_p)] - 2\frac{T_i^2 \tau_p^2}{T_i + \tau_p}[1 - \exp(-\Delta t/T_i)\exp(-\Delta t/\tau_p)] \tag{138}$$

$$\langle \gamma_i(t)\Gamma_i(t) \rangle = \breve{B}_i^2 \theta_i T_i \left\{ \frac{1}{2}[1 - \exp(-2\Delta t/T_i)] - \frac{\tau_p}{T_i + \tau_p}[1 - \exp(-\Delta t/T_i)\exp(-\Delta t/\tau_p)] \right\} \tag{139}$$

$$\langle \gamma_i(t)\Omega_i(t) \rangle = \breve{B}_i^2 \theta_i T_i \left\{ (T_i - \tau_p)[1 - \exp(-\Delta t/T_i)] - \frac{T_i}{2}[1 - \exp(-2\Delta t/T_i)] + \frac{\tau_p^2}{T_i + \tau_p}[1 - \exp(-\Delta t/T_i)\exp(-\Delta t/\tau_p)] \right\} \tag{140}$$

$$\frac{1}{\breve{B}_i^2 \theta_i^2}\langle \Gamma_i(t)\Omega_i(t) \rangle = (T_i - \tau_p)\{T_i[1 - \exp(-\Delta t/T_i)] - \tau_p[1 - \exp(-\Delta t/\tau_p)]\} - \frac{T_i^2}{2}[1 - \exp(-2\Delta t/T_i)]$$
$$- \frac{\tau_p^2}{2}[1 - \exp(-2\Delta t/\tau_p)] + T_i\tau_p[1 - \exp(-\Delta t/T_i)\exp(-\Delta t/\tau_p)] \tag{141}$$

$$\begin{cases} U_{s,i}(t) = \langle U_i \rangle, \\ U_{p,i}(t) = U_{p,i}(t_0)\exp(-\Delta t/\tau_p) + [\langle U_i \rangle + \mathcal{A}_i \tau_p][1 - \exp(-\Delta t/\tau_p)], \\ x_{p,i}(t) = x_{p,i}(t_0) + \tau_p[1 - \exp(-\Delta t/\tau_p)]U_{p,i}(t_0) + [\langle U_i \rangle + \mathcal{A}_i \tau_p]\{\Delta t - \tau_p[1 - \exp(-\Delta t/\tau_p)]\}, \end{cases} \tag{74}$$

which is the analytical solution to system (44) when the coefficients are constant.

5.3.3. Weak first-order scheme

The derivation of the weak first order scheme is now rather straightforward since the analytical solutions to system (40) with constant coefficients have already been calculated. Indeed, the Euler scheme (which is a weak scheme of order 1 [17]) is simply obtained by freezing the coefficients at the beginning of the time intervals $\Delta t = [t_n, t_{n+1}]$. Let Z_i^n and Z_i^{n+1} be the approximated values of $Z_i(t)$ at time t_n and t_{n+1}, respectively. The Euler scheme is then simply written by using the results of Tables 2 and 3 as shown in Table 4. Before showing that the scheme is consistent with all limit cases, some clarifications must be given. Here, the limit systems are considered in the *discrete sense*. The observation timescale dt has now become the time step Δt. The timescales τ_p and T_i do not go to zero, as in the continuous sense (Section 4), but their values, depending on the history of the particles, can be

smaller or greater than Δt. The continuous limits, i.e. Eqs. (41)–(44), represent a mathematical limit, whereas in the discrete formulation, as we shall see just below, the limit systems correspond to a numerical solution where the ratios $\Delta t/T_i$ and $\Delta t/\tau_p$ become large (the limit systems are obtained by Taylor expansions).

In limit case 1, when $\tau_p \to 0$ in the continuous sense and $\tau_p \ll \Delta t \ll T_i$ in the discrete sense, the numerical scheme gives $U_{p,i}^{n+1} = U_{s,i}^{n+1}$, see Table 4, which is consistent with the results of Section 4.2.

In limit case 2, in the continuous sense $T_i \to 0$ and $\breve{B}_i T_i = \text{cst}$, i.e. the fluid velocity seen $\mathbf{U}_s(t)$ becomes a fast variable, which is eliminated. In the discrete case, $\mathbf{U}_s(t)$ is simply observed at a timescale which is great compared to its memory, i.e. $T_i \ll \Delta t \ll \tau_p$, and the numerical scheme yields (see Table 4)

$$U_{s,i}^{n+1} = \langle U_i^n \rangle + \sqrt{\frac{[\breve{B}_n^i]^2 T_i^n}{2}}\,\mathcal{G}_{1,i}, \tag{75}$$

where $\langle U_i^n \rangle = \langle U_i(t_n, \mathbf{x}_p^n) \rangle$. The fluid velocity seen becomes a Gaussian random variable, a result which is physically sound since $\mathbf{U}_s(t)$ is observed at time steps which are greater than its memory. This result is in line with that of the model problem presented in Section 4.1. Furthermore, by Taylor expansion, it can be shown that the numerical scheme is consistent with Eq. (72).

In limit case 3, i.e. when $1 \ll \Delta t/T_i$ and $1 \ll \Delta t/\tau_p$ (discrete case), one obtains for the velocity of the particles and for the fluid velocity seen (see Table 4)

Table 4
Weak first-order scheme (Euler scheme)

Numerical integration of the system:

$x_{p,i}^{n+1} = x_{p,i}^n + A_1 U_{p,i}^n + B_1 U_{s,i}^n + C_1 [T_i^n C_i^n] + \Omega_i^n,$

$U_{s,i}^{n+1} = U_{s,i}^n \exp(-\Delta t/T_i^n) + [T_i^n C_i^n][1 - \exp(-\Delta t/T_i^n)] + \gamma_i^n,$

$U_{p,i}^{n+1} = U_{p,i}^n \exp(-\Delta t/\tau_p^n) + D_1 U_{s,i}^n + [T_i^n C_i^n](E_1 - D_1) + \Gamma_i^n.$

The coefficients A_1, B_1, C_1, D_1 and E_1 are given by:

$A_1 = \tau_p^n[1 - \exp(-\Delta t/\tau_p^n)],$

$B_1 = \theta_i^n[T_i^n(1 - \exp(-\Delta t/T_i^n)) - A_1], \quad \text{with } \theta_i^n = T_i^n/(T_i^n - \tau_p^n),$

$C_1 = \Delta t - A_1 - B_1,$

$D_1 = \theta_i^n[\exp(-\Delta t/T_i^n) - \exp(-\Delta t/\tau_p^n)],$

$E_1 = 1 - \exp(-\Delta t/\tau_p^n).$

The stochastic integrals γ_i^n, Ω_i^n, Γ_i^n are simulated by:

$\gamma_i^n = P_{11} \mathcal{G}_{1,i},$

$\Omega_i^n = P_{21} \mathcal{G}_{1,i} + P_{22} \mathcal{G}_{2,i}$

$\Gamma_i^n = P_{31} \mathcal{G}_{1,i} + P_{32} \mathcal{G}_{2,i} + P_{33} \mathcal{G}_{3,i},$

where $\mathcal{G}_{1,i}$, $\mathcal{G}_{2,i}$, $\mathcal{G}_{3,i}$ are independent $\mathcal{N}(0, 1)$ random variables. The coefficients P_{11}, P_{21}, P_{22}, P_{31}, P_{32}, P_{33} are defined as:

$P_{11} = \sqrt{\langle(\gamma_i^n)^2\rangle},$

$P_{21} = \dfrac{\langle \Omega_i^n \gamma_i^n \rangle}{\sqrt{\langle(\gamma_i^n)^2\rangle}}, \quad P_{22} = \sqrt{\langle(\Omega_i^n)^2\rangle - \dfrac{\langle \Omega_i^n \gamma_i^n \rangle^2}{\langle(\gamma_i^n)^2\rangle}},$

$P_{31} = \dfrac{\langle \Gamma_i^n \gamma_i^n \rangle}{\sqrt{\langle(\gamma_i^n)^2\rangle}}, \quad P_{32} = \dfrac{1}{P_{22}}(\langle \Omega_i^n \Gamma_i^n \rangle - P_{21}P_{31}),$

$P_{33} = \sqrt{\langle(\Gamma_i^n)^2\rangle - P_{31}^2 - P_{32}^2}.$

$$\left\{ \begin{array}{l} U_{p,i}^{n+1} = \langle U_i^n \rangle + \mathcal{A}_i^n \tau_p^n \\[2mm] + \sqrt{\dfrac{[\check{B}_i^n]^2}{2} \dfrac{T_i^n}{T_i^n + \tau_p^n}} \left(\sqrt{T_i^n} \mathcal{G}_{1,i} + \sqrt{\tau_p^n} \mathcal{G}_{2,i} \right), \\[4mm] U_{s,i}^{n+1} = \langle U_i^n \rangle + \sqrt{\dfrac{[\check{B}_i^n]^2 T_i^n}{2}} \mathcal{G}_{1,i}. \end{array} \right\} \quad (76)$$

Once again, $U_{p,i}(t)$, and $U_{s,i}(t)$, which were eliminated in the continuous case, do not disappear. They become Gaussian random variables, a result which is physically sound since these two random variables are observed at time steps, which are greater than their respective memories. Moreover, by Taylor expansion, one can show that the numerical scheme is consistent with Eq. (73).

In limit case 4, $T_i = 0$, and the flow becomes laminar. It can be easily shown that the numerical scheme is consistent with Eqs. (74). For instance, one has for the fluid velocity $U_{s,i}^{n+1} = \langle U_i^n \rangle$, cf. Table 4.

The previous results show that the Euler scheme presented in Table 4 is consistent with all limit cases. Therefore, the scheme gives numerical solutions, which are physically sound, i.e. a consistent representation of the multiscale character of the model is obtained.

5.3.4. Weak second-order scheme

Most of the time, dynamical Monte Carlo methods are used with first-order schemes only, for example in nuclear or particle physics. In those cases, the time-step value is not a very important factor, and attention is rather focused on obtaining accurate statistics. On the contrary, in industrial fluid mechanics applications with complex geometries and strong inhomogeneities in the flow, a higher-order accuracy in time can be critical in order to avoid prohibitively small time steps resulting in huge computational time. Such an example will be presented in Section 7.1.

From a formal point of view, weak high-order schemes for a set of SDEs can be derived for any desired accuracy, though this is much more complicated than for ODEs. Such high-order schemes are generally based on truncated stochastic Taylor expansions, see for example Refs. [17,48]. These techniques cannot be applied directly in our particular case since neither the unconditional stability nor the consistency in limit cases can be obtained.

5.3.4.1. Property of the system of SDEs. The diffusion matrix of system (29) has a singular property of crucial importance here [30]. In the present case, this nine-dimensional matrix can be written, using block

notation, as (we recall that $\mathbf{Z}(t) = (\mathbf{x}_p(t), \mathbf{U}_p(t), \mathbf{U}_s(t))$)

$$\sigma(t, \mathbf{Z}(t)) = \begin{bmatrix} 0 & 0 & 0 \\ 0 & 0 & 0 \\ 0 & 0 & \mathbf{B}_s(t, \mathbf{x}_p(t)) \end{bmatrix}, \qquad (77)$$

where each block represents a three-dimensional matrix. Indeed, from Eq. (24), it can be noticed that $B_{s,ij}$ depends only on time, position, $\mathbf{x}_p$, and the mean value of the relative velocity, $\langle \mathbf{U}_r \rangle$. Therefore, the only variable of the state vector on which $B_{s,ij}$ depends is position, because $\langle \mathbf{U}_r \rangle (t, \mathbf{x}_p(t))$ is a mean field. The fact that σ_{ij} depends neither on $\mathbf{U}_p$ nor on $\mathbf{U}_s$ implies that quantities such as $\partial \sigma_{ij}/\partial z_k$ are non-zero only when $1 \leq k \leq 3$ and $7 \leq i,j \leq 9$. For these values of k and j, one has $\sigma_{kj} = 0$.

Thus, the diffusion matrix σ_{ij} has the following singular property

$$\sum_k \sum_j \sigma_{kj} \frac{\partial \sigma_{ij}}{\partial z_k} = 0, \quad \forall i. \qquad (78)$$

5.3.4.2. General idea. Let us consider the following model problem

$$dX_i(t) = \mathfrak{A}_i(\mathbf{X}(t))dt + \sum_j \mathfrak{B}_{ij}(\mathbf{X}(t))dW_j(t), \qquad (79)$$

where $\mathfrak{B}_{ij}$ verifies property (78). It can be shown, for example by stochastic Taylor expansions [17], that a predictor–corrector scheme of the type

$$\begin{cases} \tilde{X}_i^{n+1} = X_i^n + \mathfrak{A}_i^n \Delta t + \sum_j \mathfrak{B}_{ij}^n \Delta W_j, \\[2mm] X_i^{n+1} = X_i^n + \dfrac{1}{2}(\mathfrak{A}_i^n + \tilde{\mathfrak{A}}_i^{n+1})\Delta t \\[2mm] \qquad\qquad + \sum_j \dfrac{1}{2}(\mathfrak{B}_{ij}^n + \tilde{\mathfrak{B}}_{ij}^{n+1})\Delta W_j, \end{cases} \qquad (80)$$

is a weak second-order scheme: $\tilde{\mathfrak{A}}_i^{n+1} = \mathfrak{A}_i(\tilde{\mathbf{X}}^{n+1})$), $\tilde{\mathfrak{B}}_{ij}^{n+1} = \mathfrak{B}_{ij}(\tilde{\mathbf{X}}^{n+1})$, $\Delta t = t_{n+1} - t_n$ and $\Delta W_j = W_j^{n+1} - W_j^n$. This result is true, once again, only when the diffusion matrix verifies property (78), cf. Ref. [47]. If this property is not verified, the problem is more complex and other terms are needed to enforce second-order accuracy, see for example [32]. Since the predictor step of the scheme above is the Euler scheme (already developed in Section 5.3.3), the remaining task consists in finding a suitable correction step, which ensures the fulfilment of the constraints listed above.

5.3.4.3. Derivation of the numerical scheme. How should the coefficients of the predictor step, $\tilde{\mathfrak{A}}_i^{n+1}$ and

$\tilde{\mathfrak{B}}_{ij}^{n+1}$, be computed? The main idea here is to generate a correction step based on the analytical solutions by considering that the acceleration terms vary linearly with time. This idea originates from considerations related to Taylor series expansions. The numerical solution obtained from the analytical solution with constant coefficients is an approximation of first-order accuracy. Mathematically, the solution is given in terms of the integral of acceleration terms. Thus, one can state that the solution based on the zeroth order (constant terms) development of the acceleration terms gives a first-order approximation in time. By analogy, it can be guessed that approximating the acceleration terms by piecewise linear functions in time yields a second-order approximation in time.

Let us introduce the following notation: $\tilde{U}_{p,i}^{n+1}$ and $\tilde{U}_{s,i}^{n+1}$ stand for the predicted velocities and $\tilde{T}_i^{n+1}$ and $\tilde{\tau}_p^{n+1}$ are the predicted timescales. The values of the fields related to the fluid taken at $(t_{n+1}, \mathbf{x}_p^{n+1})$ are denoted, for example, $\langle U_i^{n+1} \rangle$ or $\langle P^{n+1} \rangle$. As far as the computation of the mean fields extracted from the discrete particles are concerned, it is worth emphasising that none of them are computed at $(t_{n+1}, \mathbf{x}_p^{n+1})$, because the scheme would become implicit, i.e. fields such as the expected value of the particle velocity are computed from the predicted velocities. For example, one has

$$\begin{aligned} C_i(t_{n+1}, \mathbf{x}_p^{n+1}) &= C_i^{n+1} \\ &= \frac{\langle U_i^{n+1} \rangle}{\tilde{T}_i^{n+1}} + f(\langle \tilde{\mathbf{U}}_p^{n+1} \rangle, \langle \mathbf{U}^{n+1} \rangle, \langle P^{n+1} \rangle). \end{aligned} \qquad (81)$$

Let us first consider the fluid velocity seen. The analytical solution to system (40) when the coefficients are constant is, by applying the rules of Itô's calculus

$$\begin{aligned} U_{s,i}(t) = {}&U_{s,i}(t_0)\exp(-\Delta t/T_i) \\ &+ \int_{t_0}^{t} C_i(s, \mathbf{x}_p)\exp[(s-t)/T_i]ds + \gamma_i(t), \end{aligned} \qquad (82)$$

where the temporal coefficients (the timescales) are considered constant, while the term C_i is retained in the integral. Following the previous ideas, let us suppose that $C_i(s, \mathbf{x}_p)$ varies linearly on the integration interval $[t_0, t]$, i.e. ($\Delta t = t - t_0$)

$$\begin{aligned} C_i(s, \mathbf{x}_p(s)) = {}&C_i(t_0, \mathbf{x}_p(t_0)) + \frac{1}{\Delta t}[C_i(t, \mathbf{x}_p(t)) \\ &- C_i(t_0, \mathbf{x}_p(t_0))](s - t_0). \end{aligned} \qquad (83)$$

By inserting Eq. (83) into Eq. (82), integration gives

$$U_{s,i}(t) = U_{s,i}(t_0)\exp(-\Delta t/T_i)$$

$$+ [T_i C_i(t_0, \mathbf{x}_p(t_0))]A_2(\Delta t, T_i)$$

$$+ [T_i C_i(t, \mathbf{x}_p(t))]B_2(\Delta t, T_i) + \gamma_i(t), \quad (84)$$

where the functions $A_2(\Delta t, x)$ and $B_2(\Delta t, x)$ are given by (x is a positive real variable)

$$\begin{cases} A_2(\Delta t, x) = -\exp(-\Delta t/x) + [1 - \exp(-\Delta t/x)][\Delta t/x], \\ B_2(\Delta t, x) = 1 - [1 - \exp(-\Delta t/x)][\Delta t/x]. \end{cases}$$
$$(85)$$

Accounting for the time dependence of the coefficients, i.e. T_i, it is proposed to write the following correction step, which is in line with the treatment of the acceleration terms

$$U_{s,i}^{n+1} = \frac{1}{2} U_{s,i}^n \exp(-\Delta t/T_i^n)$$

$$+ \frac{1}{2} U_{s,i}^n \exp(-\Delta t/\tilde{T}_i^{n+1}) + A_2(\Delta t, T_i^n)$$

$$\times [T_i^n C_i^n] + B_2(\Delta t, \tilde{T}_i^{n+1})[\tilde{T}_i^{n+1} C_i^{n+1}] + \tilde{\gamma}_i^{n+1},$$
$$(86)$$

where a consistent formulation for the stochastic integral $\tilde{\gamma}_i^{n+1}$ is needed. The same procedure is used, i.e. the diffusion matrix B_{ij} is linearised and integration is carried out. The final expression is

$$\tilde{\gamma}_i^{n+1} = \sqrt{[B_i^*]^2 \frac{\tilde{T}_i^{n+1}}{2} [1 - \exp(-2\Delta t/\tilde{T}_i^{n+1})]}\mathcal{G}_{1,i}, \quad (87)$$

where $\mathcal{G}_{1,i}$ is the same $\mathcal{N}(0, 1)$ random variable used in the simulation of γ_i^n in the Euler scheme (cf. Table 4) and where B_i^* is defined by

$$[1 - \exp(-2\Delta t/\tilde{T}_i^{n+1})]B_i^*$$

$$= A_2(2\Delta t, \tilde{T}_i^{n+1})\sqrt{(B_i^n)^2} + B_2(2\Delta t, \tilde{T}_i^{n+1})\sqrt{(\tilde{B}_i^{n+1})^2}.$$
$$(88)$$

Here, some explanations must be given. During integration, another step is necessary in order to achieve the closed form presented in Eq. (88). Indeed, two parts derive from the integration by parts carried out when B_{ij} varies linearly. The first term is an analytical function, while the second term is still a stochastic integral, therefore the global integral can be written formally $\tilde{\gamma}_i^{n+1} = \delta_1 + \delta_2$. It has been considered that a projection of this second integral on the first remains of second-order accuracy for the global scheme. Therefore, the following hypothesis has been used, $\delta_2 \approx (\langle \delta_1 \delta_2 \rangle / \langle \delta_1^2 \rangle)\delta_1$.

In the case of the velocity of the particles, the same approach followed for the fluid velocity seen is adopted. Let us start from the exact solution with constant coefficients for $\mathbf{U}_p(t)$. By resorting to the rules of Itô's calculus, one can write

$$U_{p,i}(t) = U_{p,i}(t_0)\exp(-\Delta t/\tau_p) + \frac{1}{\tau_p}\exp(-\Delta t/\tau_p)$$

$$\times \int_{t_0}^{t} \exp(s/\tau_p)[U_{s,i}(s) + \tau_p \mathcal{A}_i(s, \mathbf{x}_p)]\mathrm{d}s, \quad (89)$$

and by inserting Eq. (82) in the previous equation, one has

$$U_{p,i}(t)$$
$$= U_{p,i}(t_0)\exp(-\Delta t/\tau_p) + U_{s,i}(t_0)\theta_i[\exp(-\Delta t/T_i)$$

$$- \exp(-\Delta t/\tau_p)] + \Gamma_i(t) + \frac{1}{\tau_p}\exp(-t/\tau_p)\int_{t_0}^{t}\exp(s/\tau_p)$$

$$\times \left[\exp(-s/T_i)\int_{t_0}^{s} C_i(u, \mathbf{x}_p)\exp(u/T_i)\mathrm{d}u + \tau_p \mathcal{A}_i(s, \mathbf{x}_p)\right]\mathrm{d}s.$$
$$(90)$$

Two deterministic integrals must be treated in Eq. (90). A multiple one, involving $C_i(t, \mathbf{x}_p)$ and a simple one with the acceleration term $\mathcal{A}_i(t, \mathbf{x}_p)$. Both integrals are handled as done previously for the fluid velocity seen, i.e. it is assumed that both accelerations vary linearly on the integration interval, see for example Eq. (83) for $C_i(t, \mathbf{x}_p)$. By integration by parts of both integrals, one finds after some derivations

$$U_{p,i}(t) = U_{p,i}(t_0)\exp(-\Delta t/\tau_p) + U_{s,i}(t_0)\theta_i[\exp(-\Delta t/T_i)$$
$$- \exp(-\Delta t/\tau_p)] + [T_i C_i(t_0, \mathbf{x}_p(t_0))]A_{2c}(\tau_p, T_i)$$
$$+ [T_i C_i(t, \mathbf{x}_p(t))]B_{2c}(\tau_p, T_i)$$
$$+ [\tau_p \mathcal{A}_i(t_0, \mathbf{x}_p(t_0))]A_2(\Delta t, \tau_p)$$
$$+ [\tau_p \mathcal{A}_i(t, \mathbf{x}_p(t))]B_2(\Delta t, \tau_p) + \Gamma_i(t),$$
$$(91)$$

where the functions $C_{2c}(x, y)$, $A_{2c}(x, y)$ and $B_{2c}(x, y)$ are given by (x and y are two positive real variables)

$$\begin{cases} C_{2c}(x, y) = [y/(y-x)][\exp(-\Delta t/y) - \exp(-\Delta t/x)], \\ A_{2c}(x, y) = -\exp(-\Delta t/x) + [(x+y)/\Delta t] \\ \qquad\qquad \times [1 - \exp(-\Delta t/x)] - (1 + y/\Delta t)C_{2c}(x, y), \\ B_{2c}(x, y) = 1 - [(x+y)/\Delta t][1 - \exp(-\Delta t/x)] \\ \qquad\qquad + (y/\Delta t)C_{2c}(x, y). \end{cases}$$
$$(92)$$

In analogy with the expression proposed for the fluid velocity seen, cf. Eq. (86), the following correction step is proposed

$$
\begin{aligned}
U_{\mathrm{p},i}^{n+1} =& \frac{1}{2} U_{\mathrm{p},i}^n \exp(-\Delta t/\tau_{\mathrm{p}}^n) + \frac{1}{2} U_{\mathrm{p},i}^n \exp(-\Delta t/\tilde{\tau}_{\mathrm{p}}^{n+1}) \\
& + \frac{1}{2} U_{\mathrm{s},i}^n C_{2c}(\tau_{\mathrm{p}}^n, T_i^n) + \frac{1}{2} U_{\mathrm{s},i}^n C_{2c}(\tilde{\tau}_{\mathrm{p}}^{n+1}, \tilde{T}_i^{n+1}) \\
& + A_{2c}(\tau_{\mathrm{p}}^n, T_i^n)[\tau_i^n C_i^n] \\
& + B_{2c}(\tilde{\tau}_{\mathrm{p}}^{n+1}, \tilde{T}_i^{n+1})[\tilde{T}_i^{n+1} C_i^{n+1}] \\
& + A_2(\Delta t, \tau_{\mathrm{p}}^n)[\tau_{\mathrm{p}}^n \mathcal{A}_i^n] \\
& + B_2(\Delta t, \tilde{\tau}_{\mathrm{p}}^{n+1})[\tilde{\tau}_{\mathrm{p}}^{n+1} \mathcal{A}_i^{n+1}] + \tilde{I}_i^{n+1}. \quad (93)
\end{aligned}
$$

For the simulation of the stochastic integral, one has ($\mathcal{G}_{2,i}$ is the $\mathcal{N}(0, 1)$ random variable used in the simulation of Γ_i^n in the Euler scheme, see Table 4)

$$
\begin{aligned}
\tilde{I}_i^{n+1} =& \frac{\langle \tilde{I}_i^{n+1} \tilde{\gamma}_i^{n+1} \rangle}{\langle (\tilde{\gamma}_i^{n+1})^2 \rangle} \tilde{\gamma}_i^{n+1} \\
& + \sqrt{\langle (\tilde{I}_i^{n+1})^2 \rangle - \frac{[\langle \tilde{I}_i^{n+1} \tilde{\gamma}_i^{n+1} \rangle]^2}{\langle (\tilde{\gamma}_i^{n+1})^2 \rangle}} \mathcal{G}_{2,i}, \quad (94)
\end{aligned}
$$

where the second-order moments $\langle (\tilde{I}_i^{n+1})^2 \rangle$ and $\langle \tilde{I}_i^{n+1} \tilde{\gamma}_i^{n+1} \rangle$ are computed from Eqs. (137) and (139), respectively, by inserting the suitable timescales and diffusion matrix, i.e. τ_{p}^n, $\tilde{T}_i^{n+1}$ and B_i^*. This completes the weak second-order scheme.

It can be shown, by means of stochastic Taylor expansion [17], that the present scheme is a weak scheme of order 2 in time for system (40). It is worth emphasising that no correction is done on position, $\mathbf{x}_{\mathrm{p}}(t)$, since the prediction is already of order 2. The complete scheme is summarised in Table 5.

5.3.4.4. Limit cases. In limit case 1, when $1 \ll \Delta t/\tau_{\mathrm{p}}$, one has $A_{2c}(\tau_{\mathrm{p}}, T_i) \rightarrow A_2(\Delta t, T_i)$, $B_{2c}(\tau_{\mathrm{p}}, T_i) \rightarrow B_2(\Delta t, T_i)$ and $C_{2c}(\tau_{\mathrm{p}}, T_i) \rightarrow \exp(-\Delta t/T_i)$. For the stochastic integral, one can show that $\tilde{I}_i^{n+1} \rightarrow \tilde{\gamma}_i^{n+1}$. Inserting these results in Eq. (93) yields $U_{\mathrm{p},i}^{n+1} = U_{\mathrm{s},i}^{n+1}$, which is consistent with Eq. (41). This result is a second-order scheme for $\mathbf{U}_{\mathrm{p}}(t)$, and therefore the scheme remains of order 2 in limit case 1.

When $1 \ll \Delta t/T_i$ and $\check{B}_i T_i = \mathrm{cst}$ (limit case 2), one has $A_{2c}(\tau_{\mathrm{p}}, T_i) \rightarrow A_2(\Delta t, \tau_{\mathrm{p}})$ and $B_{2c}(\tau_{\mathrm{p}}, T_i) \rightarrow B_2(\Delta t, \tau_{\mathrm{p}})$, which gives for the numerical correction of the velocity of the particles

$$
\begin{aligned}
U_{\mathrm{p},i}^{n+1} =& \frac{1}{2} U_{\mathrm{p},i}^n \exp(-\Delta t/\tau_{\mathrm{p}}^n) \\
& + \frac{1}{2} U_{\mathrm{p},i}^n \exp(-\Delta t/\tilde{\tau}_{\mathrm{p}}^{n+1}) + A_2(\Delta t, \tau_{\mathrm{p}}^n) \\
& \times [\langle U_i^n \rangle + \tau_{\mathrm{p}}^n \mathcal{A}_i^n] + B_2(\Delta t, \tilde{\tau}_{\mathrm{p}}^{n+1})[\langle U_i^{n+1} \rangle \\
& + \tilde{\tau}_{\mathrm{p}}^{n+1} \mathcal{A}_i^{n+1}] + \tilde{I}_i^{n+1}. \quad (95)
\end{aligned}
$$

For the simulation of the stochastic integral, one can prove by looking at the limit values (when $1 \ll \Delta t/T_i$ and $\check{B}_i T_i = \mathrm{cst}$) in Eqs. (136), (137) and (139) that (here $\mathcal{G}'_{\mathrm{p},i}$ is a $\mathcal{N}(0, 1)$ random variable)

$$
\tilde{I}_i^{n+1} \rightarrow \sqrt{\frac{[B_i^* \tilde{T}_i^{n+1}]^2}{2\tau_{\mathrm{p}}^n} [1 - \exp(-2\Delta t/\tau_{\mathrm{p}}^n)]} \mathcal{G}'_{\mathrm{p},i}, \quad (96)
$$

which is in accordance with Eq. (72). Unfortunately, it can be established, again by Taylor stochastic expansion, that the scheme is not of second-order in time for system (42), but of first order. This is due to the treatment of the correction step for the stochastic integral $\Gamma_i(t)$ where τ_{p}^n has been retained in order to avoid anticipation and inconsistent numerical expressions of the Itô integral. As far as the fluid velocity seen is concerned, one has

$$
U_{\mathrm{s},i}^{n+1} = \langle U_i^{n+1} \rangle + \sqrt{\frac{[B_i^*]^2 \tilde{T}_i^{n+1}}{2}} \mathcal{G}_{1,i}, \quad (97)
$$

which is in line with the previous result. This scheme is of second order, but the whole scheme is not. Indeed, as mentioned above, the scheme is only of first order for the velocity of the particles.

When both the fluid velocity seen and the velocity of the particles become fast variables (limit case 3), i.e. when $1 \ll \Delta t/T_i$, $1 \ll \Delta t/\tau_{\mathrm{p}}$ and $\check{B}_i T_i = \mathrm{cst}$, one can write for the velocity of the particle, for example from Eq. (95) with $1 \ll \Delta t/\tau_{\mathrm{p}}$

$$
U_{\mathrm{p},i}^{n+1} = \langle U_i^{n+1} \rangle + \tilde{\tau}_{\mathrm{p}}^{n+1} \mathcal{A}_i^{n+1} + \sqrt{\frac{[B_i^* \tilde{T}_i^{n+1}]^2}{2\tau_{\mathrm{p}}^n}} \mathcal{G}'_{\mathrm{p},i}. \quad (98)
$$

For the fluid velocity seen, Eq. (97) is unchanged. These results are consistent with the expressions of Section 5.3.3. In limit case 3, the numerical scheme for the position of the particles is equivalent to the Euler scheme written previously and is of first order in time.

When the flow becomes laminar, i.e. when $T_i \rightarrow 0$ with no condition on the product $\check{B}_i T_i$, one has the following limits: $A_2(\Delta t, T_i) \rightarrow 0$, $B_2(\Delta t, T_i) \rightarrow 1$ and

Table 5
Weak second-order scheme

Prediction step: Euler scheme, see Table 4.
Correction step:

$$U_{p,i}^{n+1} = \frac{1}{2} U_{p,i}^n \exp(-\Delta t/\tau_p^n) + \frac{1}{2} U_{p,i}^n \exp(-\Delta t/\tilde{\tau}_p^{n+1}) + \frac{1}{2} U_{s,i}^n C_{2c}(\tau_p^n, T_i^n) + \frac{1}{2} U_{s,i}^n C_{2c}(\tilde{\tau}_p^{n+1}, \tilde{T}_i^{n+1}) + A_{2c}(\tau_p^n, T_i^n)[T_i^n C_i^n] + B_{2c}(\tilde{\tau}_p^{n+1}, \tilde{T}_i^{n+1})[\tilde{T}_i^{n+1} C_i^{n+1}]$$

$$+ A_2(\Delta t, \tau_p^n)[\tau_p^n \mathcal{A}_i^n] + B_2(\Delta t, \tilde{\tau}_p^{n+1})[\tilde{\tau}_p^{n+1} \mathcal{A}_i^{n+1}] + \tilde{I}_i^{n+1},$$

$$U_{s,i}^{n+1} = \frac{1}{2} U_{s,i}^n \exp(-\Delta t/T_i^n) + \frac{1}{2} U_{s,i}^n \exp(-\Delta t/\tilde{T}_i^{n+1}) + A_2(\Delta t, T_i^n)[T_i^n C_i^n] + B_2(\Delta t, \tilde{T}_i^{n+1})[\tilde{T}_i^{n+1} C_i^{n+1}] + \tilde{\gamma}_i^{n+1}.$$

The coefficients A_2, B_2, A_{2c} and C_{2c} are defined as:

$$A_2(\Delta t, x) = -\exp(-\Delta t/x) + [1 - \exp(-\Delta t/x)][\Delta t/x],$$

$$B_2(\Delta t, x) = 1 - [1 - \exp(-\Delta t/x)][\Delta t/x],$$

$$A_{2c}(x, y) = -\exp(-\Delta t/x) + [(x + y)/\Delta t][1 - \exp(-\Delta t/x)] - (1 + y/\Delta t)C_{2c}(x, y),$$

$$B_{2c}(x, y) = 1 - [(x + y)/\Delta t][1 - \exp(-\Delta t/x)] + (y/\Delta t)C_{2c}(x, y),$$

$$C_{2c}(x, y) = [y/(y - x)][\exp(-\Delta t/y) - \exp(-\Delta t/x)].$$

The stochastic integrals $\tilde{\gamma}_i^{n+1}$ and $\tilde{I}_i^{n+1}$ are simulated as follows:

$$\tilde{\gamma}_i^{n+1} = \sqrt{\frac{[B_i^*]^2 \tilde{T}_i^{n+1}}{2}[1 - \exp(-2\Delta t/\tilde{T}_i^{n+1})]} \mathcal{G}_{1,i},$$

with $[1 - \exp(-2\Delta t/\tilde{T}_i^{n+1})]B_i^* = A_2(2\Delta t, \tilde{T}_i^{n+1})\sqrt{(B_i^n)^2} + B_2(2\Delta t, \tilde{T}_i^{n+1})\sqrt{(\tilde{B}_i^{n+1})^2}.$

$$\tilde{I}_i^{n+1} = \frac{\langle \tilde{I}_i^{n+1} \tilde{\gamma}_i^{n+1} \rangle}{\langle (\tilde{\gamma}_i^{n+1})^2 \rangle} \tilde{\gamma}_i^{n+1} + \sqrt{\langle (\tilde{I}_i^{n+1})^2 \rangle - \frac{\langle \tilde{I}_i^{n+1} \tilde{\gamma}_i^{n+1} \rangle^2}{\langle (\tilde{\gamma}_i^{n+1})^2 \rangle}} \mathcal{G}_{2,i}$$

with $\langle \tilde{I}_i^{n+1} \tilde{\gamma}_i^{n+1} \rangle = \langle \Gamma_i \gamma_i \rangle (\tau_p^n, \tilde{T}_i^{n+1}, B_i^*)$ and $\langle (\tilde{I}_i^{n+1})^2 \rangle = \langle \Gamma_i^2 \rangle (\tau_p^n, \tilde{T}_i^{n+1}, B_i^*).$

$\gamma_i(t) \to 0$, which gives $U_{s,i}^{n+1} = \langle U_i^{n+1} \rangle$ for the fluid velocity seen. For the velocity of the particles, the coefficients have the following limits: $A_{2c}(\tau_p, T_i) \to A_2(\Delta t, \tau_p)$, $B_{2c}(\tau_p, T_i) \to B_2(\Delta t, \tau_p)$ and $C_{2c}(\tau_p, T_i) \to 0$ which gives together with the limit $\Gamma_i(t) \to 0$

$$U_{p,i}^{n+1} = \frac{1}{2} U_{p,i}^n \exp(-\Delta t/\tau_p^n) + \frac{1}{2} U_{p,i}^n exp(-\Delta t/\tilde{\tau}_p^{n+1})$$
$$+ A_2(\Delta t, \tau_p^n)[\langle U_i^n \rangle + \tau_p^n \mathcal{A}_i^n]$$
$$+ B_2(\Delta t, \tilde{\tau}_p^{n+1})[\langle U_i^{n+1} \rangle + \tilde{\tau}_p^{n+1} \mathcal{A}_i^{n+1}].$$
(99)

It can be shown, by regular Taylor expansion, that this scheme, together with the prediction step (Euler scheme) is a second-order scheme for system (44).

In summary, a weak second-order scheme for system (40) has been derived. This scheme satisfies all conditions listed in Section 5.3. However, second-order convergence is not obtained in limit cases 2 and 3. In this latter case, the first-order convergence is inherent to the spirit of the scheme, i.e. a single step to compute position $\mathbf{x}_p(t)$ (in order to minimise the number of particle localisations in the algorithm).

6. Specific and open issues

The main objective of this paper is to present a consistent and rigorous numerical method for the computations of polydispersed turbulent two-phase

flows using a mean-field/PDF approach. The mathematical framework and the models used in this approach have been put forward (Sections 2 and 3) and a general methodology for the derivation of weak numerical schemes for the set of SDEs describing the dynamics of the stochastic particles has been given in the context of particle-mesh methods (Sections 4 and 5).

In this general methodology, the derivation of the weak numerical schemes has been performed only in the case of one-way coupling. As mentioned before, this is not a limitation of the methodology and it is simply the status of the developments so far. The extension of the present results to two-way coupling is now discussed. Two issues are addressed:

(i) the computations of the source terms in the PDEs describing the dynamics of the fluid mean fields. When two-way coupling is accounted for. When the particle mass fraction is high enough and the influence of the particles on the fluid mean fields must be taken into account, particle source terms are added to the fluid equations, cf. Eqs. (125) and (126),

(ii) the extension of the methodology introduced in Sections 4 and 5, i.e. when two-way coupling is considered, an acceleration is added to the SDE describing the dynamics of the fluid velocity seen, cf. Eqs. (28) and (29), and the structure of the system of SDEs is changed.

The first point is a specific issue, i.e. a practical solution is given for the computational procedure of the source terms. The second point is considered as an open issue since only explanations on the procedure to follow, for the extension of the weak numerical schemes to two-way coupling, are provided.

After the treatment of the two-way coupling issues and before showing computational examples, some possible improvements and some open questions related to the numerical method will be discussed. The list of open questions related to the present numerical (particle-mesh) method is long. Here, attention is focused on two open issues:

(iii) the formulation of boundary conditions in wall-bounded flows,

(iv) the development of new numerical methods based on the present one.

We start now with aspects related to two-way coupling, i.e. issues (i) and (ii).

6.1. Computation of the source terms

As can be seen from the equations given in Table 1, i.e. Eqs. (125) and (126), two source terms are present when two-way coupling is considered. The first one, say $\mathbf{S}_U$, represents the exchange of momentum between the discrete particles and the fluid. In the present paper, the only force exerted by the fluid on the discrete particles is the drag force, see Eqs. (1), and by reaction the force exerted by the particles on the fluid is the reverse drag force. The mean momentum source term is expressed by

$$(S_U)_i = \chi \left\langle \frac{U_{p,i} - U_{s,i}}{\tau_p} \right\rangle, \qquad (100)$$

where $\chi = (\alpha_p \rho_p)/(\alpha_f \rho_f)$. From the particle equation of motion, cf. Eqs. (29), the drag term is equal to the discrete particle acceleration (when gravity is first subtracted) and $\mathbf{S}_U$ can be re-expressed as

$$(S_U)_i = -\chi \left\langle \frac{dU_{p,i}}{dt} \right\rangle. \qquad (101)$$

From the discrete point of view, if we use the NGP technique, as explained in Section 5.2.1, for the sake of simplicity (since most of what is presented below concern particle instantaneous quantities that can be put within the CIC formalism), this source term is the sum of the reverse drag force due to the discrete particles that are found in a given fluid cell. Then, the total fluid momentum in a cell $[k]$, whose volume is $\mathcal{V}_f^{[k]}$ can be written as

$$\alpha_f \rho_f \mathcal{V}_f^{[k]} (S_U)_i^{[k]} = \sum_{l=1}^{N_k} m_p^l \frac{(U_{p,i}^l)^{n+1} - (U_{s,i}^l)^n}{\Delta t}, \qquad (102)$$

where m_p^l and $U_{p,i}^l$ stand for the mass and the velocity of the discrete particle labelled l, respectively. The sum is performed over the N_k particles that are located in cell $[k]$ at iteration n ($t = n\Delta t$).

The source term for the fluid Reynolds-stress equations, see Eq. (126), raises new questions and its numerical evaluation is an interesting example of the specificities of stochastic calculus, cf. Section 2.2. For the discussion of its expression, we limit ourselves to the simplified case of a stationary one-dimensional system and to the source term, S_k, for the fluid kinetic energy k. The system of SDEs that we consider is

$$\begin{cases} dU_p(t) = \dfrac{U_s(t) - U_p(t)}{\tau_p} dt, \\[4mm] dU_s(t) = -\dfrac{U_s(t)}{T} dt - \chi \left(\dfrac{U_s(t) - U_p(t)}{\tau_p} \right) dt + \sqrt{K}\, dW(t), \end{cases}$$

$$(103)$$

and the fluid kinetic source term which represents the work performed by the drag force is

$$S_k = \chi \left\langle U_s \left(\frac{U_p - U_s}{\tau_p} \right) \right\rangle. \tag{104}$$

For this simplified case, and when the coefficients of the equations are constant, we can derive the analytical expression of the second-order moments. Indeed, for a long-enough time after the initial conditions, the stochastic process $\mathbf{Z}(t) = \{U_p(t), U_s(t)\}$ (since here $x_p(t)$ is irrelevant) reaches a stationary state and $\langle U_p^2 \rangle$, $\langle U_p U_s \rangle$ and $\langle U_s^2 \rangle$ become constant. Therefore, using Itô's calculus, we have that

$$\begin{cases} d\langle U_p^2 \rangle = 2\langle U_p\, dU_p \rangle = 0, \\[2mm] d\langle U_p U_s \rangle = \langle U_p\, dU_s + U_s\, dU_p \rangle = 0, \\[2mm] d\langle U_s^2 \rangle = 2\langle U_s\, dU_s \rangle + K\, dt = 0. \end{cases} \tag{105}$$

The first two equations yield the equilibrium formulae for the second-order moments

$$\begin{cases} \langle U_p^2 \rangle = \langle U_p U_s \rangle, \\[2mm] \langle U_p U_s \rangle = \langle U_s^2 \rangle \dfrac{1}{1 + \tau_p/T}, \end{cases} \tag{106}$$

while the third one gives the expression of the diffusion coefficient K to maintain a constant value of the fluid kinetic energy

$$K = 2\langle U_s^2 \rangle \left(\frac{1}{T} + \frac{\chi}{T + \tau_p} \right). \tag{107}$$

Using these formulae, the (equilibrium) analytical expression of the kinetic source term can be written as

$$S_k = -\chi \langle U_s^2 \rangle \frac{1}{T + \tau_p}. \tag{108}$$

This source term is always negative which indicates that the drag force, which is indeed a friction force, induces a loss of energy in the fluid energy budget. This is valid for the total energy budget, whereas if we consider the fluid energy spectrum and its modulation by particles, particles may enhance turbulence at some lengthscales (or wave numbers) due, for example, to wakes generated behind the particles. In the present

model, we consider only S_k, which is the integrated value of the exchange term over the whole spectrum, and, if we leave out the (possible) energy injected from particles by their initial conditions, the total energy gained by the particles comes from the fluid and the fluid kinetic energy source term is negative. However, when $\tau_p \to 0$, i.e. when the discrete particles behave as fluid elements (but with a constant mass fraction, χ), we expect the kinetic source term to vanish ($S_k \to 0$) since we consider a stationary case. Yet, from Eq. (108), it is seen that the limit is

$$S_k \xrightarrow[\tau_p \to 0]{} -\chi \langle U_s^2 \rangle \frac{1}{T}. \tag{109}$$

This spurious non-zero limit for vanishing particle characteristic timescale can be traced back to the Langevin model and is related to the fact that acceleration is indeed replaced by a white-noise term, cf. in Ref. [8, Chapter 6.8].

Nevertheless, it is possible to retrieve the correct limit in the numerical evaluation of S_k by resorting to a discretisation based on the Stratonovich definition, see Section 2.2. The first step is to write the source term with the particle acceleration as

$$S_k = -\chi \left\langle U_s \frac{dU_p}{dt} \right\rangle. \tag{110}$$

Therefore, if we consider the integration of the source term in a time interval, we get

$$S_k\, dt = -\chi \langle U_s\, dU_p \rangle \tag{111}$$

and, in a formal sense, when $\tau_p \to 0$, we expect the source term to become

$$S_k\, dt \to -\chi \langle U_s\, dU_s \rangle, \tag{112}$$

since in that case $U_p \to U_s$, cf. Eq. (41) in Section 4.2. Now, from Section 2.2, we know that the above expression can have different meanings. If we decide to regard the term $\langle U_s\, dU_s \rangle$ as being defined in the Itô sense, as it should be in order to be consistent with the algebra retained throughout the paper, we would find the non-zero limit given above. Yet, if for this expression of the source term, we decide to consider it as being defined in the Stratonovich sense, then

$$S_k\, dt \xrightarrow[\tau_p \to 0]{} -\chi \langle U_s \circ dU_s \rangle = -\frac{\chi}{2} \langle d(U_s)^2 \rangle, \tag{113}$$

which is indeed zero since we are in a stationary case.

The difference between the two stochastic calculus is only presented here since it provides a useful guideline. In the present case, it is seen that the interest

of the Stratonovich expression is that the formal quantity dU_s/dt can still be handled as if it were a normal derivative (and, in our case, the limit of dU_p/dt when $\tau_p \to 0$). This suggests therefore to express the kinetic source term numerically, in a fluid cell $[k]$ at time $t = n\,\Delta t$ with N_k particles, as

$$\alpha_f \rho_f \mathcal{V}_f^{[k]} S_k^{[k]} = -\sum_{l=1}^{N_k} m_p^l \frac{1}{2}((U_s^l)^{n+1} + (U_s^l)^n)$$

$$\times \frac{(U_p^l)^{n+1} - (U_p^l)^n}{\Delta t}. \tag{114}$$

From the properties of the numerical schemes developed in the previous sections, we have that $(U_p^l)^n \to (U_s^l)^n$ when $\tau_p \to 0$. Thus, in that limit

$$\alpha_f \rho_f \mathcal{V}_f^{[k]} S_k^{[k]} \to -\sum_{l=1}^{N_k} m_p^l \frac{1}{2}((U_s^l)^{n+1} + (U_s^l)^n)$$

$$\times \frac{(U_s^l)^{n+1} - (U_s^l)^n}{\Delta t} = -\sum_{l=1}^{N_k} m_p^l \frac{1}{2}([(U_s^l)^{n+1}]^2 - [(U_s^l)^n]^2)$$

$$\simeq \alpha_p \rho_p \mathcal{V}_f^{[k]} \langle [(U_s^l)^{n+1}]^2 - [(U_s^l)^n]^2 \rangle \tag{115}$$

and when the stationarity of U_s is indeed enforced numerically, this term is zero. Finally, going back to the exact fluid Reynolds stress equations, we propose to express the numerical source terms as

$$\alpha_f \rho_f \mathcal{V}_f^{[k]} S_{R_{ij}}^{[k]} = -\sum_{l=1}^{N_k} m_p^l \left\{ \frac{1}{2}[(U_{s,j}^l)^{n+1} \right.$$

$$+ (U_{s,j}^l)^n] \frac{(U_{p,i}^l)^{n+1} - (U_{p,i}^l)^n}{\Delta t} + \frac{1}{2}[(U_{s,i}^l)^{n+1}$$

$$\left. + (U_{s,i}^l)^n] \frac{(U_{p,j}^l)^{n+1} - (U_{p,j}^l)^n}{\Delta t} \right\}. \tag{116}$$

As mentioned at the beginning of this section, most of the arguments that have been presented concern the discrete evaluation of each particle term $U_s(dU_p/dt)$. The expression proposed above in the NGP formulation can be used directly within the CIC technique. Another interesting question is to ask to what cell (or cells) the different source terms should be assigned. Indeed, within one time step, particles may cross several fluid cells and the source terms, say S_U and S_R, which represent the total momentum and energy exchange terms, should be distributed between the different cells crossed by the particles. One possibility is to apply to each fluid cell crossed by a particle, the different reverse expressions, say dU_p/dt and $U_s(dU_p/dt)$ in proportion of the time spent in that cell (the residence time) which is then a fraction of the time step. This is

probably the most precise expression and the most accurate discrete formulation, but it implies to keep track of the different fluid cells along the particle trajectory within one time step. In a complex geometry discretised with unstructured meshes, given present localisation algorithms, this is not an easy task and it induces computational overloads. For these reasons, at the moment, it is proposed to evaluate the total source terms from the particles that were located in that cell at the beginning of the time step. This evaluation has been applied in various computational examples presented in Section 7. It can be seen as a first-order spatial approximation or based on an implicit assumption that the particle Courant number remains of order one in most cases.

6.2. Extension of the weak numerical schemes

When two-way coupling is accounted for, the SDE describing the dynamics of the fluid velocity seen is supplemented with an acceleration term, cf. Eqs. (28) and (29), in order to account for the influence of the discrete particles on the statistics of the fluid velocity sampled along the trajectory of a discrete particle. This supplementary acceleration changes drastically the nature of the equation system and one has (the equation for position is omitted for the sake of clarity)

$$\begin{cases} dU_{p,i}(t) = -\frac{1}{\tau_p} U_{p,i}\,dt + \frac{1}{\tau_p} U_{s,i}\,dt + g_i\,dt, \\ \\ dU_{s,i}(t) = \frac{\chi}{\tau_p} U_{p,i}\,dt - \left(\frac{1}{T_i} + \frac{\chi}{\tau_p}\right) U_{s,i}\,dt + C_i\,dt \\ \qquad\qquad + \sum_j B_{ij}\,dW_j(t), \end{cases} \tag{117}$$

i.e. the SDE for the fluid velocity seen, $\mathbf{U}_s(t)$, depends explicitly on the velocity of the discrete particle, $\mathbf{U}_p(t)$. This dependence complicates the analysis of the system, in particular the limit systems when the timescales go to zero, cf. Section 4. If one is able to find the limit systems in the continuous sense, the extension of the numerical schemes can be obtained in the same way as presented in Section 5.3. However, in order to calculate the analytical solution with constant coefficients, one has to express the following matrix in diagonal or triangular form (depending on the roots of the characteristic polynomial)

$$\begin{bmatrix} -1/\tau_{\mathrm{p}} & 1/\tau_{\mathrm{p}} \\ \chi/\tau_{\mathrm{p}} & -(1/T_i + \chi/\tau_{\mathrm{p}}) \end{bmatrix}. \tag{118}$$

Once this is done, the previous analysis can be used, but in the frame of much more complex algebra. Once the analytical solution is obtained for the eigensystem, one has to go back to the original system (state vector) with some transformation matrix (which is formed by the eigenvectors).

This difficulty is actually not a typical feature of two-way coupling. As a matter of fact, in the one-way coupling case, if the alternative model is chosen, cf. Section 3.1.2, the drift term is written in terms of the local instantaneous velocities. Therefore, an acceleration, which has the same form as $\mathbf{A}_{\mathrm{p}\rightarrow\mathrm{s}}$, is introduced

$$\sum_j \frac{1}{T_{ij}}(U_{\mathrm{p},j} - U_{\mathrm{s},j}), \tag{119}$$

where the timescales of the mean flow, T_{ij}, are given by $T_{ij}^{-1} = \partial \langle U_i \rangle / \partial x_j$. As a consequence, if such a model is used for the drift term, the problems inherent to the derivation of the present schemes with two-way coupling are already encountered for the one-way coupling case. There is, to our knowledge, no specific work in the literature dealing with this subject.

6.3. Boundary conditions in wall-bounded flows

In the present work, for the computational examples, cf. Section 7, the wall boundary conditions for the system of SDEs are treated as follows: for the discrete particle velocity, $\mathbf{U}_{\mathrm{p}}(t)$, an elastic wall-particle collision is applied whereas for the fluid velocity seen, $\mathbf{U}_{\mathrm{s}}(t)$, we build on ideas from turbulent single-phase flows [36,49] in order to ensure consistency when $\tau_{\mathrm{p}} \rightarrow 0$. As a matter of fact, in one-point PDF models for single-phase turbulent flows, cf. Section 3.1.1, or in one-point PDF models for the discrete particles, cf. Section 3.1.2, the derivation of boundary conditions for fluid or discrete particles, when solid boundaries are present, has not received the needed attention. Here, for the sake of simplicity, we make our point by considering, as an example, only the motion of fluid particles.

In the framework of PDF methods for single-phase turbulent flows, boundary conditions of the *wall function* kind have been studied and proposed [36,50]. This solution has been investigated rigorously from the mathematical and physical (based on the knowledge of the phenomenology of the near-wall region) points of view. In practice, the numerical treatment is developed in analogy with the wall-function approach used in

RANS computations, a method which is perfectly in line with one-point high-Reynolds number PDF models. However, in some engineering applications where a precise description of the near-wall region is needed, it may be of interest to replace the wall-function boundary conditions with a direct particle-wall interaction, i.e. $\mathbf{U}_{\mathrm{f}}(t) = 0$ at the wall. According to Section 3.1.1, a one-point PDF model for single-phase turbulent flows reads

$$\begin{cases} \mathrm{d}x_{\mathrm{f},i}(t) = U_{\mathrm{f},i}(t)\mathrm{d}t, \\ \mathrm{d}U_{\mathrm{f},i}(t) = \mathfrak{A}_i(t,\mathbf{x}_{\mathrm{f}}(t),\mathbf{U}_{\mathrm{f}}(t))\mathrm{d}t + \sum_j \mathfrak{B}_{ij}(t,\mathbf{x}_{\mathrm{f}}(t))\mathrm{d}W_j(t), \end{cases} \tag{120}$$

and it has been shown in Section 5.3.4 that a possible weak second-order scheme is (when $\mathfrak{B}_{ij}$ verifies property (78))

$$\begin{cases} \tilde{x}_{\mathrm{f},i}^{n+1} = x_{\mathrm{f},i}^n + U_{\mathrm{f},i}^n \Delta t \\ \tilde{U}_{\mathrm{f},i}^{n+1} = U_{\mathrm{f},i}^n + \mathfrak{A}_i^n \Delta t + \mathfrak{B}_{ij}^n \Delta W_i(t), \\ U_{\mathrm{f},i}^{n+1} = U_{\mathrm{f},i}^n + \frac{1}{2}(\mathfrak{A}_i^n + \tilde{\mathfrak{A}}_i^{n+1})\Delta t \\ \qquad\qquad + \sum_j \frac{1}{2}(\mathfrak{B}_{ij}^n + \tilde{\mathfrak{B}}_{ij}^{n+1})\Delta W_j(t), \end{cases} \tag{121}$$

where $\tilde{\mathfrak{A}}_i^{n+1} = \mathfrak{A}_i(t+\Delta t, \tilde{x}_{\mathrm{f},i}^{n+1}, \tilde{U}_{\mathrm{f},i}^{n+1})$ and $\tilde{\mathfrak{B}}_{ij}^{n+1} = \mathfrak{B}_{ij}(t+\Delta t, \tilde{x}_{\mathrm{f},i}^{n+1})$. This scheme is used for our present discussion and it is different from the one developed above, cf. Table 5. With this *stochastic* framework in mind, some open questions remain.

  (i) Is it possible to propose a general form of wall boundary conditions for the fluid particles, independently of our particular Langevin model?
 (ii) What boundary condition ensures that the impermeability condition is valid just at the wall (as in the real world)?
(iii) What is the order of accuracy of the boundary conditions in the frame of our numerical schemes?
(iv) Is it possible to propose high-order (second-order) boundary conditions?

The above questions might seem easy to answer at first glance, but the subtleties of stochastic calculus make these open issues difficult to solve. At present, only one proposition has been made [51]. In that work, the authors have proposed to impose a zero velocity to the particles reaching the wall during a time step and to

move them in space by symmetry at the wall. The proposed treatment is sensible, but it presents some shortcomings, i.e. it remains dependent on the particular model used (a Wiener process was used in the equation for position to account for viscous effects in the vicinity of the wall), and the order of accuracy is not given. A mathematical approach to this problem can be found in the book of Öttinger [31].

The scarcity of the literature on this subject calls for future rigorous development in the formulation of boundary conditions at the wall in one-point PDF methods. A good illustration of the lack of knowledge will be presented in Section 7 for a computational example of particle deposition phenomena.

6.4. New hybrid methods

In the present work, a hybrid method has been used: the fluid is described with a mean-field (RANS) approach whereas the statistics (the pdf) of the discrete particles are reproduced by introducing stochastic particles (SDEs).

In stand-alone methods for one-point PDF models for single-phase turbulent flows, it is known that the bias (cf. Section 5.1.2) is the main concern in the control of the numerical error [41]. If this is also the case for the numerics put forward for one-point PDF models for discrete particles, every idea improving this shortcoming is welcome. A solution could be to resort to VRT that have been developed in disparate fields. A possibility could be to resort to a hybrid algorithm for the numerical treatment of the discrete particles where some variables could be solved by a mean-field method and others by a PDF method. In such configurations, duplicate fields usually arise, and consistency conditions must be imposed. These consistency conditions give the opportunity of introducing VRT. Indeed, the mean variables computed from a mean-field method are by construction not biased. If the PDF method contains the evolution in time of the corresponding instantaneous variables, the operation of centering the moments extracted from the PDF approach with the ones computed from the mean-field algorithm leads to an excellent reduction of variance [37]. Moreover, it would be helpful to find a criterion, in the frame of domain decomposition, in order to use the mean-field or PDF algorithms where it is most appropriate. For example, in some parts of the flow where the knowledge of some mean-fields is sufficient, one would resort to mean-field algorithms whereas in other regions, where the physics are complex and the pdf is needed, one would use a PDF algorithm. In such an approach, the central issue becomes the consistency at the boundaries between the contiguous domains. Some work in that sense has been carried out in the field of Direct Monte Carlo Simulations (DSMC) [52].

At last, in the present work, the proposed particle algorithm (the numerical algorithm for the set of SDEs, cf. Section 5.1.1) is compatible with other approaches for the fluid. It is one of the strong points of this numerical method. Therefore, it is conceptually possible to think about some other configuration and in particular to a LES/PDF one, i.e. the set of SDEs is provided with filtered fluid fields instead of mean fluid fields. Even though, in such a configuration, an increase of the computational effort is expected, the quality of results, in particular, for cases where RANS models are known to be inadequate, could be improved, cf. the computational example for particle deposition in Section 7. In such an algorithm, the challenge is to reconstruct the subgrid scale fluid velocity along the discrete particle trajectories [6,7,53]. A possibility is to use PDF methods; it has been attempted in single-phase flows [54] and it remains to be developed for dispersed two-phase flows.

7. Computational examples

Three numerical computations of polydispersed turbulent two-phase flows are now presented. The first one (*swirling flow*) is chosen in order to show that significant improvements in the computing efficiency can be achieved by using, for the integration of the set of SDEs, a second-order scheme instead of a first-order scheme. The second computation (*bluff-body flow*) demonstrates the ability of the models to capture the main physics of the flow and the specificity of PDF models from which valuable information can be extracted. The third example (*particle deposition*) illustrates the ability of PDF models to treat flows where complex physics are involved.

In the first and third examples, i.e. swirling flow and particle deposition, both flows are dilute enough so that only one-way coupling is under consideration. The numerical schemes presented in Section 5.3 can therefore be used directly. In the second example, bluff-body flow, the suspension is rather dense and one has to take into account two-way coupling. Numerically, for the integration in time of the set of SDEs, this is done by resorting to the first-order scheme and by treating the coupling term, cf. Eq. (28), as an explicit source term. Collisions that might occur in some restricted areas of the computational domain are not taken care of. It is, however, fully possible to treat collisions between discrete particles in the frame of the present PDF approach. This has been discussed

elsewhere [8] on a theoretical basis and the inherent numerical developments remain to be done.

7.1. Swirling flow

In this particular example, no comparison with experimental data is attempted since the purpose of the computations is to show the benefits of using second-order schemes instead of first-order schemes for the integration of the set of SDEs.

7.1.1. Experimental setup

The turbulent polydispersed two-phase flow under investigation corresponds to a gas–solid flow (air and solid particles) in a cyclone of Stairmand type [55], see Fig. 10. Cyclone separators are devices used to separate particles from gas flows. The gas flow inside the cyclone has quite complicated patterns, i.e. a reverse swirling flow with quite high rotational velocities. The swirl is created by the tangential inlet, but it is well-known from experiments that the gas flow exhibits a double helix structure. The flow spirals downwards (with a constant intensity) to the vortex finder (exit tube of the cyclone at the bottom) where it reverses and spirals upwards in a cylindrical volume having roughly the diameter of the exit. In such a device, the separation

De/D	H/D	h/D	a/D	b/D	S/D	B/D
1/2	4	3/2	1/2	1/5	1/2	9/25

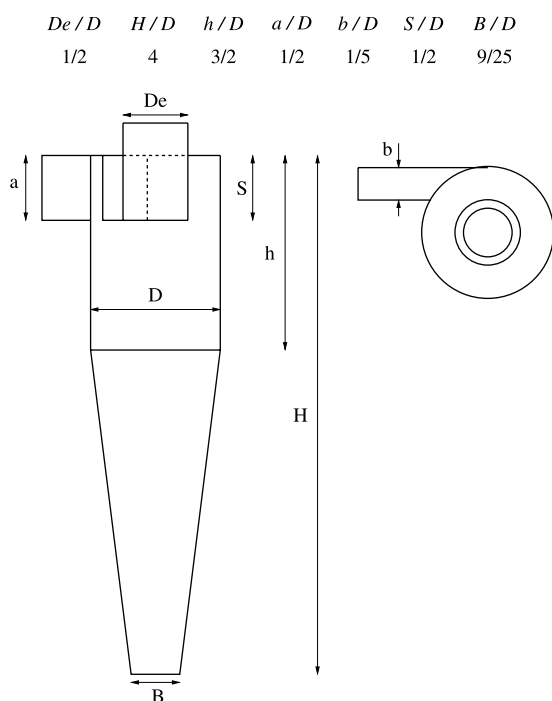

Fig. 10. Definition of the geometry of a cyclone of the Stairmand design. All dimensions are given as a function of the diameter D of the cyclone.

between air and particles is not due to gravity but to the effect of the double helix. Indeed particles entering the device are entrained towards the outer wall (by centrifugal forces) where they flow downwards to the exit (the axial velocity of the gas is oriented downwards at the walls).

The efficiency of a cyclone is characterised by its selectivity curve. This curve expresses the ratio (in mass) of captured particles as a function of their diameter. For very small particles, this curve goes to zero efficiency as their inertia decreases ($\tau_p \rightarrow 0$), i.e. particles tend to behave as fluid elements. On the contrary, large particles are all collected and the efficiency attains 1. Between these two asymptotic cases, the cyclone efficiency is an increasing function of the particle diameter.

7.1.2. Numerical simulations

The simulated cyclone [56,57] has a diameter $D = 0.2$ m, the glass particles have a density of $\rho_p = 2500$ kg/m^3 and diameters ranging between 0.5 and 5 μm. The gas (air at ambient temperature = 293 K) is injected with a constant velocity of 30 m/s. In the present simulations, the flow is dilute enough (the mass of particles per unit of gas is quite low) not to consider two-way coupling effects (the particles have no influence on the flow field). In addition, it is well established from experiments that such flows are stationary. Consequently, the flow field is computed in advance and all the particles are tracked in a *frozen* field. The prediction of the flow field is rather challenging given the complex structure of the flow. In this work, a second-order turbulence model (Rotta model [13], which is consistent with the form of the SDEs) was used with a fine grid (approximately 4×10^5 nodes) in order to obtain mesh-independent calculations. Figs. 11 and 12 show the axial and radial mean velocity profiles of the air flow at two different heights: it can be seen that the numerical results are in good agreement with the measurements.

Particles are then tracked in this frozen field. The diameter range of the glass particles has been discretised as follows, $d_p = [0.5; 1; 1.5; 2; 3; 4; 5]$ μm. For each class (diameter of particles), a number N_{pc} of particles is released (this number is identical for each class). The computation stops when all particles have left the computational domain.

7.1.3. Results and discussion

A numerical study has been carried out to show that the results (the obtained selectivity curves) are
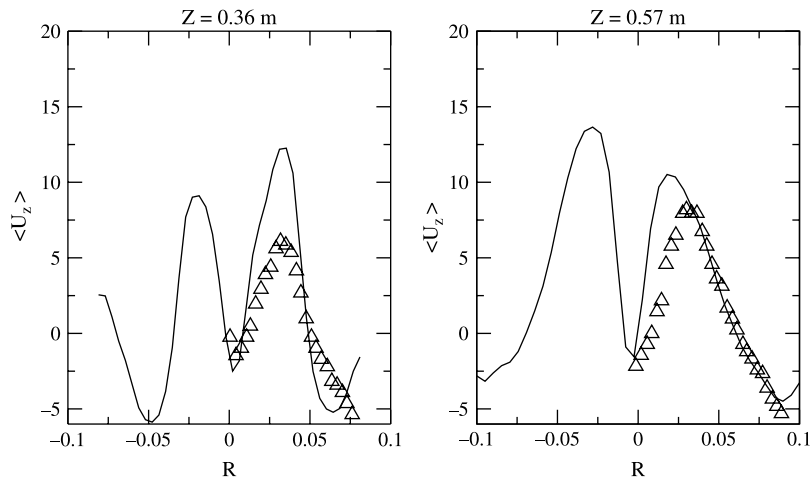
Fig. 11. Gas mean axial velocity profiles at two different heights: $z=0.36$ m (left) and $z=0.57$ m (right). The velocities are plotted as functions of the radius R. Continuous lines: computations. Experimental data: $\triangle$.

independent of the time step, Δt, and the number of particles per class, N_{pc}. For instance, for the second-order scheme, the computations show, for two different time steps, that roughly 400 particles per class are necessary to obtain selectivity curves, which do not depend on N_{pc}, see Fig. 13. The time step of $\Delta t = 10^{-4}$ s guarantees that the results do not depend on the time discretisation, Fig. 13. For the first-order scheme, similar results are obtained: $\Delta t = 5 \times 10^{-6}$ s and $N_{pc} = 400$ ensure that the results depend neither on the time step nor on the number of particles per class, Fig. 13.

It is then observed that, for this particular flow, there is a great difference between the respective time steps for the first- and second-order schemes, see Fig. 13, and

this for the same numerical results (selectivity curve). In fact, with a second-order scheme, the time step can be multiplied by a factor 20 compared to a first-order scheme. If one accounts for the computer time (the computation of a time step takes approximately 30% extra time compared to the first-order scheme), there is a gain in CPU time by a factor 15 by using a second-order scheme. Therefore, in this case, it is seen that the complexity of the second-order scheme is balanced by the reduction of computing time.

It can be stated that for flows where velocities and the curvature of the trajectories of the discrete particles are important, it is recommended to use a second-order scheme rather than a first-order one, unless one is ready
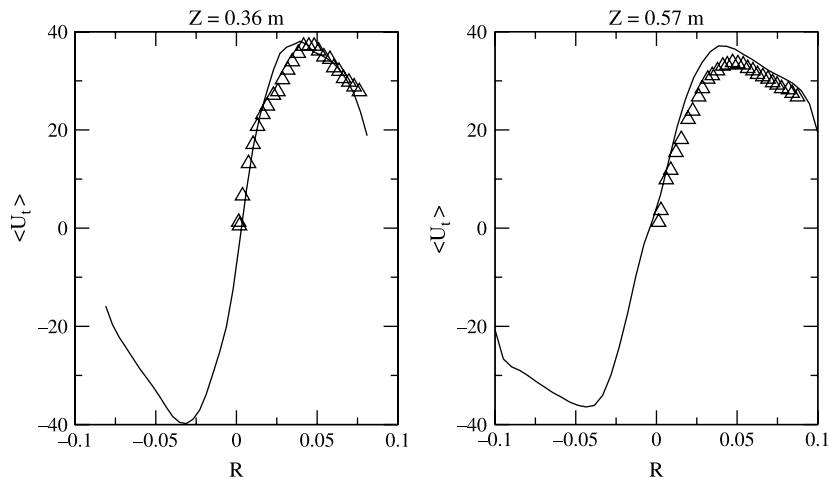

Fig. 12. Gas mean tangential velocity profiles at two different heights: $z=0.36$ m (left) and $z=0.57$ m (right). The velocities are plotted as functions of the radius R. Continuous lines: computations. Experimental data: $\triangle$.
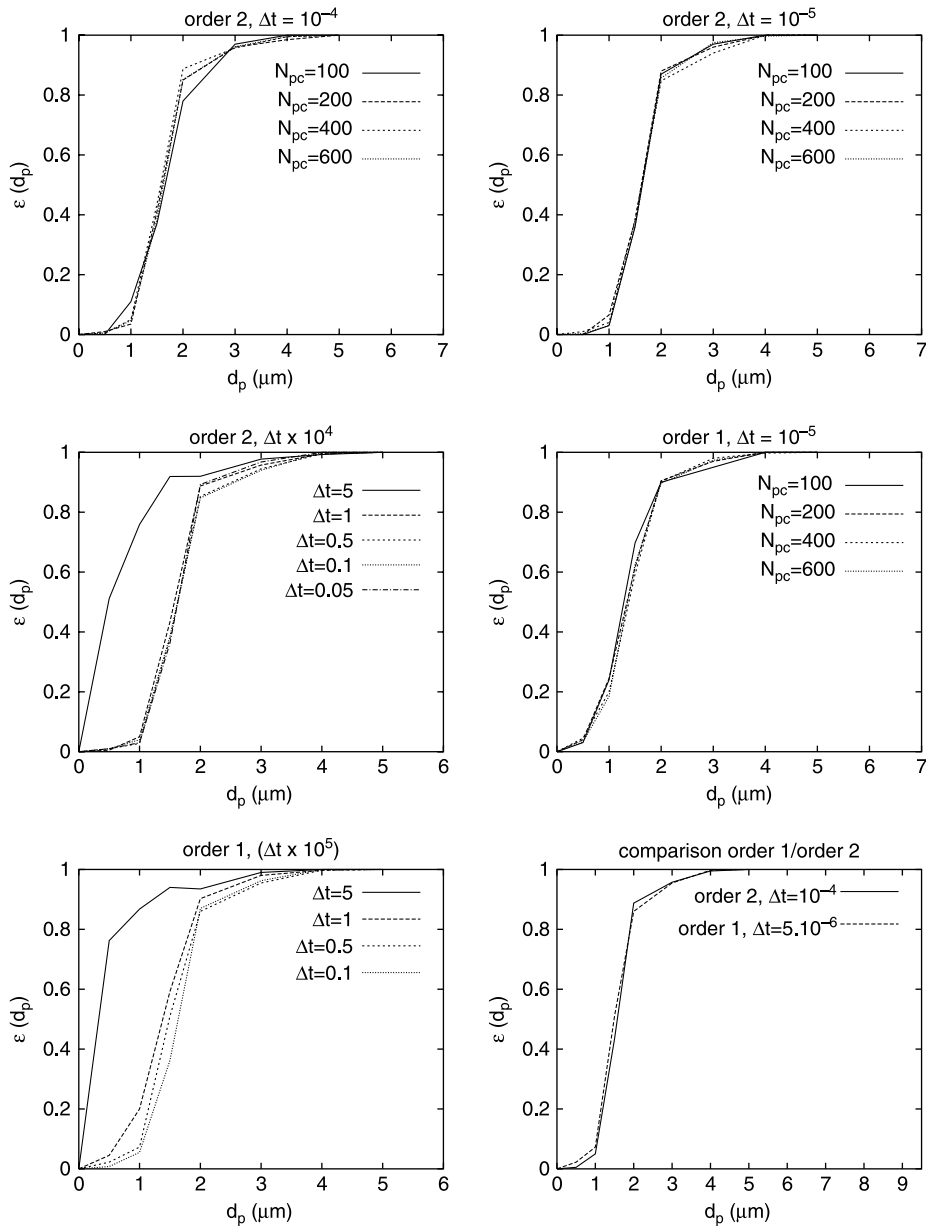
Fig. 13. Sensitivity analysis for the second-order and first-order schemes. The sensitivity analysis is carried out for the number of particles per class, N_{pc}, and the time step, Δt (with $N_{pc}=400$). At last, comparison of the time steps for the first- and second-order schemes for identical numerical results (bottom right corner). All numerical results represent the selectivity curve which gives the efficiency of the cyclone, ε, as a function of the particle diameter, d_p, *i.e.* $\varepsilon(d_p)$.

to pay the computational price. This is clearly seen in this computational example, where the time step of the first-order scheme is extremely small: as a matter of fact, in such a flow, a precise prediction of the particle velocity is needed because the numerical error on this quantity amounts at simulating an additional centrifugal force.

7.2. Bluff body flow

In this second example, the numerical results are compared to experimental data in order to show the ability of the present approach to reproduce the main trends of complex turbulent polydispersed two phase-flows. Other results are displayed to enhance

the specificity of the mean-field/PDF approach, i.e. the type of information, which can be extracted.

7.2.1. Experimental setup

The 'Hercule' experimental setup [58,59] is characteristic of pulverised coal combustion where primary air and coal are injected in the centre and secondary air is introduced on the periphery, Fig. 14. This is a typical bluff-body flow where the gas (air at ambient temperature and atmospheric pressure) is injected both in the inner region (jet) and the outer cylinders (exterior). The ratio between the gas velocity in the inner region, U_j, and the gas velocity in the outer region, U_e, is low enough so that a recirculation zone downstream of the injection is created. Two honeycombs are used in the experimental setup in order to stabilise the flow so that no swirl is present. Solid particles (glass spheres) are then injected from the inner cylinder with a given mass flow rate. The injected glass spheres have a density $\rho_p = 2470 \text{ kg/m}^3$ and a known

Fig. 14. The 'Hercule' experimental setup. The mean streamlines are shown for the fluid (solid lines) and the particles (dashed lines). Two stagnation points in the fluid flow can be observed (S_1 and S_2). Experimental data is available for radial profiles of different statistical quantities at five axial distances downstream of the injection ($x = 0.08, 0.16, 0.24, 0.32, 0.40$ m) (experimental data is also available on the symmetry axis).

diameter distribution, typically between $d_p = 20$ and $110 \,\mu\text{m}$ around a mass-weighted average of $d_p \sim 65 \,\mu\text{m}$. A polydispersed turbulent two-phase flow, which is *stationary* and *axisymmetric*, is then obtained. Moreover, two-way coupling takes place since the particle mass loading, $\phi = \chi \langle U_p \rangle / \langle U_f \rangle$, at the inlet is high enough. Experimental data are available for radial profiles of different statistical quantities at five axial distances downstream of the injection, Fig. 14 (axial profiles along the axis of symmetry have also been measured). The 'Hercule' experimental setup is a very interesting test case for polydispersed turbulent two-phase flow modelling and numerical simulations since most of the different aspects encountered in such flows are present. The particles are dispersed by the turbulent flow but in return modify it. Furthermore, the existence of a recirculation zone (with two stagnation points, S_1 and S_2 in Fig. 14) where particles interact with negative axial fluid velocities constitutes a much more stringent test case compared to cases where the fluid and the particle mean velocities are of the same sign (the problem is then mostly confined to radial dispersion issues). These features are displayed in Fig. 14, where mean streamlines are shown (solid lines for the fluid and dashed lines for the particles). For the fluid, there is a rather large recirculation zone with stagnation points. For the particles, depending on their inertia, several behaviours can be observed: some particles do not 'feel' the recirculation zone and leave the test section immediately. Others are partially influenced and change direction before leaving the apparatus, whereas some particles follow closely the recirculation pattern. This will be seen in the results showing the pdf of the particle residence time at different locations in the flow.
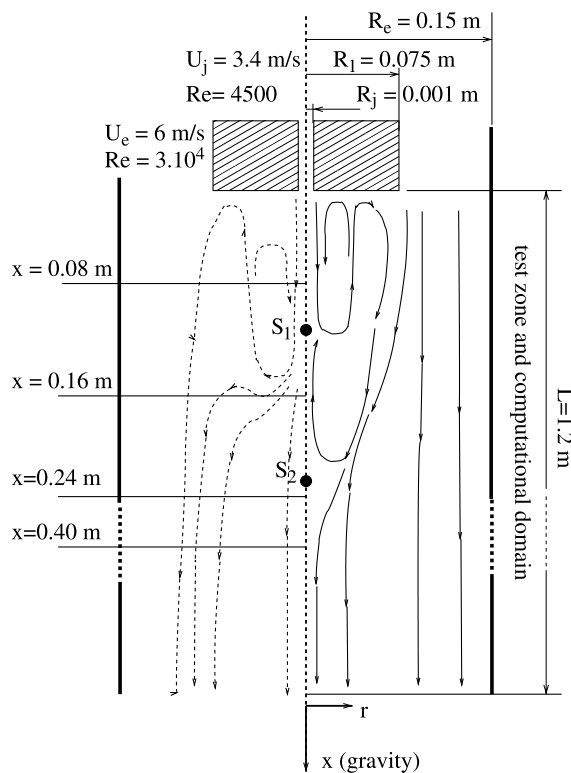
7.2.2. Numerical simulation

A two-dimensional, single block, non-Cartesian, non-uniform mesh ($142 \times 3 \times 75$ nodes for the (x, r, θ) coordinate system) has been generated in accordance with the axisymmetric property of the flow. It was carefully checked that the results are not too sensitive either to the time and spatial discretisations or to the number of stochastic particles ($\Delta t = 10^{-3}$ s and $N = 14,000$ particles). A second-order turbulence model (Rotta model, which is consistent with the form of SDEs) was used. The projection and averaging operators were approximated with a NGP technique [33]. For further details on numerical computations, see Ref. [60].

In the simulations, the following procedure is adopted. The single-phase flow case is first computed

until the stationary state is reached. By doing so, it is possible to check that the prediction of the flow field, without the particles, is accurate. Then the discrete particles are introduced until the stationary state is obtained again. At that point, the number of particles in the flow is roughly constant (it fluctuates around a mean value). From this state, computations are continued to extract the statistics, which are compared to the experimental values. The last computation is performed to allow time averaging on the ensemble averages so that the statistical noise can be reduced to a minimum.

7.2.3. Results and discussion

In this particular flow, there is almost no difference between the predictions with the first- and second-order schemes. The main difference takes place in regions, where only few particles are present (large diameters) and consequently the statistical results contain some noise.

Three sets of results are given: (i) radial profiles of the particle axial velocity, Fig. 15, (ii) radial profiles of the particle radial velocity, Fig. 16 and (iii) radial profiles of the fluid axial velocity, Fig. 17. All sets of numerical results compare relatively well

with the experimental data, in terms of the shape of the curve and of the magnitude, which are observed. The recirculation zone ($x=0.16$ m) is well predicted as indicated by the velocity profiles. All (mean and fluctuating) velocities go to zero when no particles are present. The widths of the numerical curves indicate that the predicted radial dispersion of the particles is also in line with experimental findings.

In Figs. 15–17, only first- and second-order moments of the variables of interest have been displayed (mean and fluctuating velocities for the fluid and the particles). This information could have been obtained by resorting to classical mean-field equations. However, in many engineering applications (for example combustion), it is necessary to know the distribution of the residence time of the particles at a certain time. In other words, one would like to know for all the particles found in a certain zone how much time they have spent inside the domain, or even if they have previously entered a marked region. This kind of information is not available in a mean-field model whereas in the present hybrid approach, this information is directly provided without additional costs: the pdf of the variables attached to each particle, which contains far
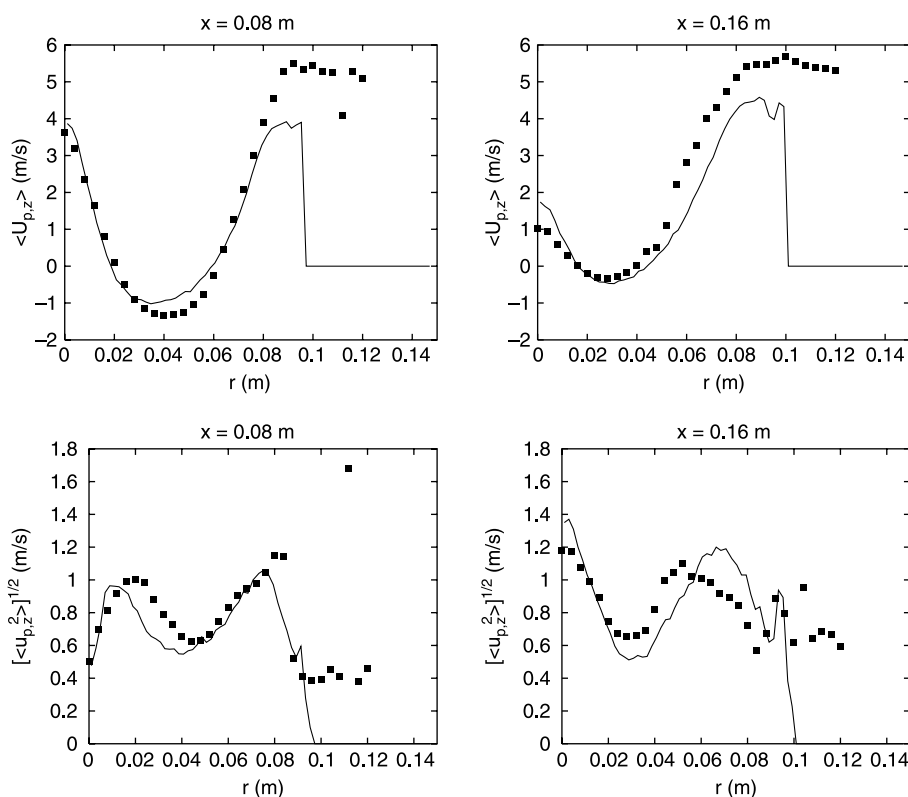

Fig. 15. Radial profiles of the particle axial velocity at $x=0.08$ and 0.16 m. Mean velocities (top) and fluctuating velocities (bottom). Continuous lines: computations (first order scheme). Experimental data: ■.
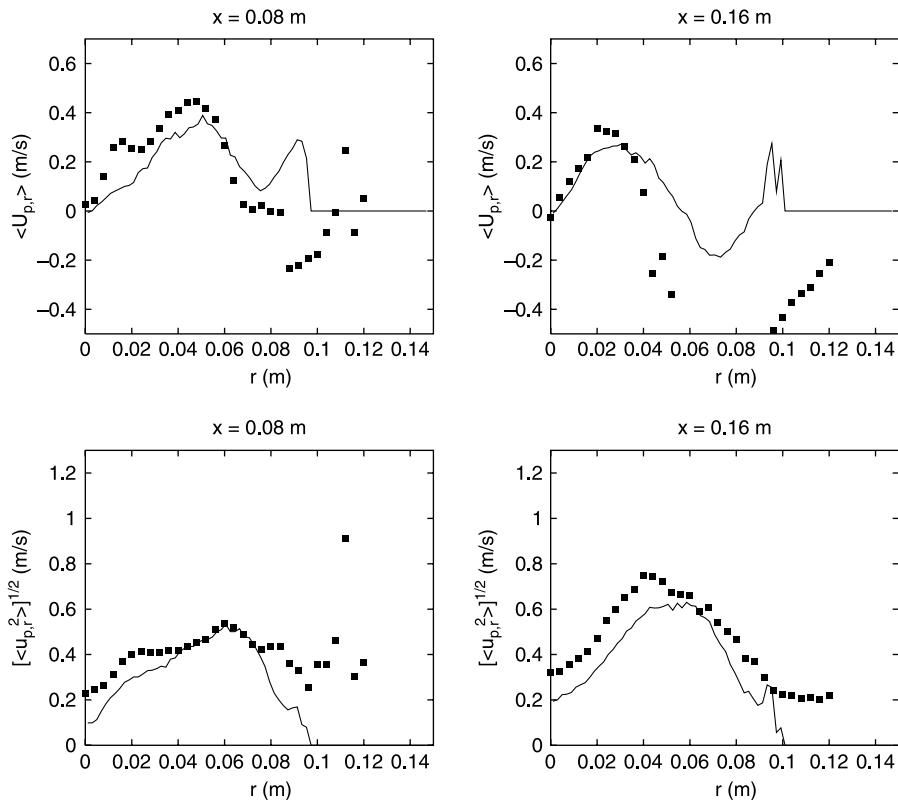
Fig. 16. Radial profiles of the particle radial velocity at $x = 0.08$ and 0.16 m. Mean velocities (top) and fluctuating velocities (bottom). Continuous lines: computations (first order scheme). Experimental data: ■.

more information than a few moments, is explicitly computed.

A typical example of this type of information is given in Fig. 18. In the first plot, on the left-hand side, a snap shot of the local instantaneous positions of the particles is given, where particles are coloured by their residence time. Two distributions are extracted, one in a cell close to the inlet and the other one in a cell close to the outlet. The pdf in the cell near the inlet clearly shows the recirculation pattern: the distribution is highly peaked, which represents particles which have just entered the domain, but a small number of particles
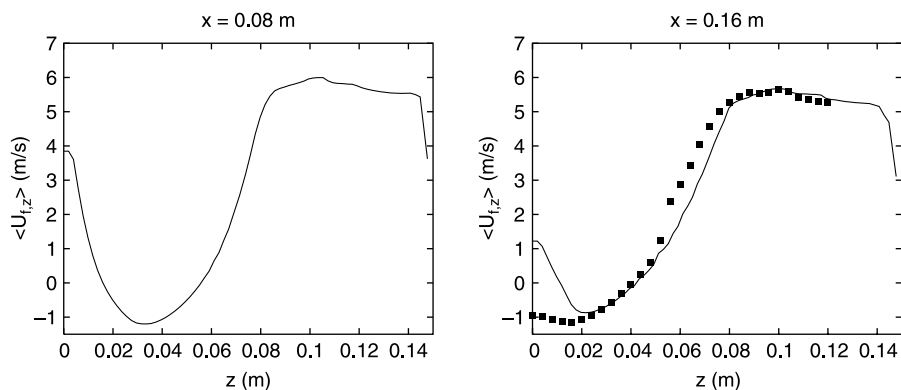
Fig. 17. Radial profiles of the fluid axial velocity at $x = 0.08$ and 0.16 m (mean velocities only). Continuous lines: computations (first-order scheme). Experimental data: ■.
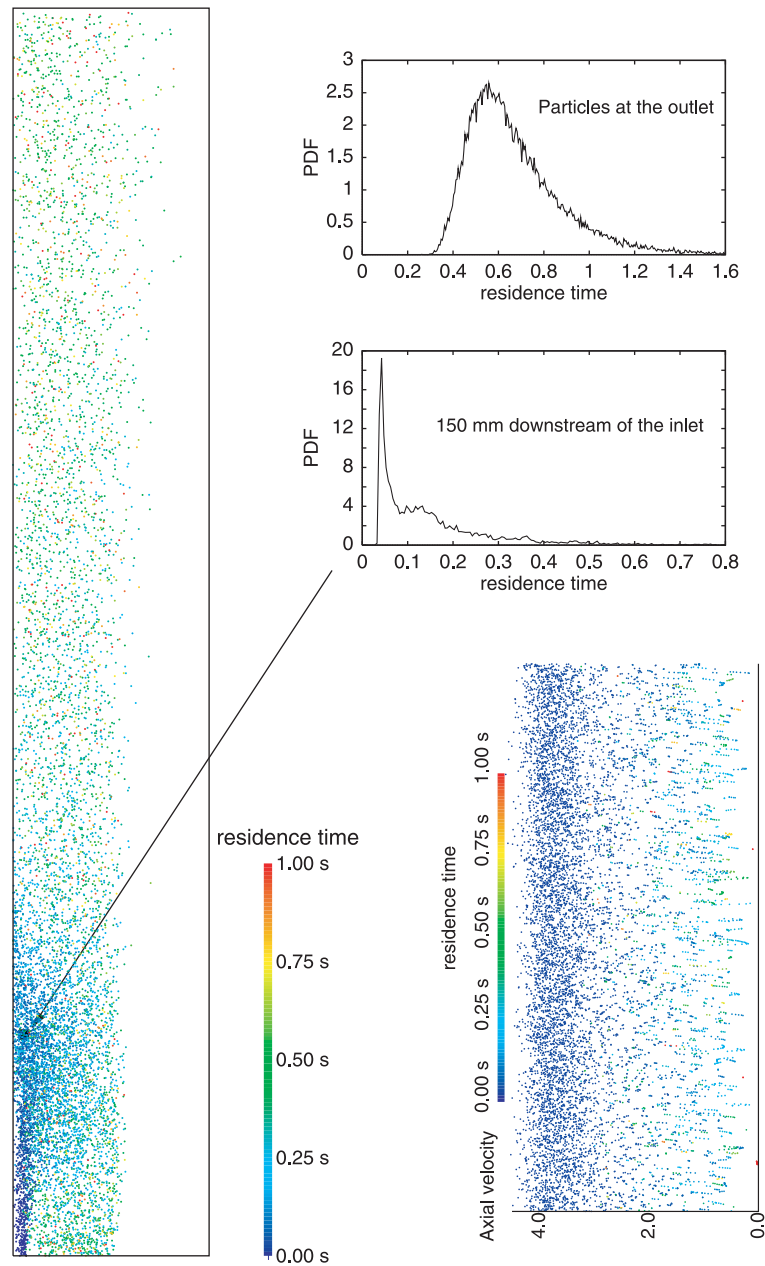
Fig. 18. Left-hand side: snapshot of the flow, at a given time, where the particles are coloured by their residence time in the computational domain. Right-hand side (upper corner): probability density functions of the particle residence time inside the domain (close to the injection and close to the outlet of the domain). Right-hand side (bottom corner): axial velocity (horizontal axis) of the particles (coloured by their residence time in the computational domain) close to the inlet at different time steps (vertical axis).

have a quite high residence time, i.e. they recirculate. At the outlet, since the particles have different trajectories in the domain, a continuous spread in residence time is observed. In the region near the inlet, more information can be gathered, for example the local instantaneous axial velocity, see the RHS graph in Fig. 18. Most particles have the same axial velocity,

around 4 m/s which is actually the inlet velocity. These particles correspond to the peak observed in the residence time: they have just entered the domain and travel directly to this region. The rest of the particles have a smaller axial velocity but with much wider fluctuations: these particles correspond to particles, which are recirculating.

At last, it is often argued that the mean-field/PDF approach is time-consuming. As a matter of fact, in this computation, the time spent by both solvers (the mean-field solver for the fluid and the PDF solver for the particles) has been compared for the *same number of computational elements* (mesh points and particles, respectively). It is found that the PDF solver is slightly faster: this is not really surprising since the mean-field fluid solver implies the use of a full second-order turbulence model (six coupled PDEs).

7.3. Pipe flow: deposition

In this last example of numerical applications with the mean-field/PDF approach, a flow where complex physics are involved, i.e. *particle deposition*, is under investigation. Particle deposition from a turbulent flow on walls is a phenomenon, which is observed in many engineering applications (for example thermal and nuclear systems, cyclone separators, spray cooling) and also in various environmental situations. Given the large number of possible applications, a lot of interest has been devoted to this subject and many studies have been carried out in the last decades.

7.3.1. Experimental setup

Different experiments have been conducted to observe deposition in turbulent flows. In most of them, attention is focused on the deposition velocity [61,62] which is defined as $k_p = m_p/\bar{C}$, where m_p is the mass flux and $\bar{C}$ is the bulk mean particle concentration. This deposition rate, often presented as the dimensionless deposition velocity k_p/u^*, is a function of the dimensionless particle relaxation time, τ_p^+, defined as

$$\tau_p^+ = S^+ \frac{u^*}{U_{p0}} = \frac{d_p^2 \rho_p U_{p0} u^*}{18 \mu_f \nu_f} \frac{u^*}{U_{p0}} = \frac{d_p^2 \rho_f^2 u^{*2}}{18 \mu_f^2} \frac{\rho_p}{\rho_f},$$

(122)

where S^+ is the dimensionless stopping distance, U_{p0} is the particle initial velocity and u^* is the friction velocity. u^* is evaluated with the Blasius formula, $u^* = [0.03955 Re^{0.25}]^{0.5} U_m$, where U_m is the bulk mean velocity. The deposition velocity is the key point in many engineering applications, where one seeks the law that gives k_p/u^* as a function of τ_p^+, i.e. as a function of the particle diameter. Recently, several experimental studies and DNS studies of particle deposition have been presented, for example [63,64], and have improved the understanding of the physical mechanisms at play. In particular, a lot of information has been obtained on the dynamical

structures of wall-bounded flows, like the coherent structures, which manifest themselves in the near-wall region.

In the present computational example, the principal interest is to show the advantage of solving the set of SDEs with a numerical scheme consistent with all limit cases, see Sections 4, 5.3.3 and 5.3.4. Indeed, in pipe flows with particle diameters ranging from 1 to 100 μm, all limit cases can be encountered:

1. for the smallest particles ($\tau_p \to 0$ in the continuous sense and $\tau_p \ll \Delta t$ in the discrete sense), limit case 1 is obtained,
2. in the near wall region, i.e. $T_{L,i}^* \ll \Delta t$, for example in the peak-production region where turbulent kinetic energy is maximal, one has $B_{ij} T_{L,i}^* = $ cst, a situation which is characteristic of limit case 2,
3. in the same region as above with small particles, one has limit case 3,
4. in the close vicinity of the wall, i.e. $T_{L,i}^* \ll \Delta t$, with no condition on the other moments, the flow is laminar, i.e. limit case 4.

The need to cope with limit cases is the result of practical considerations. Indeed, if the numerical schemes were not consistent with the limit cases, it would be very inefficient to carry out computations with a time step limited by the smallest timescale.

In the present work, numerical simulations corresponding to the experimental setup of Liu and Agarwal [61] are presented, i.e. the deposition of particles (920 kg/m³ in density and diameters in the range 1.4–68.5 μm) in a vertical pipe flow at a Reynolds number of 10^4.

7.3.2. Numerical simulation

In order to describe the particle phase, 10^4 stochastic particles (distributed in 10 diameter classes, cf. Table 6) are released in a frozen field, i.e. the flow is stationary and dilute enough so that only one-way coupling is under consideration. Two frozen fields are computed with a standard k–ϵ turbulence model and with a R_{ij}–ϵ (Rotta model) both with wall-function boundary conditions. The computations are performed with a 2D mesh, $100 \times 20 \times 3$ nodes (the flow is axisymmetric).

To compute the deposition velocity, the fraction of particles remaining in the flow, F, is evaluated as a function of the axial position x [65]. F is calculated as the number of particles that reach the sampling cross-section, divided by the total number of released particles. The particle deposition velocity is then

Table 6

Mean near-wall ($y^+ < 30$) residence time t^+ for different diameters (the simulation is carried out with the exact frozen field)

τ_p^+	d_p (μm)	t^+ (wall units)
0.2	1.4	29.5
0.4	2.0	29.9
0.9	2.9	28.7
1.9	4.3	30.9
3.5	5.8	31.5
6.4	7.8	31.6
13.2	11.2	35.4
29.6	16.8	40.6
122.7	34.2	55.3
492.2	68.5	96.8

The residence time is given in non-dimensional form (it is normalised with the viscous timescale, $\nu_f/(u^*)^2$, i.e. $t^+ = t(u^*)^2/\nu_f$).

computed as follows [65]

$$k_p = \frac{U_m D_h}{4(x_2 - x_1)} \ln\left(\frac{F_1}{F_2}\right), \tag{123}$$

where D_h is the diameter of the pipe and F_i is the value of F at a given sampling cross section labelled i (axial position x_i).

Numerical tests have been performed to check that the numerical results are independent of the values of numerical parameters, in particular the number of particles, N, and the time-step, Δt. It was checked beforehand that the numerical prediction of the fluid field is grid-independent.

Both numerical schemes (first- and second-order) were tested with different time steps, cf. Fig. 19. All computations were then performed with the weak second-order scheme and a time step of 10^{-4} s. Indeed, Fig. 19 shows that both schemes give similar results and that a time step $\Delta t = 10^{-4}$ s ensures that the computations are independent of Δt. The independence of the deposition velocity for the whole range of particle diameters with respect to the time step illustrates the benefits of a numerical scheme which is consistent in all limit cases: for instance, the values of the particle relaxation timescales given in Table 6 cover three orders of magnitude (limit case 1). Computations can anyway be carried out with by using the same constant time-step for all classes and in the whole domain.

An analysis of the statistical error has also been carried out. Since particle deposition velocities are calculated by a Monte Carlo method, it is important to check that the number of particles (which represent samples of the pdf) is sufficiently large so that statistical error is reasonably small. In Fig. 20, results obtained with three different values of N_{pc} (the number of particles used for each class of diameter) are presented
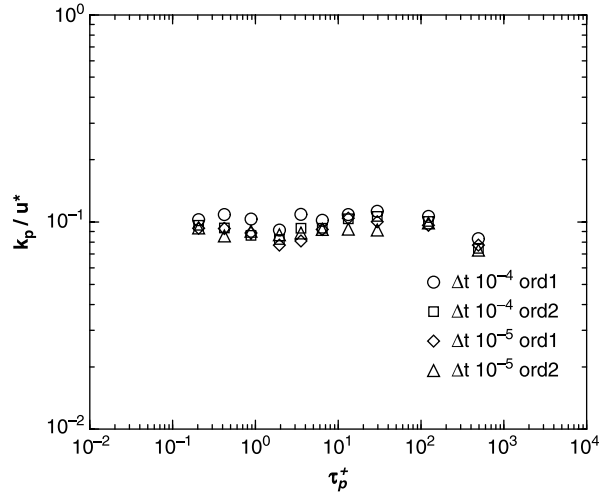

Fig. 19. Sensitivity analysis: deposition velocity computed with different time steps Δt and with the first and second order schemes. $\Delta t = 10^{-4}$ s ($\bigcirc$) and $\Delta t = 10^{-5}$ s ($\diamond$) with the first-order scheme. $\Delta t = 10^{-4}$ s ($\square$) and $\Delta t = 10^{-5}$ s ($\triangle$) with the second-order scheme.

($N_{pc} = 500$, 1000 and 5000). Fig. 20 shows that there is no clear difference between the results obtained with different values of N_{pc}. As a matter of fact, it seems that 500 particles for each class of diameter are enough. Nevertheless, for all the following simulations, the value of $N_{pc} = 1000$ particles for each class of diameter has been chosen, in order to reduce statistical noise.

7.3.3. Results and discussion

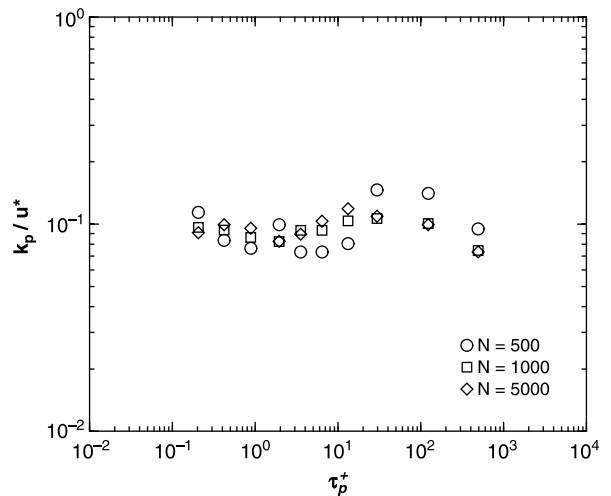The numerical results are now compared to experiments and some sensitivity tests are conducted.

Fig. 20. sensitivity analysis: deposition velocity computed with different number of particles per class N_{pc} for the same fluid mean-fields ($N_{pc} = 500$ ($\bigcirc$), $N_{pc} = 1000$ ($\square$), $N_{pc} = 5000$ ($\diamond$)).
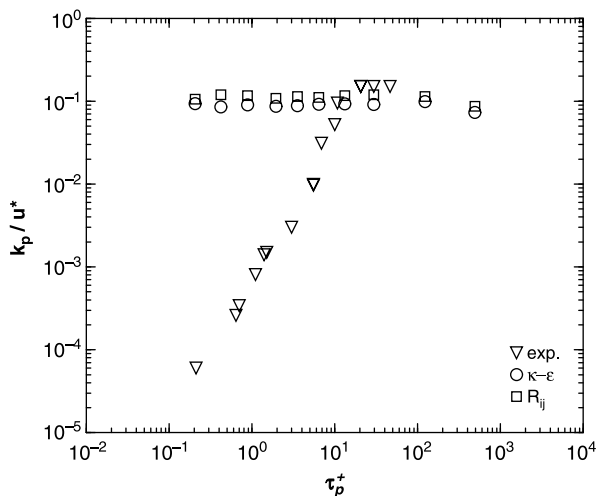
Fig. 21. Deposition velocity with different mean fields for the fluid. Fluid mean-fields calculated with a k–ϵ model ($\bigcirc$). Fluid mean-fields computed with a R_{ij}–ϵ model ($\square$). Experimental data ($\triangledown$).

Some proposals are put forward for the features, which seem to be the most significant ones for a good representation of deposition phenomena. Possible improvements of the computational method shall be exposed.

In Fig. 21, results obtained with the general PDF model, Eqs. (1) and (24), and two turbulence models (k–ϵ and R_{ij}–ϵ), are displayed. The difference between the simulations performed with two different turbulence models is negligible; this is not too surprising, since for turbulent pipe flow, both models give similar mean fluid velocity profiles. The standard PDF model is integrated with wall-function conditions for the fluid and pure-deposition boundary conditions for the particles. These results are coherent with those obtained in an analogous configuration by Schuen [66].

Fig. 21 shows that for heavy particles ($\tau_p^+ > 10$), the model predictions are in good agreement with experiments whereas for light particles ($\tau_p^+ < 10$), the deposition velocities are strongly overestimated (they remain at the same level as that of the heavy particles). Therefore, the model is not suitable for simulations of deposition phenomena in the range $\tau_p^+ < 10$. This statement is consistent with experimental and DNS findings [67]: heavy particles are slightly affected by near-wall boundary layer and more especially by the specific features of the local instantaneous turbulent structures in the near-wall region. On the contrary, for light particles, the physical mechanism of deposition changes with a growing importance of turbulent structures and near-wall physics. In the current PDF model, near wall physics are mainly described by

wall-function boundary conditions which may be sufficient for heavy particles deposition but not for light particle deposition.

Wall-functions give a reasonable approximation of the mean fluid velocity profile in the logarithmic region, but in any case they do not describe the viscous sub-layer. Therefore, a question arises: is the prediction of small particle deposition velocity sensitive to changes in the fluid mean-field profiles? This matter was recently investigated for other Lagrangian models [65]. Following the same reasoning, simulations have been carried out with a given frozen field (consequently, wall-function boundary conditions are suppressed). The frozen field can be obtained, in this particular case, either from analytical solutions for the mean fluid fields ($\langle \mathbf{U} \rangle, k, \langle \epsilon \rangle$) [4] and/or from DNS data. In Fig. 22, two frozen fields are tested. In the first field, the axial mean fluid velocity $\langle U_i \rangle$ is given by the law-of-the-wall equations (the values k and ϵ are that of the computations). In the second field, $\langle U_i \rangle$ is still given by the law-of-the-wall, and the turbulent kinetic energy, k, and the turbulent dissipation rate, ϵ, are curve-fitted to the DNS data that can be found in the work of Matida et al. [65]. Thus, in the second field, mean fluid profiles are exact. Fig. 22 shows that an exact frozen field hardly improves the results. An explanation might be that the eventual effect of the exact mean fluid profiles is concentrated in a very thin region. The most important quantity is expected to be the turbulent
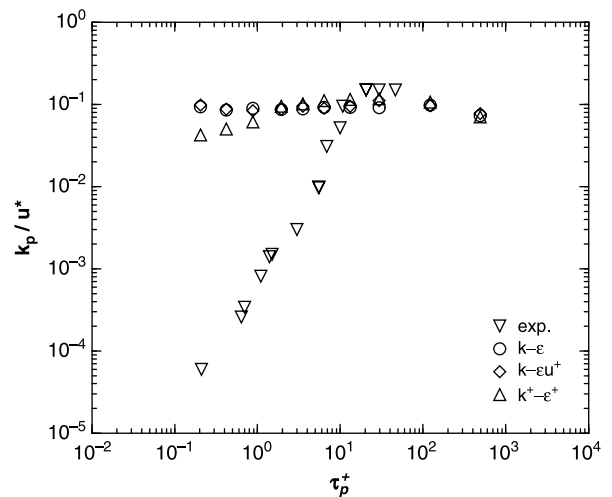

Fig. 22. Deposition velocity with different mean fields for the fluid. First, mean field obtained by computation with a standard k–ϵ model ($\bigcirc$). Second, mean field where $\langle U_i \rangle$ is computed with the law-of-the-wall equations and where the values k and ϵ are that of the computations ($\diamond$). Third, $\langle U_i \rangle$ is still given by the law-of-the-wall, and k and ϵ are curve-fitted to DNS data [65] ($\triangle$). Experimental data ($\triangledown$).

kinetic energy, which goes to zero at the wall and should affect mainly light particles. Nevertheless, k diminishes only from $y^+ \approx 10$, where it has its maximum (peak production). The resulting effect is not easy to be foreseen and it may be negligible with respect to the overall effect of migration of particles towards the wall due to the net mean flow.

In order to further support the argument above, mean near-wall residence times of deposited particles have been computed in the layer $y^+ < 30$, for each class of diameters. Indeed, this quantity has been found to properly distinguish different deposition mechanisms [67]. A rough description of the physics of deposition is that heavy particles, which are slightly influenced by near-wall structures, deposit with small near-wall residence times by the so-called *free-flight* mechanism. On the contrary, light particles are trapped and driven by turbulent structures and deposit with large near-wall residence times, this mechanism is called *diffusional*. The lighter the particles are, the more important the diffusional mechanism is. In Table 6, the results obtained for each class of diameters are given for a simulation corresponding to the exact frozen field. For the sake of clarity, the residence time is always expressed in non-dimensional form (it is normalised with the viscous timescale, $\nu_f/(u^*)^2$, $t^+ = t(u^*)^2/\nu_f$). Table 6 shows that all particles deposit after small near-wall residence time, i.e. by free-flight mechanism. Moreover, since the residence time slightly increases with d_p, the motion of particles is influenced by the migratory flux. The force exerted on the particles by the fluid being inversely proportional to d_p, light particles reach the walls faster than the coarse ones. Therefore, in the absence of representation of turbulent coherent structures (which should be able to trap particles in the near-wall region and which should describe correctly the mechanisms of deposition), the sole mean fluid profiles are not the main mechanism.

Two possibilities exist to improve the prediction of deposition phenomena and in particular of light particles:

(i) some phenomenological model can be introduced, based on the present knowledge of deposition physics. In this type of approach, some hypotheses are made in accordance with experimental findings. Some parameters may be present and may be fitted in order to find good comparison with experiments. This approach ought to verify if the hypotheses made are correct or not, and, thus, ought to show which are the dominant aspects not covered by the standard model.

(ii) it is also possible to propose extensions of the present PDF model that reproduce correctly the variations of the fluid statistical moments (such as $\langle \mathbf{U} \rangle$, R_{ij}, ϵ, etc.) throughout the near-wall region, including the viscous sublayer [49]. Such a model might lead to improvement for the deposition velocity. However, it would require a very refined mesh in the near-wall region, considering the high value of Reynolds number. Furthermore, only the statistics of the fluid would be well reproduced and, as mentioned above, it is believed that the contribution of the specific features of coherent structures should be considered for small particle deposition.

Therefore, for practical purposes, the first proposition has been retained [68]. This subject is not further developed here and it is left as a challenging open issue.

8. Conclusions and perspectives

In this paper, we have presented a comprehensive review of the numerical methods involved for the computation of polydispersed turbulent two-phase flows using a particle stochastic method based on Langevin equations. The present mean-field/PDF model is one among a host of other so-called Euler/Lagrange models. However, it is worth putting forward two main specific aspects of the present framework.

(i) The usual term Euler/Lagrange refers to the point of view adopted for the description of the two phases: an Eulerian point of view for the fluid phase and a Lagrangian one for the particle phase. This terminology can be misleading and does not clearly identify the physics involved, the level of information contained in the statistical description and the numerical tools, which are adopted. For example, the so-called Eulerian equations for the fluid phase can be directly obtained through the two-particle stochastic formulation sketched in Section 3.2.1 and Appendix A, and its numerical solution may involve Lagrangian ideas (for instance, in the method of characteristics for the discretisation of the convection terms) and, at least in theory, the PDF equation could also be solved using a mesh and an Eulerian description in phase space. In the present work, the complete model is called a *mean-field/PDF approach*. This refers directly to the level of information contained in

the description: the fluid phase is described by a limited number of statistical moments (in practice, at most two for the fluid velocity) while the particle phase is characterised by the PDF of the variables retained for its description. The complete model is therefore a *hybrid model*. The hybrid nature of the model is then reflected in the numerical approach developed in Section 5. The fluid mean fields are computed as the solution of PDEs, involving a mesh and, say, classical Finite Volume schemes. As explained in Section 2, the PDF equation is solved, in a weak sense, by a particle Monte Carlo method, where the particles should be seen as instantaneous realizations of this PDF rather than real particles. The numerical approach is thus a hybrid *PDE/Particle Stochastic* method, or a *Mesh/Particle Stochastic* method; its specificities have been discussed at length in Section 5. The various details treated in that section can be improved, but the important point is that they are developed once a clear framework about the complete hybrid method is first set forth. This framework is a necessary guideline.

(ii) Drawing on these first remarks, the second aspect of the present formulation is the fact that there is a separation between the theoretical construction of the model and its numerical solution. Indeed, given the correspondence (in a weak sense) between the PDF equation and particle stochastic equations, as explained in Section 2, it may be tempting to develop directly the model in discrete time. This amounts to treating the model and its numerical scheme without distinction. This may be confusing and may not help to identify the actual issues. In the present work, the theoretical stochastic model is developed and first written in continuous time. This requires knowledge of the mathematical background of stochastic diffusion, but actually this effort is a valuable investment and the formulation in terms of the particle trajectories of the stochastic process in continuous time simplifies the situation and the numerical developments.

The central point of the complete work presented in Section 4 concerns the multiscale character of the stochastic theoretical model which is then reflected in the numerical developments of Section 5. Placed between the mathematical background and the numerical implementations, this section illustrates the interplay between mathematical formulation, physical modelling and numerical developments. The mathematical manipulation of the system of equations reveals the property of the model: different limits are continuously reached depending upon the values of the observation timescale with respect to the different physical time-scales. These limits correspond to natural physical diffusive limits and they point out that some physical variables are not real white-noise terms, but that their effects may be regarded as such *at a certain scale*. Using the numerical time step as the observation timescale, this physical property appears in turn as a basis for the development of the numerical schemes which, while being explicit and stable, can satisfy these limits without any constraint or threshold on the time step.

Finally, the main purpose of this work has been to propose a consistent and specific framework for the simulation of polydispersed two-phase flows based on Langevin stochastic equations. Together with the presentation of the theoretical aspects [8], it provides a comprehensive description of the model and of the numerical ideas. It does not pretend to be the ultimate word in this field and much work remains to be done. The Langevin equations still require new developments [8] and, on the numerical side, boundary conditions must be properly addressed, see Section 6.3. Yet, it is hoped that the present framework paves the way for the improvement of current methods as well as for the formulation of new ideas. In particular, new hybrid methods may benefit from these first steps, by trying to go further into a mixed mean-field/PDF approach within the description of the particle phase itself. This will require a good understanding of the consistency between the mean field equations satisfied by particle statistical properties and the instantaneous stochastic equations for the trajectories, of their mathematical manipulation and of the issues involved with particle/mesh exchange of information.

Acknowledgements

Appendix A. Two-point description

Here, some additional information is given on the construction of the two-point description, i.e., the form of the acceleration term to be added in the Langevin

equation describing the velocity increments along the trajectory of a fluid particle. Once this is done, it is briefly explained how the mean-field (RANS) equations for the fluid can be extracted from this two-point description.

A.1. Model for a two-way coupling term

In the exact local instantaneous equations for the fluid (the Navier–Stokes equations), a formal treatment of the force exerted on the fluid by the discrete particles implies the use of a distribution (or density of force) acting on the fluid located in the neighbourhood of the discrete particles in order to express the resulting acceleration on nearby fluid particles. This accurate treatment, which would result in a multi-point treatment of the discrete phase, is outside the scope of the present work. Here, in the frame of the one-point approach, the influence of the discrete particles on the fluid is expressed directly in the SDEs, Eqs. (30), with stochastic tools.

As explained in Section 3.1.2, for $\mathbf{A}_{p \to s}$, the underlying force corresponds to the exchange of momentum between the fluid and the particles (drag force). The acceleration acting on the fluid element surrounding a discrete particle can be obtained as the sum of all elementary accelerations (due to the neighbouring particles), i.e., at the discrete particle location $\mathbf{x}_p$, the elementary acceleration $(\mathbf{U}_p - \mathbf{U}_s)/\tau_p$ is multiplied by $\chi = (\alpha_p \rho_p)/(\alpha_f \rho_f)$, that is the probable mass of particles divided by the probable mass of fluid (since the total force is distributed only on the fluid phase).

For $\mathbf{A}_{p \to f}$, the problem of finding a suitable stochastic model is slightly more difficult since the drag force can only be defined in terms of variables attached to the discrete particles (which are not defined at the location of a fluid particle). As a consequence, the influence of the neighbouring discrete particles on the fluid particle located, at time t, at $\mathbf{x} = \mathbf{x}_f(t)$, is ensured by considering that $\mathbf{A}_{p \to f}$ is a random variable given by

$$A_{p \to f} = \begin{cases} 0, & \text{with probability } 1 - \alpha_p(t, x), \\ \mathbf{\Pi}_p & \text{with probability } \alpha_p(t, x), \end{cases} \quad \text{(A1)}$$

where $\mathbf{\Pi}_p$ is a random variable which plays the role of an ersatz of the Eulerian random variable which is formed from the discrete particles at $\mathbf{x} = \mathbf{x}_p(t)$

$$\mathbf{\Pi}_p \equiv -\frac{\rho_p}{\rho_f} \frac{\mathbf{U}_s - \mathbf{U}_p}{\tau_p}. \quad \text{(A2)}$$

This random term mimics the reverse force due to the discrete particles and is only non zero when the fluid particle is in the close neighbourhood of a discrete particle. In addition, it is required that, at $\mathbf{x} = \mathbf{x}_f(t)$, $\mathbf{\Pi}_p$ and $\mathbf{U}(t, \mathbf{x})$ are correlated so that

$$\begin{cases} \langle \mathbf{\Pi}_p \rangle = -(\rho_p/\rho_f)\langle(\mathbf{U}_s - \mathbf{U}_p)/\tau_p\rangle, \\ \langle \mathbf{\Pi}_p \mathbf{U} \rangle = -(\rho_p/\rho_f)\langle(\mathbf{U}_s - \mathbf{U}_p)\mathbf{U}_s/\tau_p\rangle. \end{cases} \quad \text{(A3)}$$

For further explanations on the modelling of two-way coupling, see Refs. [8,29].

A.2. Mean-field (RANS) equations for the fluid

In sample space, Eqs. (30) are equivalent (in a weak sense) to a general Fokker–Planck equation for the two-point Lagrangian pdf, $p^r(t; \mathbf{z}_f, \mathbf{z}_p)$, cf. the correspondence between Eqs. (10) and (11). It can be shown [8] that the Fokker–Planck equation verified by $p^r(t; \mathbf{z}_f, \mathbf{z}_p)$ is also verified by the two-point Eulerian mass density function (mdf) and therefore by one of its marginals, $F_f^E(t, \mathbf{x}; \mathbf{V}_f)$. This mdf is given by $F_f^E(t, \mathbf{x}; \mathbf{V}_f) = \rho_f p_f^E(t, \mathbf{x}; \mathbf{V}_f)$ where p_f^E is the Eulerian distribution function of the fluid. The knowledge of the PDE verified by an Eulerian quantity allows us, using classical tools of kinetic theory [69,70], to write field equations for the velocity moments of the fluid: the PDE verified by F_f^E is multiplied by a given function of $\mathbf{V}_f$, $\mathcal{H}(\mathbf{V}_f)$. Applying the following operator

$$\alpha_f(t, \mathbf{x})\rho_f\langle \mathcal{H}(\mathbf{U}(t, \mathbf{x})\rangle = \int \mathcal{H}(\mathbf{V}_f)F_k^E(t, \mathbf{x}; \mathbf{V}_f)d\mathbf{V}_f \quad \text{(A4)}$$

to this PDE gives field equations for any $\langle \mathcal{H}(\mathbf{U}(t, \mathbf{x})\rangle$. By replacing $\mathcal{H}$ by $\mathcal{H} = 1$, $V_{f,i}$ and $V_{f,i}V_{f,j}$, the continuity equation, the momentum equations and the Reynolds-stress equations are obtained, respectively [29]. These equations are given in Table 1, i.e. Eqs. (124)–(126).

References

[1] Sreenivasan KR. Fluid turbulence. Rev Mod Phys 1999;71(2): S383–S95.

[2] de Gennes PG. Granular matter: a tentative view. Rev Mod Phys 1999;71(2):S374–S82.

[3] Clift R, Grace JR, Weber ME. Bubbles, drops and particles. New York: Academic Press; 1978.

[4] Monin AS, Yaglom AM. Statistical fluid mechanics. Cambridge, MA: MIT Press; 1975.

[5] Stock DE. Particle dispersion in flowing gases. J Fluids Eng 1996;118:4–17.

[6] Boivin M, Simonin O, Squires KD. On the prediction of gas–solid flows with two-way coupling using large eddy simulation. Phys Fluids 2000;12:2080–90.

[7] Okong'o NA, Bellan J. Consistent large-eddy simulation of a temporal mixing layer laden with evaporating drops. Part 1. Direct numerical simulation, formulation and a priori analysis. J Fluid Mech 2004;499:1–47.

[8] Minier J-P, Peirano E. The PDF approach to polydispersed turbulent two-phase flows. Phys Rep 2001;352(1–3):1–214.

[9] Gardiner CW. Handbook of stochastic methods for physics, chemistry and the natural sciences. 2nd ed. Berlin: Springer; 1990.

[10] Pope SB. PDF methods for turbulent reactive flows. Prog Energy Combust Sci 1985;11:119–92.

[11] Pope SB. Lagrangian PDF methods for turbulent reactive flows. Ann Rev Fluid Mech 1994;26:23–63.

[12] Reeks MW. On the continuum equations for dispersed particles in nonuniform flows. Phys Fluids A 1992;4(6): 1290–303.

[13] Pope SB. Turbulent flows. Cambridge: Cambridge University Press; 2000.

[14] Arnold L. Stochastic differential equations: theory and applications. New York: Wiley; 1974.

[15] Klebaner FC. Introduction to stochastic calculus with applications. London: Imperial College Press; 1999.

[16] Øksendal B. Stochastic differential equations. An introduction with applications. Berlin: Springer; 1995.

[17] Kloeden PE, Platen E. Numerical solution of stochastic differential equations. Berlin: Springer; 1992.

[18] Haken H. Synergetics: an overview. Rep Prog Phys 1989;52: 515–33.

[19] Minier J-P, Pozorski J. Derivation of a PDF model for turbulent flows based on principles from statistical physics. Phys Fluids 1997;9(6):1748–53.

[20] Minier J-P, Peirano E, Chibbaro S. PDF model based on Langevin equation for polydispersed two-phase flows applied to a bluff-body gas–solid flow. Phys Fluids A 2004;16(7): 2419–31.

[21] Reeks MW. On the constitutive relations for dispersed particles in nonuniform flows. I dispersion in a simple shear flow. Phys Fluids A 1993;5(3):750–61.

[22] Pozorski J, Minier P. On the Lagrangian turbulent dispersion models based on the Langevin equation. Int J Multiphase Flow 1998;24:913–45.

[23] Csanady GT. Turbulent diffusion of heavy particles in the atmosphere. J Atmos Sci 1963;20:201–8.

[24] Olla P, Paradisi P. Relations between Lagrangian models and synthetic random velocity fields. Phys Rev E 2004;70: 046305.

[25] Reynolds AM. On the formulation of Lagrangian stochastic models for heavy particle trajectories. J Colloid Interface Sci 2000;232:260–8.

[26] Simonin O, Deutsch E, Minier J-P. Eulerian prediction of the fluid/particle correlated motion in turbulent two-phase flows. Appl Sci Res 1993;51:275–83.

[27] Simonin O. Continuum modelling of dispersed two-phase flows Combustion and turbulence in two-phase flows. Lecture series programme: Von Karman Institute; 1996.

[28] Peirano E, Leckner B. Fundamentals of turbulent gas–solid flows applied to circulating fluidized bed combustion. Prog Energy Combust Sci 1998;24:259–96.

[29] Peirano E, Minier J-P. Probabilistic formalism and hierarchy of models for polydispersed turbulent two-phase flows. Phys Rev E 2002;65(046301):1–18.

[30] Minier J-P, Peirano E, Chibbaro S. Weak first- and second order numerical schemes for stochastic differential equations appearing in Lagrangian two-phase flow modelling. Monte Carlo Methods Appl 2003;9(2):93–133.

[31] Öttinger HC. Stochastic processes in polymeric fluids. Tools and examples for developing simulation algorithms. Berlin: Springer; 1996.

[32] Talay D. In: Kree P, Wedig W, editors. Simulation of stochastic differential equation, in probabilistic methods in applied physics. Berlin: Springer; 1995.

[33] Hockney RW, Eastwood JW. Computer simulation using particles. New York: Adam Hilger; 1988.

[34] Birdsall CK, Fuss D. Clouds-in-clouds, clouds-in-cells physics for many-body plasma simulation. J Comput Phys 1969;3: 494–511 [reprinted in 1997, 135:141–148].

[35] O'Rourke PJ, Brackbill JU, Larrouturou B. On particle-grid interpolation and calculating chemistry in particle-in-cell methods. J Comput Phys 1993;109:37–52.

[36] Minier J-P, Pozorski J. Wall-boundary conditions in the PDF method for turbulent flows. Phys Fluids 1999;11:2632–44.

[37] Pope SB. Particle method for turbulent flows: integration of stochastic model equations. J Comput Phys 1995;117:332–49.

[38] Van Slooten PR, Jayesh, Pope SB. Advances in PDF modeling for inhomogeneous turbulent flows. Phys Fluids 1998;10: 246–65.

[39] Muradoglu M, Jenny P, Pope SB, Caughey DA. A consistent hybrid finite volume/particle method for the PDF equations of turbulent reactive flows. J Comput Phys 1999;154:342–71.

[40] Minier J-P, Ouraou M. Module diphasique Lagrangien du code ESTET: calculs de validation et applications industrielles. Technical Report HI-81/01/027/A, Laboratoire National d'Hydraulique, Electricité de France, Chatou, France; 2001.

[41] Xu J, Pope SB. Assessment of numerical accuracy of PDF/Monte-Carlo methods for turbulent reacting flows. J Comput Phys 1999;152:192.

[42] Welton WC. Two-dimensional PDF/SPH simulations of compressible turbulent flows. J Comput Phys 1998;139:410–43.

[43] Kalos MH, Whitlock PA. Monte Carlo methods, vol. I. New York: Wiley; 1986.

[44] Dreeben TD, Pope SB. Nonparametric estimation of mean fields with application to particle methods for turbulent flows. Technical Report FDA 92-13, Sibley School of Mechanical and Aerospace Engineering, Cornell University, Ithaca, New York; 1992.

[45] Monaghan JJ. Smoothed particle hydrodynamics. Ann Rev Astron Astrophys 1992;30:543–74.

[46] Morris JP, Fox PJ, Zhu Y. Modeling low Reynolds number incompressible flows using SPH. J Comput Phys 1997;136: 214–26.

[47] Minier J-P, Cao R, Pope SB. Comment on the article 'An effective particle tracing scheme on structured/unstructured grids in hybrid finite volume/PDF Monte Carlo methods' by Li and Modest. J Comput Phys 2003;186:356–8.

[48] Talay D. Probabilistic models for non-linear partial differential equations and numerical applications. In: Talay D, Tubaro L, editors. Lecture notes in mathematics 1627. Berlin: Springer; 1996. p. 148–96 [CIME Summer School].

[49] Wacławczyk M, Pozorski J, Minier J-P. Probability density function computation of turbulent flows with a new near-wall model. Phys Fluids 2004;16:1410.

[50] Dreeben TD, Pope SB. Wall-function treatment in PDF methods for turbulent flows. Phys Fluids 1997;9:2692–703.

[51] Dreeben TD, Pope SB. Probability density function/Monte Carlo simulation of near-wall turbulent flows. J Fluid Mech 1998;357:141–66.

[52] Garcia AL, Bell JB, Crutchfield W, Alder BJ. Adaptive mesh and algorithm refinement using direct simulation Monte Carlo. J Comput Phys 1999;154:134–55.

[53] Pozorski J, Apte SV, Raman V. Filtered particle tracking for dispersed two-phase turbulent flows Center for Turbulence Research, Summer Program 2004, Stanford, June 20–July 16; 2004.

[54] Jaberi FA, Gicquel LYM, Givi P, Pope SB. Velocity filtered density function for large eddy simulation of turbulent flows. Phys Fluids 2002;14:1196–213.

[55] Stairmand CJ. The design and performance of cyclone separators. Trans Inst Chem Eng 1951;29:356.

[56] Boysan F, Ewan B, Swithenbank J, Ayers W. Experimental and theoretical studies in cyclone separator aerodynamics. Proc I Chem E Symp Series 1983;69:305–17.

[57] Boysan F, Swithenbank J, Ayers W. Mathematical modeling of gas-particle flows in cyclone separators. Encyclopedia Fluid Mech 1986;4:1307–29.

[58] Ishima T, Borrée J, Fanouillère P, Flour I. Presentation of a data base: confined bluff body flow laden with solid particles. In the workshop on two-phase flow predictions, Martin-Luther-Universität, Halle-Wittenburg, Germany, April 13–16 1999.

[59] Borée J, Ishima T, Flour I. The effect of mass loading and inter-particle collisions on the development of the polydispersed two-phase flow downstream a confined bluff body. J Fluid Mech 2001;443:129–65.

[60] Minier J-P. Peirano E, Talay D. Schémas numériques faibles pour les équations différentielles stochastiques intervenant dans les modèles diphasiques Lagrangiens. Technical report HI-81/01/026/A, Laboratoire National d'Hydraulique, EDF, Chatou, France; 2001.

[61] Liu B, Agarwal K. Experimental observation of aerosol deposition in turbulent flow. J Aerosol Sci 1974;5:145.

[62] McCoy DD, Hanratty TJ. Rate of deposition of droplets in annular two-phase flow. Int J Multiphase Flow 1977;3:319.

[63] Eaton JK, Fessler JR. Preferential concentration of particles by turbulence. Int J Multiphase Flow 1994;20:169.

[64] Van Haarlem B, Boersma BJ, Nieuwstadt FTM. Direct numerical simulation of particle deposition onto a free-slip and no-slip surface. Phys Fluids 1998;10:2608.

[65] Matida EA, Nishino K, Torii K. Statistical simulation of particle deposition on the wall from turbulent dispersed pipe flow. Int J Heat Fluid Flow 2000;21:389.

[66] Schuen JS, Chen LD, Faeth M. Evaluation of a stochastic model of particle dispersion in a turbulent round jet. AIChE J 1987;29:167.

[67] Narayanan C, Lakehal D, Botto L, Soldati A. Mechanisms of particle deposition in a fully developed turbulent open channel flow. Phys Fluids 2003;3:763.

[68] Chibbaro S, Douce A, Minier J-P. PDF simulation of particle deposition in turbulent two-phase flows. In: Hanjalić K, Nagano Y, Tummers MJ, editors. Turbulence, heat and mass transfer, vol. 4. New York: Begell House; 2003. p. 1025–30.

[69] Liboff RL. Kinetic theory: classical, quantum, and relativistic descriptions. 2nd ed. London: Prentice Hall Advanced Reference Series; 1998.

[70] Chapman S, Cowling TG. The mathematical theory of non-uniform gases. Cambridge: Cambridge Mathematical Library; 1970.